ACCURATE THERMOCHEMISTRY OF KEY SOOT FORMATION INTERMEDIATES

by

STEVEN EDGE WHEELER

(Under the direction of Henry F. Schaefer III)

ABSTRACT

Precise enthalpies of formation of key soot formation intermediates C_3H_3, C_4H_3, and C_4H_5 have been determined through systematic extrapolations of *ab initio* energies within the focal point method of Allen and co-workers. Electron correlation has been accounted for using second-order Z-averaged perturbation theory (ZAPT2) and coupled cluster theory through full triple excitations [CCSD, CCSD(T), and CCSDT]. We have also explicitly examined the convergence of ZAPT*n* energies and predicted spectroscopic constants for a series of systems to compare it with more oft-applied restricted open-shell perturbation theories. The results offer justification for the inclusion of ZAPT2 energies as the leading correlation contribution in the focal point method over alternative perturbation theories in cases exhibiting spin-contamination and suggest ZAPT2 as the best available open-shell perturbation theory for routine applications. Based on the extrapolated results, recommended enthalpies of formation are as follows: $\Delta_f H_0^\circ$(propargyl) = 84.7, $\Delta_f H_0^\circ$(1-propynyl) = 126.6, $\Delta_f H_0^\circ$(cycloprop-1-enyl) = 125.7, $\Delta_f H_0^\circ$(cycloprop-2-enyl) = 117.3, $\Delta_f H_0^\circ$(*i*-C_4H_3) = 119.0, $\Delta_f H_0^\circ$(*E*-*n*-C_4H_3) = 130.8, $\Delta_f H_0^\circ$(*i*-C_4H_5) = 78.4, and $\Delta_f H_0^\circ$(*E*-*n*-C_4H_5) = 89.1 kcal mol^{-1}. These constitute the most reliable enthalpies presently available, and their incorporation into detailed kinetic models of soot formation will allow for the development of more definitive models of PAH and soot formation during combustion.

INDEX WORDS: soot formation, combustion, computational chemistry, perturbation theory, ZAPT, spin contamination, thermochemistry, basis set extrapolation

ACCURATE THERMOCHEMISTRY OF KEY SOOT FORMATION INTERMEDIATES

by

STEVEN EDGE WHEELER

B.A., New College of Florida, 2002

A Dissertation Submitted to the Graduate Faculty of The University of Georgia in Partial Fulfillment of the Requirements for the Degree

DOCTOR OF PHILOSOPHY

ATHENS, GEORGIA

2006

ACCURATE THERMOCHEMISTRY OF KEY SOOT FORMATION INTERMEDIATES

by

STEVEN EDGE WHEELER

Major Professor: Henry F. Schaefer III

Committee: Geoffrey D. Smith
Henning H. Meyer

Electronic Version Approved:

Maureen Grasso
Dean of the Graduate School
The University of Georgia
May 2006

DEDICATION

For my Kristen, who loves soot so, so much.

ACKNOWLEDGEMENTS

I would like to quickly acknowledge those without whom the completion of this work and this degree would have been improbable. First, Dr. Jeremy Lloyd introduced me to chemistry ten years ago, providing much of the foundation upon which the rest of my science education was built. Furthermore, he instilled in me a love and enthusiasm for chemistry that is undying and insatiable. Without Dr. Lloyd, I would have probably tried to become a physicist, so thank you, Dr. Lloyd, for pointing me in the satisfying and fruitful direction of chemistry. I also must thank Mrs. Myrick, who instilled in me an appreciation of knowledge and scholarly pursuits. Building on this foundation was the ever-supportive faculty of New College—Don Colladay, Paul Scudder, Pat McDonald, and Malkiat Johal. Together these four challenged me and guided me as I honed in on the field of computational quantum chemistry. Vital to my decision to abandon earlier dreams of becoming an organic chemist were physical chemistry and quantum mechanics courses taught by Jane Stephens and Alice Kolakowska, respectively, and a summer research experience under the direction of Shih-I Chu at the University of Kansas.

Whether consciously or not, my parents trained me to be a scientist and a scholar essentially from birth, encouraging me to seek a deeper understanding of the physical world around me. I've found that such an understanding was not always forthcoming, but that certainly didn't spoil the fun of searching. Thank you, for instilling in me a scientific curiosity that prevented me from heading down the mundane roads toward accounting or engineering. I would also like to thank my brothers, Matt and Will (an accountant and engineer, respectively), for

allowing me to survive this long in the world and for creating the footsteps in which I have largely chosen not to follow.

The task of completing this degree would not have been the pleasant adventure it was were it not for the jovial, inspiring atmosphere of the CC(Q)C, created simultaneously by the 'grandfatherly' Henry F. Schaefer and his motley crew of graduate students, research scientists, and visitors. Thank you all of CC(Q)C for making these last few years enjoyable yet productive. Specifically, I would like to thank office-mates Joe 'Big Daddy' Larkin and Justin Boone Ingels as well as co-conspirator Justin 'Jet' Turney. I would also like to thank Wesley Allen and Yukio Yamaguchi for their support and assistance over the last four years.

In my experience, the best learning experiences arise through teaching, so I would like to thank my summer mentees Andy Simmonett, Richard Lord, and Ken Robertson, as well as my fellow graduate students Sunghwan 'Martin' Kim and Andy Simmonett. Likewise, my time at the CC(Q)C would have been far less productive and the transition to graduate school less smooth had I not starting out under the tutelage of mentors Dr. Joe Kenny and Dr. Kurt Sattelmeyer. Also, as we all know, the CC(Q)C would not function were it not for Linda Rowe and the rest of the staff at the CC(Q)C. I thank you Linda, for shielding us all from the bureaucracy and nonsense that is necessarily part of a large university.

Finally, I would like to thank my Kristen, to whom this work is dedicated, and without whom there would be little point in facing each day. Your strength and perseverance in the face of a nasty illness amazes and inspires each of us on a daily basis. Thank you for your understanding over these last four years as I slipped deeper and deeper into my own world. Sorry I think about little other than computational chemistry. Thank you also for toughing it through these harsh north Georgia winters until we can move somewhere with a proper climate.

TABLE OF CONTENTS

CHAPTER 1

INTRODUCTION AND BACKGROUND MATERIAL

1.1 INTRODUCTION

Modern computational quantum chemistry constitutes an indispensable tool for the determination of accurate thermochemical parameters for key intermediates in combustion and soot formation. These intermediates are typically transient, unsaturated hydrocarbon radicals that evade detailed experimental characterization and pose a challenge to many commonly employed methods of computational thermochemistry. However, the judicious application of electronic structure theory coupled with basis-set extrapolation techniques allows for the precise determination of enthalpies of formation and isomerization energies, which in turn provide a solid foundation upon which detailed kinetic models of combustion can be developed. Devoid of precise thermochemistry for key intermediates, the development of quantitative kinetic models of combustion progresses slowly, with the results often shrouded in doubt.[1,2]

The electronic Schrödinger equation can not be solved exactly for multi-electron systems, necessitating the invocation of some set of approximations. Ideally, these approximations are evoked in a controlled manner, yielding predicable errors without relying on empirical or *ad hoc* correction schemes. One such approach to solving the electronic Schrödinger equation is through *ab initio* molecular orbital theory, the results of which can be systemically improved towards the exact, non-relativistic Born-Oppenheimer solution. When executed properly, this framework of controlled, systematic improvement allows for the extrapolation of computed energies, often resulting in predictions whose accuracy rivals the best available experiments.

Ideally one would carry out molecular computations using a relativistic Hamiltonian and expand the wave function describing both nuclear and electronic motion in a complete basis. Instead, one generally starts with a non-relativistic Hamiltonian and then invokes the Born-Oppenheimer approximation to allow for the separation of the nuclear and electronic problems.

The errors resulting from these two approximations are generally small, though first-order corrections compensating for these effects are often necessary to achieve accuracy in predicted relative energies on the order of 0.1 kcal mol^{-1}.[3,4]

By far the largest errors in typical *ab initio* electronic structure computations are incurred through the expansion of the Born-Oppenheimer wave function in terms of finite one- and *n*-particle basis sets. The *n*-particle basis is composed of all possible Slater determinants generated from excitations out of the set of occupied molecular orbitals into virtual orbitals. At the simplest level, the electronic wave function can be represented by a single determinant (Hartree-Fock theory; HF), which is the optimal single determinant wave function for the given one-particle basis. At the other extreme is full configuration interaction (FCI), in which the wave function is optimized within the space spanned by the complete *n*-particle basis. By definition, the difference in energies between these two extremes (HF and FCI) is the electron correlation energy. While the correlation energy comprises only a small fraction of the total electronic energy, its accurate description is of paramount importance in accounting for chemical phenomena. Expansion of the wave function in terms of complete one- and *n*-particle bases yields the exact, non-Relativistic Born-Oppenheimer solution. While this is not feasible for realistic molecular systems, we can approach this tantalizing limit by systematically increasing the one- and *n*-particle basis sets and exploiting the regular convergence towards both basis set limits

1.2 Hierarchies of *ab Initio* Methods

The most robust, applicable single-reference method for the treatment of electron correlation is coupled cluster (CC) theory.[5,6] CC theory is characterized by an exponential expansion of the wave function in the *n*-particle basis,

$$\left|\Psi_{CC}\right\rangle = e^{\hat{T}}\left|\Psi_0\right\rangle, \tag{1.1}$$

where $\left|\Psi_0\right\rangle$ is generally a Hartree-Fock wave function, and the operator $\hat{T}$ a sum of excitation operators, $\hat{T} = \hat{T}_1 + \hat{T}_2 + \hat{T}_3 + \ldots$. The effect of $\hat{T}_n$ on a Hartree-Fock determinant is to excite *n* electrons from occupied MOs to virtual (unoccupied) orbitals. In practical applications the excitation operator $\hat{T}$ is truncated at some order less than the total number of electrons, yielding, for example, the familiar CCSD (where $\hat{T}$ is limited to single and double excitations) and CCSDT (where $\hat{T} = \hat{T}_1 + \hat{T}_2 + \hat{T}_3$) theories. By increasing the level at which $\hat{T}$ is truncated, more complete wave functions can be constructed, yielding a hierarchy of CC methods spanning the void between HF and FCI. The primary advantage of coupled cluster theory over truncated CI approaches is that the couple cluster method is size extensive at any level of truncation, unlike CI, while still converging to the FCI limit. Moreover, the CC expansion is generally more rapidly convergent than CI at a given level of truncation, due to the contributions of higher order excitations through the inclusion of disconnected terms in coupled cluster theory. As a result, CC theory has grown to dominate the market of high-accuracy computations on small molecules.

A major drawback to methods that explicitly include triple excitations, including CCSDT, is the unfavorable scaling with system size. However, there are numerous approximate treatments of triple excitations within the coupled-cluster framework, the most well-known of which is the perturbative CCSD(T) method of Raghavachari and co-workers.[7] CCSD(T) offers an attractive balance of computational efficiency (the method formally scales as N^7, where N is representative of the system size) and accuracy, yielding results that are generally comparable to the full inclusion of triple excitations via CCSDT (which scales formally as N^8). Moreover, it is often the case that the errors in CCSD(T), relative to CCSDT, are of comparable magnitude but

opposite sign as the correction that would arise from the inclusion of quadruple excitations through CCSDTQ.[8] Indeed, CCSD(T) often performs better than CCSDT, relative to FCI and experiment.[9]

However, even CCSD scales as N^6, prohibiting its use with large one-particle basis sets. Instead, second-order Møller-Plesset perturbation theory (MP2) is often used to recover the effects of electron correlation with large basis sets. In Møller-Plesset theory[10] one defines the zeroth-order Hamiltonian as a sum of one-electron Fock operators, of which the MOs comprising the Hartree-Fock reference wave function are eigenfunctions. The zeroth-order energy is then the sum of orbital energies (diagonal Fock matrix elements in a basis of canonical Hartree-Fock orbitals), and inclusion of the first order correction yields the Hartree-Fock energy. Second-order perturbation theory, the first order at which electron correlation energy is recovered, scales as N^5, and provides an economical treatment of electron correlation that bridges the gap between HF and CCSD.

1.2.1 Open-Shell Systems

Since the non-relativistic electronic Hamiltonian operator commutes with the total spin operator, the exact electronic wave functions can be constructed to be eigenfunctions of $\hat{S}^2$. For high-spin open-shell molecules, Hartree-Fock wave functions that are also spin-eigenfunctions can be constructed by restricting the spatial orbitals corresponding to α and β spins to be identical, resulting in restricted open-shell HF theory (ROHF). On the other hand, this constraint can be lifted, allowing α and β orbitals to vary independently (unrestricted Hartree-Fock theory; UHF), imparting additional variational flexibility to the wave function and generally resulting in a lower variational energy. This lowering of the energy comes at the cost, however, of the introduction of contributions from higher spin states—spin contamination. While the

unrestricted and restricted solutions are often similar, there are many cases in which spin contamination can become significant, with dire consequences for UHF predicted properties and correlated methods built on this spin contaminated reference.

While coupled-cluster theory is relatively insensitive to a spin contaminated reference wave function,[11] the detrimental effects of spin contamination on perturbative wave functions can be dramatic. This would suggest that Møller-Plesset theory for open-shell systems should start from a ROHF reference wave function. However, in this case there is no clear choice for the partitioning of the electronic Hamiltonian, resulting in a slew of different formulations of ROHF-reference perturbation theories in the literature. While some of these theories result in correlated wave functions that are spin-eigenfunctions, others introduce spin contamination into the correlated wave function. However, none of the commonly employed ROHF-based perturbation theories exhibit spin contamination in the second order energy.[12] The choice then of a restricted open-shell second-order perturbation theory should depend primarily on the computational efficiency, performance in chemical applications, and convergence properties of the particular formulation.

1.2.2 Convergence of Møller-Plesset Perturbation Theory

While Møller-Plesset perturbation theory can be readily implemented to fourth-order, the explicit implementation of higher-order perturbation methods rapidly becomes intractable, involving the evaluation of 1000s of terms. However, in 1985, Laidig *et al.*[13] and Handy and co-workers[14,15] independently published a method by which FCI programs can be coaxed to yield MP*n* energies up to very high order for any system accessible by FCI. In 1996, Olsen *et al.*[16] used such methods to examine high-order MP*n* energy series for several systems, revealing highly oscillatory and divergent behavior for Ne, HF, and H_2O. Furthermore, the convergence

properties were strongly dependent on the one-particle basis set, with the inclusion of diffuse functions often causing previously convergent series to oscillate and diverge. Subsequent work has shed light on the underlying causes of this and related phenomena. Together, these investigations have cast doubt on the convergence of the Møller-Plesset energy series for most chemical systems, providing further incentive to abandon all but MP2 theory in favor of the more robust coupled cluster methods.

1.3 Convergence of the One-Particle Basis

Having discussed the hierarchy of *ab initio* methods, we now turn to the one-particle basis. The one-electron functions used to build the *n*-particle determinants, usually chosen such that they yield a diagonal representation of the Fock operator, are most often constructed as linear combinations of atom-centered Gaussian functions (AOs). The convergence of the Hartree-Fock energy with respect to the completeness of this atomic orbital basis is relatively quick, since the Hartree-Fock energy depends only on the occupied molecular orbitals, the accurate description of which requires primarily AOs resembling the valence orbitals of the constituent atoms. The convergence of the correlation energy, on the other hand, is quite slow with respect to completeness of the one-particle basis. Early work on the convergence of the electron correlation energy is due to Schwartz,[17] who found that the correlation energy in two-electron systems decays as $\left(l+\frac{1}{2}\right)^{-4}$ for basis sets saturated up to angular momentum level *l*. Thirty years later, Kutzelnigg and Morgan[18] demonstrated similar convergence behavior for MP2 correlation energies based on a Hartree-Fock reference wave function. This slow convergence is generally attributed at least in part to the inability of a determinantal wave function expanded in terms of one-electron functions to properly describe the cusp in the electronic wave function at the electron coalescence point.[19]

There are two commonly-employed approaches to rectify the slow convergence of the correlation energy with respect to the one-particle basis within standard *ab initio* molecular orbital theories: explicit inclusion of the inter-electronic distance in the wave function (via so-called r_{12} methods) and extrapolations of energies computed using carefully constructed basis sets. While the former solution is perhaps more satisfying from a theoretical standpoint, the area of open-shell r_{12} methods is in its infancy, leaving the latter choice as the only presently viable option for applications to systems with unpaired electrons.

1.3.1 Basis Set Extrapolations

The modern use of basis-set extrapolations stems primarily from the work of Almlöf and Taylor[20] and Dunning[21] in the late 1980s, in which families of AO basis sets were constructed that result in the systematic approach of correlation energies to the complete basis set limit. The pioneering work of Almlöf and Taylor resulted in the atomic natural orbital (ANO) basis sets, though the large number of primitive Gaussian functions on which these basis sets were built made them prohibitively expensive for routine applications, and their use was not widespread. Two years later, Dunning introduced the correlation-consistent polarized valence *X*-tuple-ζ basis sets (cc-pV*X*Z), which struck a more efficient compromise between uniform convergence to the complete basis set (CBS) limit and number of Gaussian primitives. The popularity of these basis sets has been overwhelming, and their introduction credited with a revolution in the way high-accuracy electronic structure computations are carried out.[9] These sets have since been extended to include basis sets with one or two shells of diffuse functions, sets for treating core-valence correlation, sets for relativistic computations, and more. Within each family, successive basis sets are constructed by adding an additional 'shell' of valence and polarization functions to the previous basis set, and are characterized by the principle quantum number of the highest shell of

functions. For example, for first-row atoms the cc-pVDZ and cc-pVTZ basis sets are composed of the contractions 3*s*2*p*1*d* and 4*s*3*p*2*d*1*f*, respectively.

Feller investigated[22] the convergence of Hartree-Fock and correlation energies computed using the cc-pV*X*Z basis sets, arriving at the exponential functional form

$$E_{HF}(X) = E_{\infty} + be^{-cX}, \tag{1.2}$$

where X is the cardinality of the basis set, E_{∞} is the energy at the CBS limit, and b and c are adjustable parameters. While there is little sound physical rational for this functional form, experience suggest that it properly describes the convergence behavior of Hartree-Fock energies, but results in an underestimation of the CBS limit when applied to correlation energies.[9] Helgaker and co-workers[23] subsequently proposed the following for the convergence of the correlation energy:

$$E_{corr}(X) = E_{\infty} + bX^{-3}. \tag{1.3}$$

While there is a similar dearth of sound theoretical basis for this functional form, empirical evidence and numerical tests reveal that it provides a robust means of extrapolating correlation energies, particularly when used in conjunction with larger basis sets. As such, it is generally advisable to extrapolate only from energies computed with triple-ζ quality basis sets or larger. While there are numerous other functional forms used in the literature for the extrapolation of both Hartree-Fock and correlation energies, Eqs. (1.2) and (1.3) constitute the standard approaches.

1.4 Computational Thermochemistry

Despite breathtaking advances in computer hardware, software, and methods of electronic structure theory, the theoretical prediction of thermochemical parameters (enthalpies of formation, heat capacities, standard entropies, *etc*.) to an accuracy that rivals typical

experiments remains a serious challenge.[24,25] However, basis set extrapolation techniques and the general availability of efficient coupled cluster programs has opened the door to extremely accurate computational thermochemistry capable of achieving agreement with the best available experiments to within 0.1 kcal mol^{-1}.[26] Moreover, in many areas in which accurate enthalpies of formation are vital (namely combustion and atmospheric chemistry), the systems of interest are often transient species. In these cases, computational methods are the most viable route to the required information, and reliable methods to compute enthalpies of formation accurate down to several tenths of a kcal mol^{-1} are mandatory.

The seemingly most straight-forward means of computing enthalpies of formation is to evaluate the energy of the formation reaction from the standard state of the constituent elements. For example, for water, this would be

$$H_{2(g)} + \tfrac{1}{2}O_{2(g)} \rightarrow H_2O_{(g)}. \qquad (1.4)$$

However, such a direct approach quickly fails for systems involving carbon, since this would require the accurate computation of the electronic energy of graphite. Instead, one typically uses either atomization reactions or more general transformations involving the target system and reference compounds for which accurate enthalpies of formation are already known. The computed reaction energy can then be used to derive enthalpies of formation of the system of interest via Hess's Law.

Atomization energies offer the clear advantage that they are uniquely defined and the reference enthalpies of formation for first-row atoms are generally well-known from experiment. However, the computation of atomization energies involves the breaking of every bond, and large errors can result from an imbalance of effects between the atomic and molecular computations. More general reactions, on the other hand, must be constructed such that the

enthalpies of formation of the reference compounds are known to sufficient accuracy. Indeed, with modern computational thermochemical techniques, the limiting factor in the accuracy of predicted enthalpies of formation is often the experimental error associated with the reference values. However, one can design specific reactions that maximize cancellation of errors while involving only compounds with precisely known enthalpies of formation.

Two types of such error-canceling reactions are the so-called isodesmic[27] and homodesmotic[28] reactions. Isodesmic reactions are those in which there are equal numbers of each 'type' of bond (*e.g.*: C–C, C–H, *etc.*) in reactants and products, while homodesmotic reactions, which constitute a subset of isodesmic reactions, are defined in the case of organic reactions as those in which there are equal numbers of carbon atoms in each state of hybridization and equal numbers of CH_3, CH_2, CH, *etc*. groups on each side of the reaction. Although initially developed to allow for the accurate computation of enthalpies of formation via low-level computations, isodesmic and homodesmotic reactions are useful even when sophisticated *ab initio* approaches are employed. Ideally, employing these types of reactions lessens the burden on the theoretical method through the natural cancellation of inherent errors, accelerating convergence with respect to completeness of the one- and *n*-particle bases. Additionally, it is often possible that several isodesmic or homodesmotic reactions can be constructed that involve complementary sets of reference compounds. In these favorable cases, uncertainties in reference enthalpies can be uncovered by predicting a single enthalpy of formation through several independent reactions.

1.4.1 Composite Methods

One particularly popular class of methods for computational thermochemistry are the so-called composite methods, typified by the Gaussian-*n* series (G2, G3, and their many

variants).[29,30] These G*n* methods strive to compute estimates of complete basis set limit QCISD(T) (quadratic CI with singles, doubles, and perturbative triples) energies primarily based on the assumption that basis set incompleteness errors in QCISD(T) energies can be properly approximated by the difference between MP2 energies with large and small basis sets. Empirical corrections are also included, calibrated against experimental thermochemical results and intended to make up for inherent deficiencies in the method. While the G*n* theories were designed to compute thermochemical parameters via atomization energies, subsequent work has revealed advantages in their use with isodesmic reactions.[31] These methods are a prime example of 'theoretical model chemistries'—methods that are precisely defined and then tested for a set of molecules. While this 'black box' approach has obvious advantages, particularly for non-experts wishing to harness the powers of computational thermochemistry, the reality is that different chemical problems require different tools, and any method that is rigidly defined will necessarily perform poorly for certain classes of systems. Moreover, when computing isomerization energies, an imbalance of errors can result in particularly poor relative energies. A similar family of methods comprises the CBS-*n* techniques of Petersson and co-workers,[32-36] which attempt to achieve accuracy on the order of 0.5 kcal mol^{-1} for small systems based on the asymptotic convergence of pair natural orbital expansions.

The G*n* methods have been tested against several large sets of experimental atomization energies, ionization potentials, and electron affinities, and for these test sets achieve an average error of only 1-2 kcal mol^{-1}.[37-40] As such, they are routinely applied to combustion intermediates, with the expectation that the accuracy of the results will be comparable to that achieved for the test sets. Unfortunately, for open-shell systems the extensive reliance in the G*n* methods on perturbative wave functions built on an UHF reference can yield unsatisfactory

results, particularly for systems with considerable spin contamination. Additionally, the black-box nature of these methods shields the user from the possibility that the theoretical methods on which they rely can be ill-suited for specific chemical systems.

1.4.2 Focal Point Analyses

Unlike the G*n* methods, the focal point procedure, developed by Allen and co-workers in the early 1990s,[4,41-43] provides a framework within which one explicitly examines the convergence with respect to completeness of the one- and *n*-particle bases. The general format of a focal point table is displayed in Fig. 1.1. Energies are computed at an accurate geometry [generally optimized using CCSD(T) theory with at least a triple-ζ quality basis set], at the HF, MP2, CCSD, CCSD(T), and CCSDT levels of theory with a series of correlation consistent basis sets. At each level, energies are computed up to the largest basis set possible. The Hartree-Fock and correlation energies are then extrapolated using Eqs (1.2) and (1.3), respectively, and the extrapolated increments (where each increment is the *correction* to the previous level of theory) then summed to yield an estimate of the complete basis set CCSDT energy. While in the present work we do not continue beyond CCSDT, the maximum level of correlation included is dictated only by computational feasibility.

By extrapolating the energies at each level of correlation treatment to the CBS limit and then examining the corrections derived from successively more complete *n*-particle expansions, the error due to incompleteness in both bases can be quantified and deficiencies remedied to yield any desired degree of error relative to the exact non-relativistic Born-Oppenheimer energy. Unlike the 'hands-free' approach of commonly employed composite methods, within the focal point procedure there is a clear indication of lingering errors due to incomplete one- and *n*-particle basis sets, allowing for the customization necessary to yield consistently reliable results.

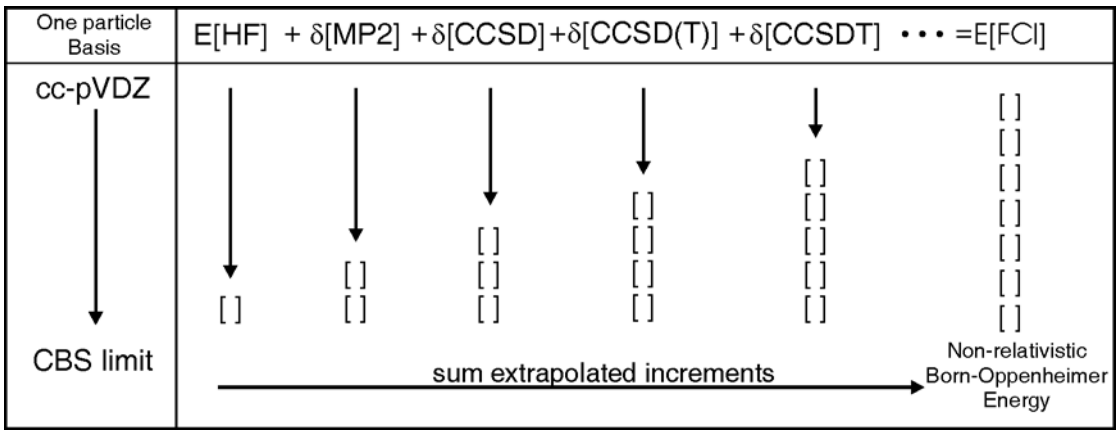

Figure 1.1 Schematic focal point table. Square brackets indicate extrapolated values, while all other energies are explicitly computed. The extrapolated increments are summed to yield an approximation to the exact non-relativistic Born-Oppenheimer energy.

The aforementioned extrapolations are carried out first within the frozen-core approximation, in which the 1*s* orbitals on first-row elements (1*s*2*s*2*p* for second-row) are excluded from the correlation treatment, using the cc-pV*X*Z basis sets. The effects of core-valence correlation are accounted for through secondary focal point extrapolations, in which the difference between all-electron and frozen-core correlated computations using the correlation-consistent polarized core-valence X-tuple-ζ basis sets (cc-pCV*X*Z) is extrapolated to the CBS limit. To achieve accuracy down to 0.2 kcal mol^{-1}, additional corrections must be appended to the energy. Specifically, effects due to non-Born-Oppenheimer behavior are accounted for through the diagonal Born-Oppenheimer correction (DBOC),[44-47] which constitutes the first-order perturbative correction to the Born-Oppenheimer energy. Scalar relativistic effects are partially accounted for through the one-electron Darwin and mass-velocity terms from the Breit-Pauli Hamiltonian.[48-52] Zero-point vibrational energies are derived from harmonic vibrational frequencies computed using CCSD(T) with the largest basis set feasible.

There is a related family of methods, developed by Martin and co-workers and referred to as the Weizmann-*n* theories (W1, W2, W3, and several lower-cost variants).[53-55] While these methods are qualitatively quite similar to the focal point method of Allen and co-workers, they are intended as black-box procedures, and therefore do not allow for the flexibility necessary to treat myriad chemical systems on equal footings. More recently, Tajti and co-workers[26] have presented the HEAT method (High accuracy Extrapolated *Ab initio* Thermochemistry), which is more computationally demanding than typical focal point applications (though strictly speaking, the HEAT method is nearly identical in design to the focal point method) and is only applicable to rather small systems. Similar approaches have also been proposed by Feller and co-workers[56] and Bauschlicher *et al*.[57,58]

1.4.3 Other Approaches

Density functional theory (DFT) has enjoyed enormous success in recent years, providing the seemingly impossible combination of accuracy and computational efficiency. As such, DFT is often the first avenue of approach for predicting thermochemical values and mapping out potential energy surfaces for complex reactions. It is ideally suited for this purpose, providing qualitative information about potential energy surfaces with minimal computational effort. However, with DFT there is a lack of means for the systematic improvement of results. As such, it is often difficult to gauge the accuracy of predicted results, and DFT can fail unexpectedly for seemingly mundane systems. Furthermore, many popular DFT functionals contain empirically adjusted parameters, so, as with all semi-empirical methods, application of these functionals to systems dissimilar to the training set used to optimize the parameters can result in expected behavior.

Quantum Monte Carlo (QMC) methods offer an orthogonal approach to the electron correlation problem, promising 'exact' solutions to the time-independent Born-Oppenheimer Schrödinger equation through stochastic methods.[59] Modern QMC implementations also offer the possibility of application to rather large chemical systems. The drawback, however, is that these techniques generally require a pre-computed nodal surface for the wave function of interest, usually taken from *ab initio* computations. The QMC energy is then evaluated within the so-called fixed node approximation.[60-64] However, the errors associated with the quality of these nodal surfaces are not fully understood,[65,66] and the result is that QMC methods can sometimes yield spurious results. Furthermore, since QMC gradients are not readily available (and, to some extent, not easily defined given the stochastic nature of the method), QMC energies are generally computed at DFT or *ab initio* predicted geometries. Even moderate deficiencies in the optimized structures used for the QMC computations can have noticeable effects on computed properties, despite the inherent accuracy of the actual QMC energy. Regardless, QMC methods, and specifically diffusion Monte Carlo (DMC) techniques, have been applied to many problems in computational thermochemistry, often with success.[67,68]

1.5 Combustion Chemistry

Combustion science has made tremendous advances in recent decades, moving from qualitative, largely phenomenological descriptions of pyrolysis to quantitative detailed kinetic models of combustion and soot formation. While some of this progress has been driven by advancements in experimental diagnostic methods that allow for the validation of combustion models, it has largely been a result of developments in computational thermochemistry and kinetics.[1,2]

Soot formation has been of interest for centuries, with soot initially valued for its light and heat producing properties.[69] With the advent of internal combustion technologies, the deposition of soot on the walls of combustion chambers was quickly seen as an obstacle to efficient combustion.[70] Only later were the deleterious effects of soot particles on human health recognized. More recently, the Clean Air Act of 1990 classified polycyclic aromatic hydrocarbons (PAHs), the primary precursors of soot particles, as air toxins and strictly regulated their emission. This legislation, coupled with studies showing that many PAHs are mutagenic and carcinogenic, has spurred intense research into soot formation mechanisms. Looming deadlines for further restrictions of small particulate emissions is further fueling these efforts. Since an understanding of the underlying mechanism of soot formation will be necessary to develop the next generation of cleaner combustion technologies, PAH and soot formation stand at the forefront of current combustion research.

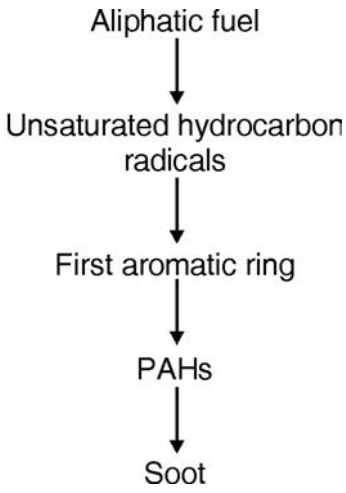

Figure 1.2 General pathway for the formation of soot particles from aliphatic fuels.

In hydrocarbon combustion, soot particles form via the general pathway given in Fig. 1.2, in which the rate-limiting step is the formation of the first aromatic ring (either benzene or

naphthalene).[1,2] The general paradigm for the accrual of additional rings on PAHs in combustion is the HACA mechanism (H-abstraction, C_2H_2-addition),[71] in which successively larger PAHs are formed through the creation of a radical via hydrogen abstraction followed by addition of acetylene. Clearly a key step in this process is the formation of the first aromatic ring, and a majority of recent soot research has focused on the mechanism and kinetics of the formation benzene in flames.

Early work by Weissman and Benson[72,73] and Cole *et al.*[74] suggested the addition of acetylene to *n*-C_4H_5 as a pathway to benzene,

$$n\text{-}C_4H_5 + C_2H_2 \rightarrow C_6H_6 + H, \qquad (1.5)$$

a process that subsequent experiments showed to be a viable cyclization step.[75,76] The first quantitative chemical kinetic model of PAH formation was due to Frenklach and co-workers,[77] in which benzene was formed primarily through

$$n\text{-}C_4H_3 + C_2H_2 \rightarrow C_6H_6 + H, \qquad (1.6)$$

with reaction (1.5) contributing under some conditions. These so-called even-carbon-atom pathways have subsequently fallen from favor, largely due to a theoretical study predicting that *n*-C_4H_3 and *n*-C_4H_5 will isomerize to the lower-lying *i*-C_4H_3 and *i*-C_4H_5, which will not readily combine with acetylene to form benzene.[78] However, recent experimental and theoretical work has spurred renewed interest in these even-carbon-atom pathways as viable means of forming soot, at least under some flame conditions, and called into question the dismissal of these reactions as inoperative in soot formation.[79]

Alternative benzene formation pathways, for which there is considerable experimental and theoretical evidence, involve the reactions of resonance-stabilized free-radicals such as propargyl, allyl, and cyclopentadienyl. The enhanced stability afforded by the delocalization of

these radicals, and the subsequent resistance towards oxidation in flames, allows for the build-up of significant populations during combustion, increasing the chance of radical-radical reactions. By far the most studied of such pathways is the self-reaction of propargyl radical (C_3H_3).[1]

Of paramount importance in detailed kinetic models of PAH formation are accurate enthalpies of formation and isomerization energies for key intermediates.[1,2] While there has been a great deal of theoretical work aimed at characterizing these intermediates and the associated potential energy surfaces, a vast majority of this work has been carried out using DFT and composite *ab initio* methods. The result is an unsatisfactory degree of uncertainty in key enthalpies of formation and relative energies. While there is little hope of applying the robust and computationally demanding *ab initio* focal point extrapolations described above to all intermediates and pathways known to be operative in PAH formation, it is imperative that the precise thermochemistry be determined for key intermediates in the rate limiting steps. This work constitutes a step towards this goal.

1.6 PROSPECTUS

We proceed by first examining the convergence of energies and predicted spectroscopic constants from Z-averaged perturbation theory (ZAPT) in Chapter 2. These convergence studies are accompanied by comparisons of ZAPT-predicted equilibrium bond lengths and harmonic vibrational frequencies at second and fourth order, compared to results from restricted open-shell Møller-Plesset theory (ROMP) and the closely related RMP theory. The computational efficiency of the ZAPT method, relative to ROMP and RMP theories, coupled with the robust convergence characteristics of ZAPT energies justifies the use of ZAPT2 as the leading correlation contribution in the focal point analyses applied to key soot formation intermediates.

In Chapter 3 we present a thorough theoretical treatment of the disputed soot formation intermediates C_4H_3 and C_4H_5 based on focal point extrapolations, providing definitive isomerization energies and enthalpies of formation and providing a sound basis on which the role of even-carbon-atom pathways can be investigated. In Chapter 4 we apply similar methods to compute relative energies for three low-lying isomers of the key soot formation intermediate propargyl radical, as well as accurate enthalpies of formation for all four of these C_3H_3 species. Finally, we conclude with Chapter 5, providing a brief summary of the work.

REFERENCES

1 J. A. Miller, M. J. Pilling, and J. Troe, Proc. Combust. Inst. **30**, 43 (2005).

2 H. Richter and J. B. Howard, Phys. Chem. Chem. Phys. **4**, 2038 (2002).

3 M. S. Schuurman, Ph.D. Thesis, University of Georgia, 2004.

4 A. G. Császár, G. Tarczay, M. L. Leininger, O. L. Polyansky, and W. D. Allen, in *Spectroscopy from Space*, edited by J. Demaison and K. Sarka (Kluwer, Dordrecht, 2001), pp. 317.

5 T. D. Crawford and H. F. Schaefer, in *Reviews in Computational Chemistry*, edited by K. B. Lipkowitz and D. B. Boyd (Wiley-VCH, New York, 2000), Vol. 14.

6 T. Helgaker, P. Jørgensen, and J. Olsen, *Molecular Electronic-Structure Theory*. (Wiley, Chichester, 2002).

7 K. Raghavachari, G. W. Trucks, J. A. Pople, and M. Head-Gordon, Chem. Phys. Lett. **157**, 479 (1989).

8 T. Helgaker, W. Klopper, A. Halkier, K. L. Bak, P. Jørgensen, and J. Olsen, in *Quantum Mechanical Prediction of Thermochemical Data*, edited by J. Cioslowski (Kluwer Academic, Dordrecht, 2001), pp. 1.

9 D. Feller, K. A. Peterson, and T. D. Crawford, J. Chem. Phys. **124**, 054107 (2006).

10 C. Møller and M. S. Plesset, Phys. Rev. **46**, 618 (1934).

11 J. F. Stanton, J. Chem. Phys. **101**, 371 (1994).

[12] T. J. Lee, A. P. Rendell, K. G. Dyall, and D. Jayatilaka, J. Chem. Phys. **100**, 7400 (1994).

[13] W. D. Laidig, G. Fitzgerald, and R. J. Bartlett, Chem. Phys. Lett. **113**, 151 (1985).

[14] P. J. Knowles, K. Somasundram, N. C. Handy, and K. Hirao, Chem. Phys. Lett. **113**, 8 (1985).

[15] N. C. Handy, P. J. Knowles, and K. Somasundram, Theor. Chim. Acta **68**, 87 (1985).

[16] J. Olsen, O. Christiansen, H. Koch, and P. Jørgensen, J. Chem. Phys. **105**, 5082 (1996).

[17] C. Schwartz, Phys. Rev. **126**, 1015 (1962).

[18] W. Kutzelnigg and J. D. Morgan, J. Chem. Phys. **96**, 4484 (1992).

[19] T. Kato, Commun. Pure Appl. Math. **10**, 151 (1957).

[20] J. Almlöf and P. R. Taylor, J. Chem. Phys. **86**, 4070 (1987).

[21] T. H. Dunning, J. Chem. Phys. **90**, 1007 (1989).

[22] D. Feller, J. Chem. Phys. **98**, 7059 (1993).

[23] T. Helgaker, W. Klopper, H. Koch, and J. Noga, J. Chem. Phys. **106**, 9639 (1997).

[24] *Computational Thermochemistry: Prediction and Estimation of Molecular Thermodynamics*, edited by K. K. Irikura and D. J. Frurip (American Chemical Society, Washington, D. C., 1998).

[25] *Quantum-Mechanical Prediction of Thermochemical Data*, edited by J. Cioslowski (Kluwer Academic, Dordrecht, 2001).

[26] A. Tajti, P. G. Szalay, A. G. Császár, M. Kállay, J. Gauss, E. F. Valeev, B. A. Flowers, J. Vázquez, and J. F. Stanton, J. Chem. Phys. **121**, 11599 (2004).

[27] W. J. Hehre, R. Ditchfield, L. Radom, and J. A. Pople, J. Am. Chem. Soc. **92**, 4796 (1970).

[28] P. George, M. Trachtman, C. W. Bock, and A. M. Brett, Theor. Chem. Acc. **38**, 121 (1975).

[29] L. A. Curtiss, K. Raghavachari, P. C. Redfern, V. Rassolov, and J. A. Pople, J. Chem. Phys. **109**, 7764 (1998).

[30] L. A. Curtiss, K. Raghavachari, G. W. Trucks, and J. A. Pople, J. Chem. Phys. **94**, 7221 (1991).

[31] K. Raghavachari, B. B. Stefanov, and L. A. Curtiss, J. Chem. Phys. **106**, 6764 (1997).

[32] G. A. Petersson and M. Braunstein, J. Chem. Phys. **83**, 5129 (1985).

[33] J. A. Montgomery, Jr., J. W. Ochterski, and G. A. Petersson, J. Chem. Phys. **101**, 5900 (1994).

[34] J. W. Ochterski, G. A. Petersson, and J. A. Montgomery, Jr., J. Chem. Phys. **104**, 2598 (1996).

[35] J. A. Montgomery, Jr., M. J. Frisch, J. W. Ochterski, and G. A. Petersson, J. Chem. Phys. **110**, 2822 (1999).

[36] J. A. Montgomery, Jr., M. J. Frisch, J. W. Ochterski, and G. A. Petersson, J. Chem. Phys. **112**, 6532 (2000).

[37] L. A. Curtiss, P. C. Redfern, K. Raghavachari, and J. A. Pople, J. Chem. Phys. **109**, 42 (1998).

[38] L. A. Curtiss, P. C. Redfern, and K. Raghavachari, J. Chem. Phys. **123**, 124127 (2005).

[39] L. A. Curtiss, K. Raghavachari, P. C. Redfern, and J. A. Pople, J. Chem. Phys. **112**, 7374 (2000).

[40] L. A. Curtiss, K. Raghavachari, P. C. Redfern, and J. A. Pople, J. Chem. Phys. **106**, 1063 (1997).

[41] W. D. Allen, A. L. L. East, and A. G. Császár, in *Structures and Conformations of Non-Rigid Molecules*, edited by J. Laane, M. Dakkouri, B. van der Vecken, and H. Oberhammer (Kluwer, Dordrecht, 1993), pp. 343.

[42] A. L. L. East and W. D. Allen, J. Chem. Phys. **99**, 4638 (1993).

[43] A. G. Császár, W. D. Allen, and H. F. Schaefer, J. Chem. Phys. **108**, 9751 (1998).

[44] N. C. Handy, Y. Yamaguchi, and H. F. Schaefer, J. Chem. Phys. **84**, 4481 (1986).

[45] A. G. Ioannou, R. D. Amos, and N. C. Handy, Chem. Phys. Lett. **251**, 52 (1996).

[46] N. C. Handy and A. M. Lee, Chem. Phys. Lett. **252**, 425 (1996).

[47] W. Kutzelnigg, Mol. Phys. **90**, 909 (1997).

[48] S. A. Perera and R. J. Bartlett, Chem. Phys. Lett. **216**, 606 (1993).

[49] K. Balasubramanian, *Relativistic Effects in Chemistry: Part A, Theory and Techniques*. (Wiley, New York, 1997).

[50] K. Balasubramanian, *Relativistic Effects in Chemistry: Part B, Applications*. (Wiley, New York, 1997).

[51] R. D. Cowan and D. C. Griffin, J. Opt. Soc. Am. **66**, 1010 (1976).

[52] G. Tarczay, A. G. Császár, W. Klopper, and H. M. Quiney, Mol. Phys. **99**, 1769 (2001).

[53] J. M. L. Martin and G. de Oliveira, J. Chem. Phys. **111**, 1843 (1999).

[54] J. M. L. Martin and S. Parthiban, in *Quantum-Mechanical Prediction of Thermochemical Data*, edited by J. Cioslowski (Kluwer Academic, Dordrecht, 2001), pp. 31.

[55] A. D. Boese, M. Oren, O. Atasolyu, J. M. L. Martin, M. Kállay, and J. Gauss, J. Chem. Phys. **120**, 4129 (2004).

[56] D. Feller and D. A. Dixon, J. Phys. Chem. A **104**, 3048 (2000).

[57] C. W. Bauschlicher, Jr. and A. Ricca, J. Phys. Chem. **102**, 8044 (1998).

[58] C. W. Bauschlicher, Jr. and A. Ricca, J. Phys. Chem. A **103**, 4313 (1999).

[59] J. B. Anderson, in *Quantum Mechanical Electronic Structure Calculations with Chemical Accuracy*, edited by S. R. Langhoff (Kluwer Academic, Dordrecht, 1995).

[60] J. B. Anderson, J. Chem. Phys. **63**, 1499 (1975).

[61] D. M. Ceperley and B. J. Alder, Phys. Rev. Lett. **45**, 566 (1980).

[62] D. M. Ceperley, in *Recent Progress in Many-Body Theories*, edited by J. G. Zabolitzky, M. de Llano, M. Fortes, and J. W. Clark (Springer, Berlin, 1981), pp. 262.

[63] B. J. Alder, D. M. Ceperley, and P. J. Reynolds, J. Phys. Chem. **86**, 1200 (1982).

[64] P. J. Reynolds, D. M. Ceperley, B. J. Alder, and W. A. Lester Jr., J. Chem. Phys. **77**, 5593 (1982).

[65] J. Hachmann, P. T. A. Galek, T. Yanai, G. K. L. Chan, and N. C. Handy, Chem. Phys. Lett. **392**, 55 (2004).

[66] N. C. Handy, Mol. Phys. **102**, 23 (2004).

[67] A. C. Kollias, D. Domin, G. Hill, M. Frenklach, D. M. Golden, and W. A. Lester, Jr., Int. J. Chem. Kinet. **37**, 583 (2005).

[68] A. C. Kollias, D. Domin, G. Hill, M. Frenklach, and W. A. Lester, Jr., Mol. Phys. **104**, 467 (2006).

[69] U. Colombo and M. W. Thring, Combust. Sci. Tech. **5**, 189 (1972).

[70] J. C. Street and A. Thomas, Fuel **34**, 4 (1955).

[71] M. Frenklach and H. Wang, Proc. Combust. Inst. **23**, 1559 (1991).

[72] M. Weissman and S. W. Benson, Int. J. Chem. Kinet. **16**, 307 (1984).

[73] M. Weissman and S. W. Benson, Prog. Energy Combust. Sci. **15**, 273 (1989).

[74] J. A. Cole, J. D. Bittner, J. P. Longwell, and J. B. Howard, Combust. Flame **56**, 51 (1984).

[75] A. B. Callear and G. B. Smith, Chem. Phys. Lett. **105**, 119 (1984).

[76] A. B. Callear and G. B. Smith, J. Phys. Chem. **90**, 3229 (1986).

[77] M. Frenklach, D. W. Clary, W. C. Gardiner Jr., and S. E. Stein, Proc. Combust. Inst. **20**, 887 (1984).

[78] J. A. Miller and C. F. Melius, Combust. Flame **91**, 21 (1992).

[79] M. Frenklach, Phys. Chem. Chem. Phys. **4**, 2028 (2002).

CHAPTER 2

ON THE CONVERGENCE OF Z-AVERAGED PERTURBATION THEORY (ZAPT)[1]

[1] S. E. Wheeler, W. D. Allen, and H. F. Schaefer. To be submitted to the Journal of Chemical Physics.

2.1 ABSTRACT

Very high-order Z-averaged perturbation theory (ZAPT) energies, equilibrium bond lengths, and harmonic vibrational frequencies have been computed for a set of small molecules using a determinantal algorithm. The convergence of ZAPT*n* energies is compared to alternative Møller-Plesset perturbation theories built on restricted open-shell Hartree-Fock (ROMP, RMP, OPT1, and OPT2) and unrestricted Hartree-Fock (UMP) reference wave functions for NH_2 at three N–H bond lengths and for CN. The ZAPT*n* energy series closely parallel those from RMP*n* and ROMP*n* theories for these systems. Further, we examine the convergence of ZAPT*n* energies, equilibrium bond lengths (r_e), and harmonic vibrational frequencies (ω_e) for X $^2\Sigma_g^+$ CN, X $^4\Sigma_g^+$ C_2^+, and b $^2\Delta_g$ C_2^+, tracking oscillations in the energy series for the latter system to order 1000. The r_e and ω_e values from explicit ZAPT2 and ZAPT4 computations with a triple-ζ plus double polarization basis set (TZ2P) are very close to those from second- and fourth-order RMP and ROMP theories for NO and CN, but offer improved predictions relative to experimental values in the case of $^3\Sigma_g^-$ O_2. In light of the noted robustness of ZAPT and similarity of results to the oft-applied RMP theory, coupled with the reductions in computational cost inherent in the ZAPT method relative to theories requiring different orbitals for different spins, we recommend low-order ZAPT for applications to open-shell systems.

2.2 INTRODUCTION

The early 1990s were witness to a flurry of publications of alternative formulations[1-6] of single-reference Møller-Plesset perturbation theories[7] built on a restricted open-shell Hartree-Fock (ROHF) reference wave function. These methods include[8] the restricted open-shell Møller-Plesset theory (ROMP) of Amos *et al.*,[1] the restricted Møller-Plesset theory (RMP) of Knowles and co-workers[2] [which is equivalent to the ROHF-MBPT formulation of Lauderdale *et al.*[3]], the

open-shell perturbation theory methods 1 and 2 (OPT1 and OPT2) of Murray and Davidson,[4] the Z-averaged perturbation theory (ZAPT) of Lee and Jayatilaka,[5] and the invariant open-shell perturbation theory (IOPT) of Kozlowski and Davidson.[6] Accompanying these developments were several studies[1,2,9,10] comparing the rate of convergence of electron correlation energies arising from these different partitionings of the electronic Hamiltonian, computed through the exploitation of determinant-based full configuration interaction (FCI) methodologies.[9-14] However, absent from previous studies of the convergence properties of open-shell perturbation theories is an analysis of ZAPT*n* energies.[15] Indeed, there are no results available in the literature for ZAPT computed beyond second order (ZAPT2). Additionally, while the convergence of predicted spectroscopic and molecular properties has been examined for closed-shell MP*n* theory,[16-18] there are no such results for open-shell perturbation theories beyond fourth-order.

The overwhelming conclusion of previous convergence studies[1,2,10] was that perturbation theories based on a ROHF reference wave function are generally more reliable than unrestricted Møller-Plesset theory (UMP),[7,19] particularly in cases with spin-contamination. Indeed, UMP theory has been known to yield poor results for some time,[12,14,20] which in part fueled the efforts to develop a satisfactory ROHF-based perturbation theory. Meanwhile, work on closed-shell MP*n* convergence revealed troubling, basis set dependent cases of oscillatory and divergent behavior for seemingly innocuous systems, such as Ne, HF, and H_2O.[18,21] More recent work has illuminated underlying causes and additional manifestations of these behaviors in closed-shell Møller-Plesset theory.[17,22] One would expect similar, if not more complex and devious, behavior in high-order perturbation series for open-shell systems.

ZAPT has been shown[23,24] to have a number of desirable properties, including invariance of the electron correlation energy with respect to most orbital rotations that leave the ROHF

energy unchanged[25] and the absence of direct contributions to the energy from spin contamination at any order (with no spin contamination at second-order). Furthermore, an analysis of the zeroth-order Hamiltonian utilized in ZAPT suggests that there will be less spin contamination at a given order than in RMP or ROMP theories.[23] Also, ZAPT can be implemented in terms of a single set of spatial orbitals, resulting in an open-shell theory that is nominally of the same cost as the corresponding closed-shell method.[5,23] This leads to computational savings relative to UMP, ROMP, and RMP theory, which require different orbitals for different spins. In addition, previous test applications[23] have indicated that ZAPT2 performs at least as well as OPT2(2), RMP2, and ROMP2 in reproducing experimentally derived r_e structures and harmonic vibrational frequencies. Together, these advantages suggest ZAPT2 as a suitable candidate for use in routine applications to open-shell systems, particularly when spin contamination is present.

In this paper we proceed by first reviewing the basic theory of ZAPT and the implementation of arbitrary order ZAPT*n* within our determinant-based FCI program, DETCI.[26] High-order perturbation series are provided for a set of standard test cases, to allow comparison of the convergence properties of ZAPT energies to ROMP, RMP, OPT1, OPT2, and UMP theories. In addition, we examine the convergence of ZAPT predicted energies, equilibrium bond lengths, and harmonic vibrational frequencies for CN and two electronic states of C_2^+. While the convergence properties of perturbation series are important, from a pragmatic prospective the choice of an open-shell perturbation theory comes down to computational efficiency and performance in chemical applications at low order. To this end, comparison is made of ZAPT2 and ZAPT4 predicted equilibrium bond lengths and harmonic vibrational frequencies with previously reported second and fourth order perturbative results for NO, CN,

and O_2. Lastly, conclusions are drawn regarding applications of low-order open-shell perturbation theories to open-shell molecular systems.

2.3 Theoretical Methods

In the following we utilize the following sets of indices to denote spatial molecular orbitals: *i*, *j*, … denote doubly occupied orbitals (doc); *a*, *b*, … doubly unoccupied (virtual) orbitals (uocc); *s*, *t*, … singly occupied orbitals (soc); and *p*, *q*, … refer to any orbital. In contrast to other open-shell Møller-Plesset perturbation theories, ZAPT is generally formulated in terms of the symmetric spin orbital basis of Jayatilaka and Lee.[27] In this basis, the singly occupied subspace is expanded in terms of eigenfunctions of $\hat{S}_x$, rather than the usual $\hat{S}_z$ eigenfunctions.[5] In other words, while the standard α and β spin functions are used for spin-orbitals in the doubly occupied and "doubly unoccupied" spaces, the singly occupied and unoccupied orbitals are written in terms of

$$\sigma^{+} = \tfrac{1}{\sqrt{2}}(\alpha + \beta) \tag{2.1}$$

and

$$\sigma^{-} = \tfrac{1}{\sqrt{2}}(\alpha - \beta), \tag{2.2}$$

where σ^{+} is chosen for the singly occupied orbitals and σ^{-} for the corresponding unoccupied orbitals. The result is a reference function that is unaltered under the interchange of α and β spins and a spin-orbital Fock Matrix that is symmetric with respect to spin interchange.[27]

The orbital canonicalization scheme[5] used in ZAPT is identical to that of OPT1,[4] achieved readily via the diagonalization of an averaged Fock operator, F^{av}, separately in the doubly occupied, singly occupied, and unoccupied subspaces. While the resulting molecular orbitals are identical for α and β spins, the diagonal elements of the Fock matrix in the

symmetric spin orbital basis will be different for the singly occupied and corresponding singly unoccupied orbitals. This gives ZAPT the advantage of diagonal Fock matrix elements corresponding to the singly-occupied and lowest unoccupied molecular orbitals that resemble ionization potential and electron affinities, respectively, without the introduction of energy non-invariance issues (as is the case with OPT2).[6,23,24] In a basis of determinants composed of orbitals canonicalized as described above, the zeroth-order Hamiltonian can be written

$$\begin{aligned}\hat{H}_0^{ZAPT} = &\sum_i^{doc} f_i^{av}\left(i_\alpha^\dagger i_\alpha + i_\beta^\dagger i_\beta\right) + \sum_a^{uoc} f_a^{av}\left(a_\alpha^\dagger a_\alpha + a_\beta^\dagger a_\beta\right) \\ &+ \sum_t^{soc}\left[f_t^{av}\left(t_\alpha^\dagger t_\alpha + t_\beta^\dagger t_\beta\right) + f_t^{\Delta}\left(t_\alpha^\dagger t_\beta + t_\alpha^\dagger t_\beta\right)\right]\end{aligned}, \tag{2.3}$$

where $f_p^{av} \equiv \frac{1}{2}\left(f_p^\alpha + f_p^\beta\right)$ and $f_t^{\Delta} \equiv \frac{1}{2}\left(f_t^\alpha - f_t^\beta\right)$. Alternatively, this can be expressed entirely in terms of the (σ_+, σ_-) basis as

$$\begin{aligned}\hat{H}_0^{ZAPT} = &\sum_i^{doc} f_i^{av}\left(i_{\sigma^+}^\dagger i_{\sigma^+} + i_{\sigma^-}^\dagger i_{\sigma^-}\right) + \sum_a^{uoc} f_a^{av}\left(a_{\sigma^+}^\dagger a_{\sigma^+} + a_{\sigma^-}^\dagger a_{\sigma^-}\right) \\ &+ \sum_t^{soc}\left[f_{t_\alpha}^{\alpha} t_{\sigma^+}^\dagger t_{\sigma^+} + f_{t_\alpha}^{\beta} t_{\sigma^-}^\dagger t_{\sigma^-}\right]\end{aligned}. \tag{2.4}$$

Recognizing that (σ_+, σ_-) are simply $\hat{S}_x$ eigenstates, this can equivalently be written entirely in terms of $\hat{S}_z$ eigenstates as

$$\tilde{\tilde{H}}_0^{ZAPT} = \sum_p^{all} f_p^{av}\left(p_\alpha^\dagger p_\alpha + p_\beta^\dagger p_\beta\right) - \tfrac{1}{2}\sum_t^{soc} K_t^o\left(t_\alpha^\dagger t_\alpha - t_\beta^\dagger t_\beta\right), \tag{2.5}$$

where f_p^{av} and K_t^o are given explicitly in terms of one- and two-electron repulsion integrals by

$$\begin{aligned} f_p^{av} &= h_{pp} + \sum_j^{doc}\left[2(pp|jj) - (pj|pj)\right] + \sum_u^{soc}\left[(pp|uu) - \tfrac{1}{2}(pu|pu)\right] \\ K_t^o &= \sum_t^{soc}(tu|tu)\end{aligned}. \tag{2.6}$$

We note that exclusion of the second term in Eq. (2.5) yields the zeroth-order Hamiltonian used in OPT1.

Generation of high-order perturbation series[11,12,18] using determinant-based FCI programs arises from the ability to write the (n + 1)th order energy, E_{n+1},and nth order wave function, $|\psi_n\rangle$, in a determinantal basis as

$$E_{n+1} = \langle \psi_0 | H | \psi_n \rangle \tag{2.7}$$

and

$$(H_0 - E_0)|\psi_n\rangle = \sum_{i=1}^{n} E_i |\psi_{n-i}\rangle + H_0 |\psi_{n-1}\rangle - H|\psi_{n-1}\rangle, \tag{2.8}$$

where the Hamiltonian matrix, H, has been partitioned into $H_0 + V$, and we rely on the fact that our perturbed wave function is orthogonal to the reference wave function (intermediate normalization). The resolvent matrix, $(H_0 - E_0)^{-1}$, is trivial to compute in cases where H_0 is diagonal, as in in Eq. (2.5). The utility of using existing FCI implementations arises from their strength in computing the product of the Hamiltonian matrix on a vector in a determinantal basis.[26] Further gains in computational efficiency are possible through the use of the Wigner energy formulae, which allow the computation of the (2n)th and (2n + 1)th order energies from $|\psi_n\rangle$.[28] Thus, high-order ZAPTn series can be generated via minor modifications to existing closed-shell MPn codes,[18,26] requiring primarily changes in the computation of diagonal matrix elements of H_0.

To verify results from high-order energy series and compute low-order results for systems too large for FCI, we have implemented ZAPT2, ZAPT3, and ZAPT4 within PSI3 in a spin-orbital representation[29] based on published formulae for ROMP theory.[30] The high-order ZAPTn series[31] have been generated using a modified version of DETCI[26] within PSI3.

2.4 Computational Details

To allow comparison with published high-order open-shell perturbation series,[10] we have employed the 6-31G basis[32] for ZAPT*n* energy series for NH_2 and the STO-3G basis[33] for CN. The Dunning[34] double-ζ correlation-consistent basis set (cc-pVDZ) was employed to examine the convergence of ZAPT energies and r_e and ω_e values for CN and C_2^+. Finally, a triple-ζ basis set plus polarization functions (TZ2P) was used to evaluate the performance of ZAPT2 and ZAPT4 in predicting equilibrium bond lengths and harmonic vibrational frequencies for NO, CN, and O_2, compared to ROMP and RMP results at second and fourth order. This TZ2P basis set comprised Dunning's (5*s*4*p*) contraction[35] of the (10*s*6*p*) primitive set of Huzinaga,[36] plus a pair of polarization functions (employing a set of six Cartesian *d*-functions) with exponents ($\alpha_d = 1.20$, $\alpha_d = 0.40$; $\alpha_d = 1.35$, $\alpha_d = 0.45$) for (C; N and O).[10] For all correlated computations the 1*s* core orbitals were frozen.

Equilibrium bond lengths and harmonic vibrational frequencies were determined by fitting a constrained fifth-order polynomial to a set of a minimum of six energies (of at least 10^{-10} E_h accuracy) evenly spaced at 0.01 Å intervals and surrounding the equilibrium bond length. The fit was achieved using the non-linear least squares fit capabilities of *MATHEMATICA*,[37] under a simple constraint on the quintic force constant.[38]

2.5 Results and Discussion

2.5.1 Convergence of Open-Shell Perturbation Theories

ZAPT*n* energy series are presented for NH_2 at three bond lengths (r = 1.013, 1.5195, 2.026 Å; bond angle 103.2°) using the 6-31G basis and for CN (r = 1.1619 Å) using STO-3G, to compare with results from the literature[10] for ROMP, RMP, OPT1, OPT2, and UMP theories (see Tables 2.1 and 2.2 and Figs. 2.1 and 2.2). From Fig. 2.1 (top panel), we see that errors in

ZAPT*n* energies relative to FCI are nearly identical to those arising from RMP and ROMP theories for NH_2 at its equilibrium bond length of 1.013 Å. Overall, all five perturbation series converge with similar alacrity, as expected since at this geometry NH_2 is well represented by a single-determinant reference wave function and exhibits negligible spin contamination ($\langle S^2 \rangle$ = 0.752 for UHF, compared to 0.750 for a pure doublet).

For NH_2 at $r = 1.5r_e$ (1.5195 Å; Fig. 2.1, middle panel), the perturbation series begin to differ, with RMP, ROMP, and ZAPT converging somewhat more slowly to the FCI limit than OPT1 and OPT2. UMP in turn converges even more slowly, presumably because of spin contamination causing the UHF reference to be somewhat deficient.

Stretching the N–H distance to twice the equilibrium bond length (Fig. 2.1, lower panel) results in spin-restricted series that oscillate about the FCI limit. As far out as 25th order, the (ROMP, RMP, OPT2, OPT1, ZAPT) energies are (1.04, 1.02, 0.48, 0.50, and 1.03) mE_h from the FCI limit. While OPT1 and OPT2 are closer to the FCI limit at 25th order, the oscillations in these two energy series are of greater magnitude than for the ROMP*n*, RMP*n*, and ZAPT*n* series, indicating that the OPT1(*n*) and OPT2(*n*) series are closer to diverging due to an approaching backdoor intruder state. This suggests a greater degree of stability of the RMP, ROMP, and ZAPT energy series for this system, and is in line with previous results indicating that smaller low-order energy corrections are characteristic of a more stable perturbation series.[9] The UMP energies converge monotonically, though very, very slowly (even at 25th order the UMP*n* energy is 10 mE_h above the FCI limit, so is not visible in the lower panel of Fig. 2.1), again due to the particularly poor zeroth order description of the system afforded by the UHF reference wave function.

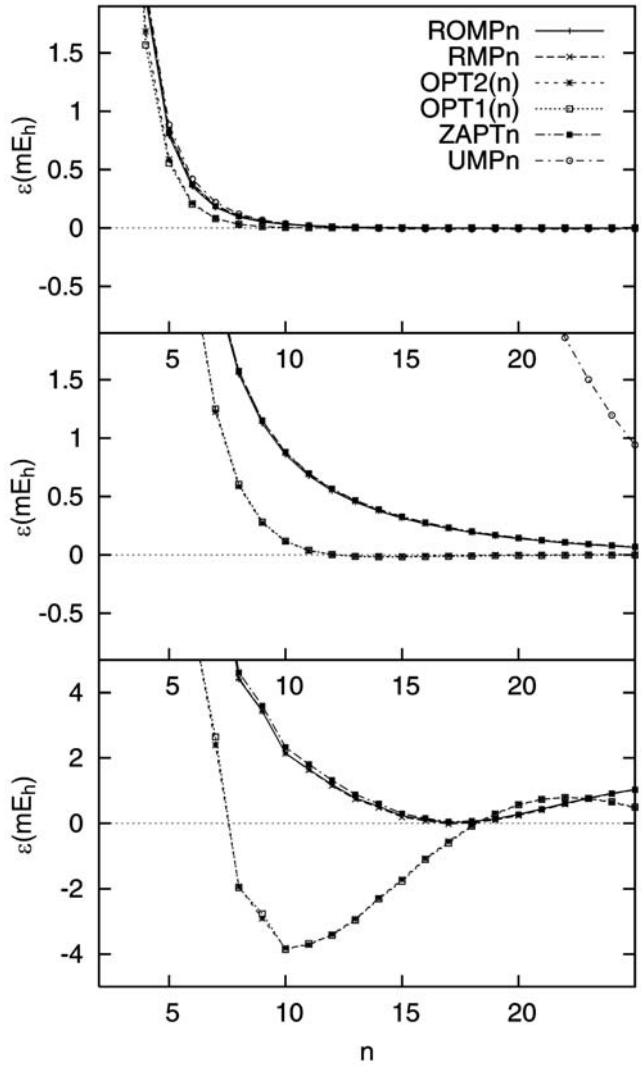

Figure 2.1 Errors in n^{th}-order perturbative energies (ε, mE_h), relative to FCI, for X $^2B_2$ NH_2 at three bond lengths (bong angle 103.2°) with the 6-31G basis and a frozen core: (top) r = 1.013 Å; (middle) r = 1.5195 Å; (bottom) r = 2.026 Å. ROMP, RMP, OPT2, OPT1, and UMP results are from Ref. 10.

At 25^{th} order it is still unclear whether the ROHF-based energy series presented for NH_2 at r = 2.026 Å will ultimately settle down and converge, or if the magnitude of the oscillations will grow for higher order terms leading to overall divergent series. As such, ZAPT*n* energies have been computed to 199^{th} order, with the errors relative to FCI falling below 1 μE_h at ZAPT101. The ROMP*n* and RMP*n* series presumably follow similar trends, while it is not clear

Table 2.1 Errors in ZAPT*n* energies relative to FCI (ε), for NH_2 ($^2B_2$) at bond lengths of r_e, 1.5 r_e, and 2 r_e (bond angle 103.2°) computed using the 6-31G basis set.[a]

	ε(mE_h)		
r =	1.013 Å	1.5195 Å	2.026 Å
ROHF	103.087	158.932	259.890
ZAPT2	16.353	37.145	84.377
ZAPT3	5.756	22.290	65.807
ZAPT4	2.034	10.204	32.502
ZAPT5	0.823	6.112	23.280
ZAPT6	0.371	3.544	11.888
ZAPT7	0.188	2.312	8.643
ZAPT8	0.101	1.576	4.622
ZAPT9	0.059	1.152	3.602
ZAPT10	0.035	0.882	2.331
ZAPT11	0.022	0.698	1.809
ZAPT12	0.014	0.567	1.321
ZAPT13	0.009	0.467	0.887
ZAPT14	0.006	0.390	0.604
ZAPT15	0.004	0.327	0.297
ZAPT16	0.002	0.277	0.161
ZAPT17	0.002	0.235	0.050
ZAPT18	0.001	0.200	0.071
ZAPT19	0.001	0.171	0.138
ZAPT20	0.000	0.147	0.272
ZAPT21	0.000	0.126	0.432
ZAPT22	0.000	0.109	0.602
ZAPT23	0.000	0.093	0.769
ZAPT24	0.000	0.081	0.913
ZAPT25	0.000	0.069	1.031
ZAPT26	0.000	0.060	1.114
ZAPT27	0.000	0.052	1.164
ZAPT28	0.000	0.044	1.180
ZAPT29	0.000	0.038	1.168
ZAPT30	0.000	0.033	1.129
ZAPT31	0.000	0.028	1.069
ZAPT32	0.000	0.024	0.993
ZAPT33	0.000	0.021	0.906
ZAPT34	0.000	0.018	0.811
ZAPT35	0.000	0.015	0.714
ZAPT36	0.000	0.013	0.618
ZAPT37	0.000	0.011	0.527
ZAPT38	0.000	0.010	0.442
ZAPT39	0.000	0.008	0.365
ZAPT40	0.000	0.007	0.299
ZAPT41	0.000	0.006	0.243
ZAPT42	0.000	0.005	0.197
ZAPT43	0.000	0.004	0.162
ZAPT44	0.000	0.004	0.137
ZAPT45	0.000	0.003	0.120
ZAPT46	0.000	0.003	0.110
ZAPT47	0.000	0.002	0.106
ZAPT48	0.000	0.002	0.106
ZAPT49	0.000	0.002	0.109[b]

[a] E(FCI) = –55.633264, –55.526661, and –55.441484 E_h for r = 1.013, 1.5195, and 2.026 Å, respectively.

[b] For r = 2.026 Å, ZAPT is not converged to within 0.001 mE_h of E(FCI) until ZAPT101.

without explicitly examining OPT1 and OPT2 energies beyond 25th order whether these series too are convergent.

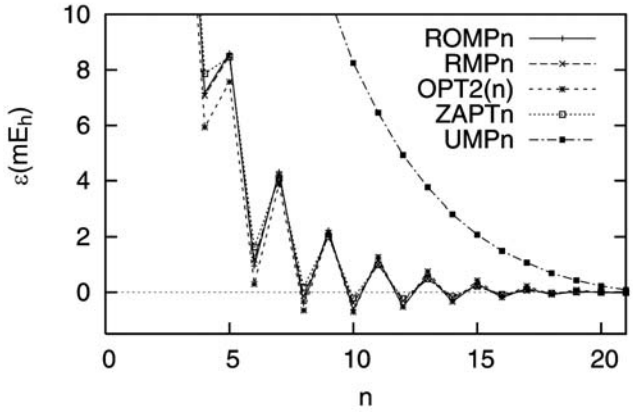

Figure 2.2 Errors in n[th]-order perturbative energies (ε, mE_h), relative to FCI, for X $^2\Sigma^+$ CN (r = 1.1619 Å) with a STO-3G basis and a frozen core. The OPT1 series rapidly diverges so is not displayed on the plot. ROMP, RMP, OPT2, OPT1, and UMP results are from Ref. 10.

The restricted open-shell perturbation series for STO-3G CN, on the other hand, exhibit rapidly oscillatory behavior, though overall the series are converged to within 0.1 mE_h by 16th order for RMP, ROMP, OPT2, and ZAPT (see Table 2.2 and Fig. 2.2). All four of these series exhibit qualitatively similar behavior for this system, in contrast to OPT1, which diverges.[10] The UMP*n* series converges monotonically, though slowly, remaining an order of magnitude further from the FCI limit than the ROHF-based methods at 16th order. As with NH_2, ZAPT*n* energies for CN are seen to very closely follow those from RMP and ROMP theories, suggesting that ZAPT*n* will consistently exhibit convergence behavior similar to RMP and ROMP theories.

Table 2.2 Errors in ZAPT*n* energies relative to FCI (ε), for X $^2\Sigma^+$ CN (r = 1.1619 Å) computed using the STO-3G basis set.[a]

	ε(mE_h)		ε(mE_h)
ROHF	172.564	ZAPT19	0.023
ZAPT2	18.164	ZAPT20	–0.003
ZAPT3	21.611	ZAPT21	–0.006
ZAPT4	7.869	ZAPT22	0.010
ZAPT5	8.463	ZAPT23	–0.016
ZAPT6	1.633	ZAPT24	0.013
ZAPT7	4.104	ZAPT25	–0.017
ZAPT8	0.176	ZAPT26	0.012
ZAPT9	2.005	ZAPT27	–0.013
ZAPT10	–0.207	ZAPT28	0.009
ZAPT11	1.005	ZAPT29	–0.009
ZAPT12	–0.229	ZAPT30	0.006
ZAPT13	0.493	ZAPT31	–0.006
ZAPT14	–0.156	ZAPT32	0.003
ZAPT15	0.227	ZAPT33	–0.003
ZAPT16	–0.083	ZAPT34	0.001
ZAPT17	0.090	ZAPT35	–0.001
ZAPT18	–0.032	ZAPT36	0.000

[a] E(FCI) = –97.170081 E_h

2.5.2 Convergence of Spectroscopic Constants

To gauge the convergence of ZAPT*n* predicted spectroscopic constants, we present predicted equilibrium bond lengths and harmonic vibrational frequencies, as well as errors in correlation energies relative to FCI, for X $^4\Sigma_g^+$ C_2^+, b $^2\Delta_g$ C_2^+, and X $^2\Sigma^+$ CN using the cc-pVDZ basis.[34] The results are summarized in Tables 2.3-2.5 and Figs. 2.3-2.6.

ZAPT*n* results for X $^4\Sigma_g^+$ C_2^+ are shown in Table 2.3 and Fig. 2.3. This cation is derived from neutral C_2 by ionization of one of the ($1\pi_u$) electrons and excitation of another ($1\pi_u$) electron to the ($3\sigma_g$) orbital, for a final occupation of [core]$(2\sigma_g)^2(2\sigma_u)^2(3\sigma_g)^1(1\pi_u)^2$. This electronic state is well-represented by a single determinant reference wave function and at the FCI equilibrium bond distance (1.43156 Å) there are no influential intruder states. As a result, the ZAPT*n* energy series for $^4\Sigma_g^+$ C_2^+ converges rapidly and monotonically to within 1 μE_h of E(FCI) by ZAPT20.

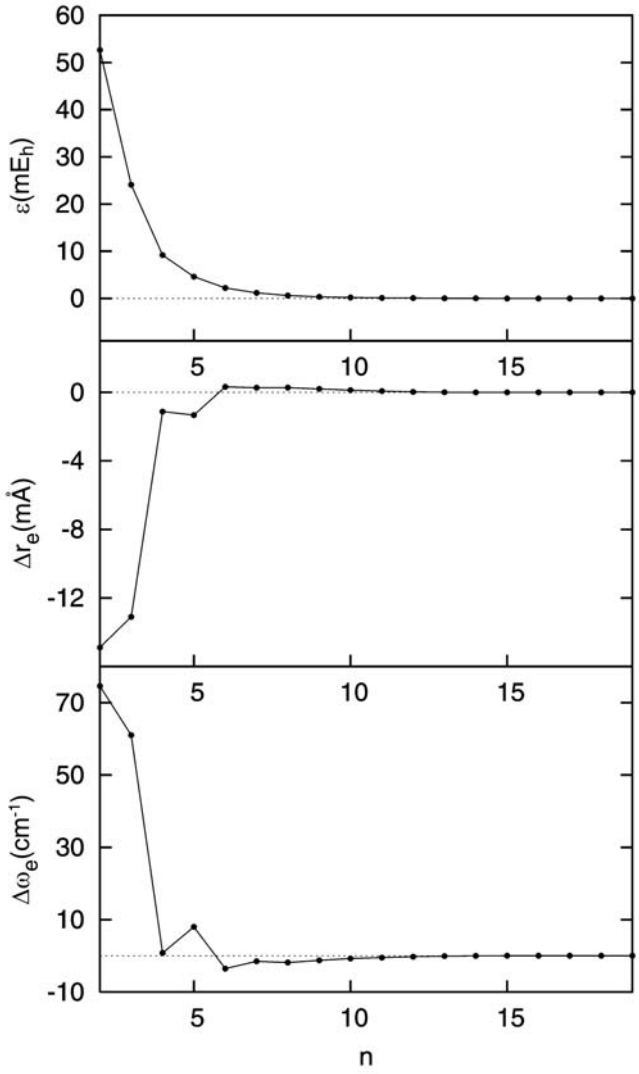

Figure 2.3 Errors in ZAPT*n* energies (ε, mE_h) and predicted equilibrium bond length (Δr_e, mÅ) and harmonic vibrational frequency ($\Delta\omega_e$, cm^{-1}), relative to FCI, for X $^4\Pi_u$ C_2^+ with the cc-pVDZ basis and a frozen *1s* core.

Table 2.3 ZAPT*n* energies (relative to FCI), equilibrium bond lengths, and harmonic vibrational frequencies for X $^4\Sigma_g^+$ C_2^+.

	cc-pVDZ		
	$\varepsilon(mE_h)$[a]	r_e(Å)	$\omega_e(cm^{-1})$
ROHF	217.63	1.38314	1496.7
ZAPT2	52.636	1.41667	1395.9
ZAPT3	24.102	1.41846	1382.3
ZAPT4	9.181	1.43043	1322.1
ZAPT5	4.615	1.43022	1329.3
ZAPT6	2.231	1.43187	1317.8
ZAPT7	1.169	1.43182	1319.8
ZAPT8	0.624	1.43183	1319.5
ZAPT9	0.340	1.43175	1320.1
ZAPT10	0.189	1.43168	1320.6
ZAPT11	0.106	1.43162	1320.9
ZAPT12	0.060	1.43159	1321.1
ZAPT13	0.344	1.43157	1321.2
ZAPT14	0.020	1.43155	1321.3
ZAPT15	0.011	1.43155	1321.3
ZAPT16	0.006	1.43155	1321.4
ZAPT17	0.003	1.43155	1321.4
ZAPT18	0.001	1.43155	1321.4
ZAPT19	0.001	1.43155	1321.3
ZAPT20	0.000	1.43155	1321.3
FCI	b	1.43156	1321.3

[a] Error with respect to E(FCI) at the FCI r_e value.
[b] E(FCI) = –75.313364 E_h

Examination of the ZAPT*n* predicted r_e and ω_e values for X $^4\Sigma_g^+$ C_2^+ reveals a brief period of oscillation in the low-order series, followed by a rapid convergence to the FCI limit analogous to the energy series. That the bond length and frequency series exhibit oscillations not present in the energy series is due to sensitivity of r_e and ω_e to the curvature of the potential energy surface surrounding the equilibrium distance—oscillations in the ZAPT*n* energies at stretched geometries alter the potential energy surface and introduce the observed variations in predicted r_e and ω_e values.

For b $^2\Delta_g$ C_2^+, which requires a two-determinant zeroth-order wave function (and is therefore far from suited for treatment with single-reference perturbation theory), the ZAPT*n* energies appear to converge monotonically (though very slowly) to the FCI limit (See Fig. 2.4

and Table 2.4). However, examining the ZAPT*n* energy series out to ZAPT999 (Fig. 2.5), one sees a slow, damped oscillation with a period of roughly 300 in the order of the perturbation. Even at ZAPT200, the correlation energy is 0.5 mE_h from the FCI limit, while by ZAPT999 the error has only been trimmed down to 0.03 mE_h. The predicted spectroscopic constants exhibit similar slow convergence, following small oscillations in the low-order series, analogous to the case of $X\ ^4\Sigma_g^+\ C_2^+$.

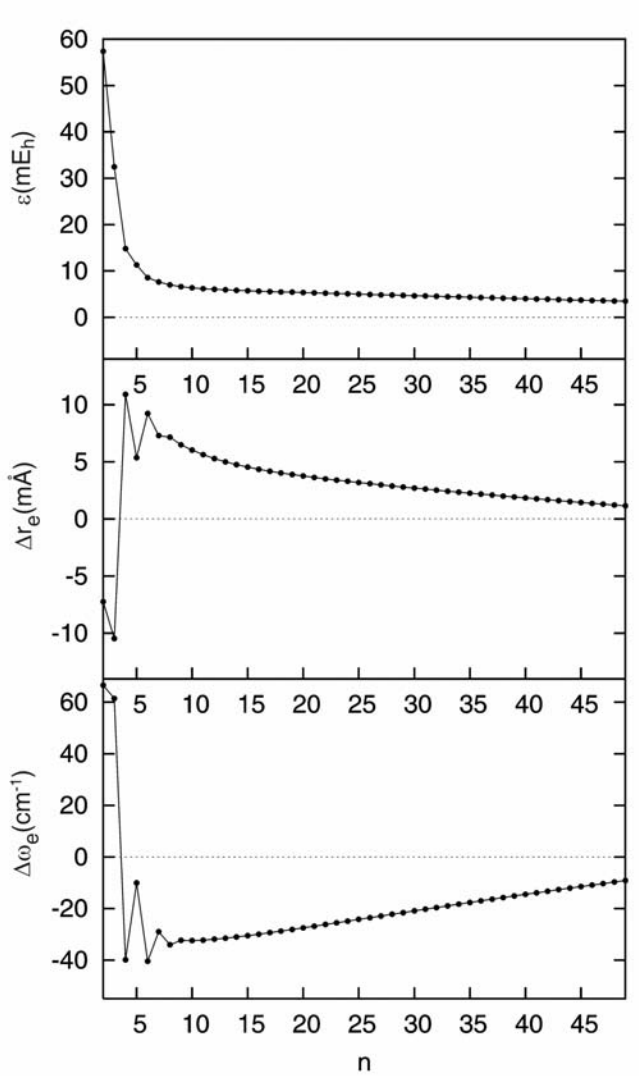

Figure 2.4 Errors in ZAPT*n* energies (ε, mE_h) and predicted equilibrium bond length (Δr_e, mÅ) and harmonic vibrational frequency ($\Delta\omega_e$, cm^{-1}), relative to FCI, for b $^2\Delta_g\ C_2^+$ with the cc-pVDZ basis and a frozen *1s* core.

Table 2.4 ZAPT*n* energies (relative to FCI), equilibrium bond lengths, and harmonic vibrational frequencies for b $^2\Delta_g$ C_2^+.

	cc-pVDZ		
	$\varepsilon(mE_h)$[a]	r_e(Å)	$\omega_e(cm^{-1})$
ROHF	246.214	1.407 63	1420.3
ZAPT2	57.394	1.459 07	1242.9
ZAPT3	32.467	1.455 84	1237.7
ZAPT4	14.815	1.477 22	1136.5
ZAPT5	11.282	1.471 68	1166.2
ZAPT6	8.571	1.475 55	1135.9
ZAPT7	7.618	1.473 61	1147.4
ZAPT8	6.986	1.473 47	1142.3
ZAPT9	6.621	1.472 81	1144.0
ZAPT10	6.371	1.472 33	1143.9
ZAPT11	6.187	1.471 95	1144.1
ZAPT12	6.043	1.471 60	1144.5
ZAPT13	5.925	1.471 32	1144.8
ZAPT14	5.822	1.471 07	1145.3
ZAPT15	5.730	1.470 85	1145.8
ZAPT16	5.645	1.470 66	1146.4
ZAPT17	5.565	1.470 49	1147.0
ZAPT18	5.489	1.470 34	1147.6
ZAPT19	5.415	1.470 20	1148.2
ZAPT20	5.342	1.470 06	1148.8
ZAPT21	5.271	1.469 94	1149.5
ZAPT22	5.201	1.469 82	1150.1
ZAPT23	5.132	1.469 71	1150.8
ZAPT24	5.064	1.469 60	1151.5
ZAPT25	4.996	1.469 50	1152.1
ZAPT26	4.928	1.469 40	1152.8
ZAPT27	4.861	1.469 30	1153.4
ZAPT28	4.794	1.469 20	1154.1
ZAPT29	4.728	1.469 11	1154.8
ZAPT30	4.662	1.469 02	1155.4
ZAPT31	4.596	1.468 92	1156.1
ZAPT32	4.530	1.468 83	1156.7
ZAPT33	4.465	1.468 75	1157.4
ZAPT34	4.400	1.468 66	1158.0
ZAPT35	4.336	1.468 57	1158.7
ZAPT36	4.272	1.468 48	1159.3
ZAPT37	4.208	1.468 40	1159.9
ZAPT38	4.144	1.468 32	1160.6
ZAPT39	4.081	1.468 23	1161.2
ZAPT40	4.018	1.468 15	1161.8
ZAPT41	3.955	1.468 07	1162.4
ZAPT42	3.893	1.467 99	1163.0
ZAPT43	3.831	1.467 91	1163.6
ZAPT44	3.769	1.467 84	1164.2
ZAPT45	3.707	1.467 76	1164.8
ZAPT46	3.646	1.467 68	1165.4
ZAPT47	3.586	1.467 61	1166.0
ZAPT48	3.525	1.467 53	1166.6
ZAPT49	3.465	1.467 46	1167.2
FCI	b	1.466 31	1176.4

[a] Error with respect to E(FCI) at the FCI r_e value.
[b] E(FCI) = –75.264433 E_h

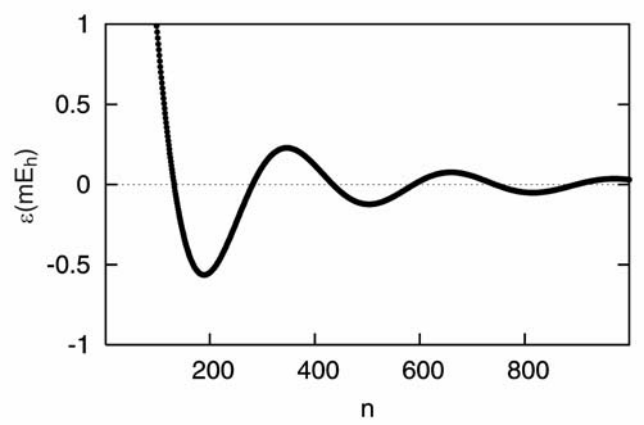

Figure 2.5 Errors in higher-order ZAPT*n* energies (ε, mE_h), relative to FCI, for b $^2\Delta_g$ C_2^+ with the cc-pVDZ basis and a frozen *1s* core.

ZAPT*n* energy, bond length, and harmonic vibrational frequency series for X $^2\Sigma^+$ CN are shown in Table 2.5 and Fig. 2.6, relative to FCI results. Neutral CN is derived from CN^+ by the population of the low-lying (5σ) LUMO, resulting in an electronic structure with the dominant determinant derived from the electron configuration $[\text{core}](3\sigma)^2(4\sigma)^2(5\sigma)^1(1\pi)^4$. In the FCI wave function, there is a significant ($C_0 = 0.894$; $C_1 = -0.198$) contribution from a second determinant arising from the excitation of an electron from (4σ) to (5σ). For low orders, the accuracy ordering is ZAPT6 > ZAPT4 > ZAPT5 > ZAPT2 > ZAPT3 for energies, ZAPT2 > ZAPT5 > ZAPT4 > ZAPT6 > ZAPT3 for r_e, and ZAPT5 > ZAPT3 > ZAPT2 > ZAPT4 > ZAPT6 for ω_e. Such erratic accuracy ordering with respect to order of the perturbation is not unique to CN, nor is it limited to ZAPT, but is instead a relatively common problem with Møller-Plesset perturbation theories. The result is that inclusion of higher-order perturbative corrections is not uniformly beneficial, with different properties exhibiting quite different behavior with respect to the order of the perturbation. As with CN^+, the ZAPT*n* series ultimately diverge for neutral CN, though at higher order than in the cation. Additionally, beyond 10$^{\text{th}}$ order, ZAPT*n* predicts an unbound potential for even orders *n*, and successively shorter bond lengths (and unphysical

frequencies) for odd *n*. Similar behavior was observed in the MP*n* results for CN^+.[18] This prediction of an unbound potential curve for cc-pVDZ CN will not be unique to ZAPT; the ROMP and RMP series are expected to exhibit qualitatively similar behavior.

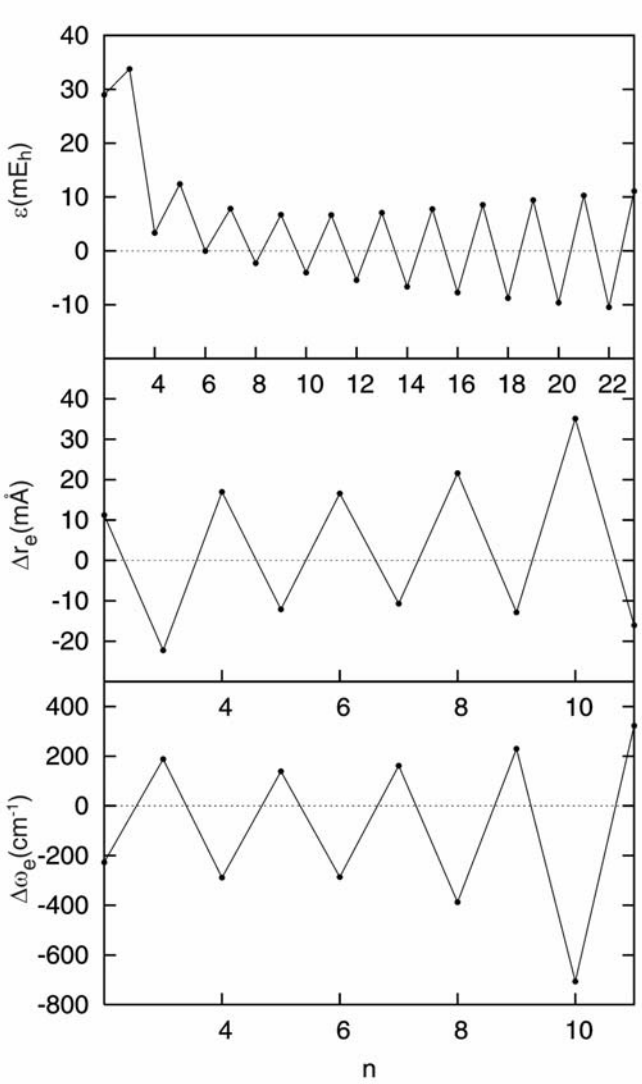

Figure 2.6 Errors in ZAPT*n* energies (ε, mE_h) and predicted equilibrium bond length (r_e, mÅ) and harmonic vibrational frequency (ω_e, cm^{-1}), relative to FCI, for X $^2\Sigma^+$ CN with the cc-pVDZ basis and a frozen *1s* core.

Table 2.5 ZAPT*n* energies (relative to FCI), equilibrium bond lengths, and harmonic vibrational frequencies for X $^2\Sigma^+$ CN.

	cc-pVDZ		
	$\varepsilon(mE_h)$[a]	r_e(Å)	$\omega_e(cm^{-1})$
ROHF	303.547	1.13897	2461.2
ZAPT2	28.977	1.20809	1793.5
ZAPT3	33.773	1.17463	2209.3
ZAPT4	3.319	1.21387	1732.6
ZAPT5	12.400	1.18478	2159.5
ZAPT6	–0.034	1.21346	1734.2
ZAPT7	7.839	1.18619	2182.3
ZAPT8	–2.290	1.21848	1633.8
ZAPT9	6.711	1.18400	2250.4
ZAPT10	–4.058	1.23200	1314.5
ZAPT11	6.663	1.18082	2343.6
ZAPT12	–5.465	c	c
ZAPT13	7.072	1.17762	2334.4
ZAPT14	–6.667	c	c
ZAPT15	7.750	1.17430	2550.6
ZAPT16	–7.763	c	c
ZAPT17	8.553	1.17142	2647.4
ZAPT18	–8.798	c	c
ZAPT19	9.419	1.16894	2741.1
ZAPT20	–9.774	c	c
ZAPT21	10.287	1.16686	2828.8
ZAPT22	–10.672	c	c
ZAPT23	11.095	1.16517	2908.0
FCI	b	1.19687	2020.9

[a] Error with respect to E(FCI) at the FCI r_e value.
[b] E(FCI) = –92.494449 E_h
[c] X $^2\Sigma^+$ CN is unbound at these levels of theory.

2.5.3 Comparison of Low-Order Results

To assess the performance of ZAPT at low order (ZAPT2, ZAPT4) in chemical applications, we present predicted r_e and ω_e values for NO, CN, and O_2 alongside ROMP and RMP results[10] and experimental values[39] in Table 2.6, computed using a TZ2P basis set. ZAPT2 and ZAPT4 are seen to provide results very similar to RMP and ROMP theory, though at reduced computational cost. This is particularly true for NO and CN, for which ZAPT predicted bond lengths are within 0.003 Å and frequencies within 40 cm^{-1} of the RMP and ROMP results at a given order. In each case, the ZAPT result is closer to the experimental value than the corresponding RMP and ROMP results, though clearly the ordering is of little significance given

the small differences among the results. For $^3\Sigma_g^-$ O_2, on the other hand, ZAPT2 and ZAPT4 predictions are noticeably closer to experiment than ROMP and RMP (though of course even 4th order perturbation theory is far from sufficient for this system): ZAPT2 offers an improvement of 0.014 Å and 112 cm^{-1} over the RMP2 bond length and frequency, respectively, while ZAPT4 bests RMP4 by 0.013 Å and 66 cm^{-1}. That the three perturbation theories exhibit larger differences for this system with two unpaired electrons is not entirely unexpected, since differences among the theories involve primarily the treatment of the singly occupied orbital subspace. The begging question, naturally, is whether the improvement offered by ZAPT over RMP and ROMP theories for O_2 is systematic or not.

Table 2.6 Second- and fourth-order ROMP, RMP, and ZAPT predicted equilibrium bond lengths (r_e) and harmonic vibrational frequencies (ω_e).[a]

	X $^2\Pi$ NO		X $^2\Sigma^+$ CN		X $^3\Sigma_g^-$ O_2	
	r_e(Å)	ω_e(cm^{-1})	r_e(Å)	ω_e(cm^{-1})	r_e(Å)	ω_e(cm^{-1})
ROMP2	1.160	1907	1.189	1834	1.265	1190
RMP2	1.162	1893	1.190	1818	1.260	1213
ZAPT2	1.160	1907	1.187	1856	1.246	1325
ROMP4	1.176	1707	1.197	1734	1.253	1239
RMP4	1.174	1718	1.197	1744	1.246	1294
ZAPT4	1.173	1730	1.195	1772	1.239	1360
Expt.[b]	1.151	1904	1.172	2069	1.208	1580

[a] ROMP and RMP results are from Ref. 10.
[b] Experimental values are from Ref. 39.

2.6 Summary and Conclusions

We have presented high-order ZAPT*n* energy series for a set of test systems to gauge the convergence relative to ROMP, RMP, OPT2, OPT1, and UMP theories. For the systems considered (6-31G NH_2 at r_e, 1.5 r_e, and 2 r_e and STO-3G CN), the ZAPT*n* energy series closely parallel published RMP and ROMP results.[10] These RMP and ROMP energies are generally

more robust (with respect to smooth convergence to the FCI limit) than those from OPT1, OPT2, and UMP theories.

We have also presented ZAPT*n* predicted energies, harmonic vibrational frequencies, and equilibrium bond lengths for X $^4\Sigma_g^+$ C_2^+, b $^2\Delta_g$ C_2^+, and X $^2\Sigma^+$ CN with the cc-pVDZ basis set. The energy and spectroscopic constant series for $^4\Sigma_g^+$ C_2^+ exhibit rapid convergence to the FCI limit, following slight oscillations at low order. In the case of $^2\Delta_g$ C_2^+, which requires two determinants for a proper zeroth order description, the ZAPT*n* energy series (tracked out to ZAPT999) exhibits spectacularly slow, oscillatory convergence to the FCI limit, remaining 0.5 mE_h from convergence even at 200th order. The ZAPT*n* series for $^2\Sigma^+$ CN are qualitatively similar to the corresponding MP*n* series for the closed shell CN^+, exhibiting highly oscillatory and ultimately divergent behavior. Indeed, for even orders past ZAPT10, $^2\Sigma^+$ CN is predicted to be unbound.

Explicit ZAPT2 and ZAPT4 energy computations were used to determine equilibrium geometries and harmonic vibrational frequencies for NO, CN, and O_2 using a TZ2P basis set, yielding results in very close agreement with second and fourth order ROMP and RMP results[10] for NO and CN. ZAPT offers significant improvement over ROMP and RMP theories in the prediction of experimental r_e and ω_e values in the case of $^3\Sigma_g^-$ O_2.

The efficient, parallel implementations[40] of ZAPT2 energies in MPQC[41] and GAMESS[42] open the door to the computation of ZAPT energies for large open-shell systems. Furthermore, the formulation[43] and recent parallel implementation of ZAPT2 analytic gradients by Aikens and co-workers[44] will permit the efficient optimization of geometries and harmonic vibrational frequencies, putting ZAPT2 on similar ground as RMP theory regarding utility in routine applications. The present work on the convergence of ZAPT*n* energies and spectroscopic

constants underscores previous findings[1,2,10,12,14,20] concerning the poor convergence of Møller-Plesset perturbation theory built on a spin-contaminated UHF wave function. Regardless, many popular composite *ab initio* methods (*e.g.*: G2, G3, etc.)[45] rely primarily on low-order UMP theory for energies and geometries for open-shell systems, with little regard for the deleterious effects of spin-contamination. ZAPT2 and ZAPT4 offer a more reliable and computationally efficient means of including electron correlation when predicting energies, geometries, and frequencies compared to UMP and RMP theories. Given the similarity of convergence properties and predicted spectroscopic properties of ZAPT to the oft-applied ROMP and RMP theories, coupled with the computational advantages of a method that requires only a single set of spatial orbitals, we recommend the use of low-order ZAPT in routine applications to open-shell systems.

2.7 Acknowledgements

This research was supported by the U. S. Department of Energy, Office of Basic Energy Sciences, Combustion Program (Grant No. DE-FG02-00ER14748). One author (S.E.W.) was also supported by a University of Georgia Presidential Fellowship, and would like to thank T. J. Lee and T. D. Crawford for illuminating comments and time-saving suggestions, respectively.

References

1 R. D. Amos, J. S. Andrews, and N. C. Handy, Chem. Phys. Lett. **185** (3,4), 256 (1991).

2 P. J. Knowles, J. S. Andrews, R. D. Amos, N. C. Handy, and J. A. Pople, Chem. Phys. Lett. **186**, 130 (1991).

3 W. J. Lauderdale, J. F. Stanton, J. Gauss, J. D. Watts, and R. J. Bartlett, Chem. Phys. Lett. **187**, 21 (1991).

4 C. Murray and E. R. Davidson, Chem. Phys. Lett. **187**, 451 (1991).

[5] T. J. Lee and D. Jayatilaka, Chem. Phys. Lett. **201**, 1 (1993).

[6] P. M. Kozlowski and E. R. Davidson, Chem. Phys. Lett. **226**, 440 (1994).

[7] C. Møller and M. S. Plesset, Phys. Rev. **46**, 618 (1934).

[8] Hubac and Carsky had previously presented a ROHF-based open-shell perturbation theory, though this generally yielded unsatisfactory results. See Ref. XXX

[9] C. W. Murray and E. R. Davidson, Int. J. Quant. Chem. **43**, 755 (1992).

[10] C. W. Murray and N. C. Handy, J. Chem. Phys. **97** (9), 6509 (1992).

[11] W. D. Laidig, G. Fitzgerald, and R. J. Bartlett, Chem. Phys. Lett. **113**, 151 (1985).

[12] P. J. Knowles, K. Somasundram, N. C. Handy, and K. Hirao, Chem. Phys. Lett. **113**, 8 (1985).

[13] N. C. Handy, P. J. Knowles, and K. Somasundram, Theor. Chim. Acta **68**, 87 (1985).

[14] P. M. W. Gill and L. Radom, Chem. Phys. Lett. **132**, 16 (1986).

[15] This absence is not surprising, since the ZAPT formalism was introduced the year following the aforementioned convergence studies.

[16] A. Halkier, H. Larsen, J. Olsen, and P. Jørgensen, J. Chem. Phys. **110**, 7127 (1999).

[17] H. Larsen, A. Halkier, J. Olsen, and P. Jørgensen, J. Chem. Phys. **112**, 1107 (2000).

[18] M. L. Leininger, W. D. Allen, and H. F. Schaefer, J. Chem. Phys. **112**, 9213 (2000).

[19] R. Krishnan, M. J. Frisch, and J. A. Pople, J. Chem. Phys. **72**, 4244 (1980).

[20] R. H. Nobes, J. A. Pople, L. Radom, N. C. Handy, and P. J. Knowles, Chem. Phys. Lett. **138**, 481 (1987); P. M. W. Gill, J. A. Pople, L. Radom, and R. H. Nobes, J. Chem. Phys. **89**, 7307 (1988).

[21] J. Olsen, O. Christiansen, H. Koch, and P. Jørgensen, J. Chem. Phys. **105**, 5082 (1996).

[22] D. Cremer and Z. He, J. Phys. Chem. **100**, 6173 (1996); O. Christiansen, J. Olsen, P. Jørgensen, H. Koch, and P.-A. Malmqvist, Chem. Phys. Lett. **261**, 369 (1996); B. Forsberg, Z. He, Y. He, and D. Cremer, Int. J. Quant. Chem. **76**, 306 (2000); F. H. Stillinger, J. Chem. Phys. **112**, 9711 (2000); D. Z. Goodson and A. V. Sergeev, Adv. Quantum Chem. **47**, 193 (2004); A. V. Sergeev, D. Z. Goodson, S. E. Wheeler, and W. D. Allen, J. Chem. Phys. **123** (6), 064105 (2005).

[23] T. J. Lee, A. P. Rendell, K. G. Dyall, and D. Jayatilaka, J. Chem. Phys. **100** (10), 7400 (1994).

[24] T. D. Crawford, H. F. Schaefer, and T. J. Lee, J. Chem. Phys. **105** (3), 1060 (1996).

[25] The ZAPTn energy is invariant to all orbital rotations within the doubly occupied and doubly unoccupied spaces. In the unusual situation that there are multiple singly occupied orbitals that transform as the same irreducible representation of the molecular point group, rotations among singly occupied orbitals are possible and will affect the energy.

[26] C. D. Sherrill and H. F. Schaefer, in *Advances in Quantum Chemistry*, edited by P.-O. Löwdin (Academic, New York, 1999), Vol. 34, pp. 143.

[27] D. Jayatilaka and T. J. Lee, Chem. Phys. Lett. **199** (3,4), 211 (1992).

[28] A. Dalgarno and A. L. Stewart, Proc. R. Soc. London, Ser. A **238**, 269 (1956); P.-O. Löwdin, J. Math. Phys. **6**, 1341 (1965).

[29] T. D. Crawford, C. D. Sherrill, E. F. Valeev, J. T. Fermann, R. A. King, M. L. Leininger, S. T. Brown, C. L. Janssen, E. T. Seidl, J. P. Kenny, and W. D. Allen, Psi 3.2 (2003).

[30] D. J. Tozer, N. C. Handy, R. D. Amos, J. A. Pople, R. H. Nobes, Y. Xie, and H. F. Schaefer, Mol. Phys. **79** (4), 777 (1993).

[31] Results for all series presented are available in full precision (14 decimal places) by request from the authors.

[32] W. J. Hehre, R. Ditchfield, and J. A. Pople, J. Chem. Phys. **56**, 2257 (1972).

[33] W. J. Hehre, R. F. Stewart, and J. A. Pople, J. Chem. Phys. **51**, 2657 (1969).

[34] T. H. Dunning, J. Chem. Phys. **90**, 1007 (1989).

[35] T. H. Dunning, J. Chem. Phys. **55**, 716 (1971).

[36] S. J. Huzinaga, J. Chem. Phys. **42**, 1293 (1965).

[37] MATHEMATICA 5.1 (Wolfram Research, Inc., Champaign, IL, 2003).

[38] M. L. Leininger, C. D. Sherrill, W. D. Allen, and H. F. Schaefer, J. Chem. Phys. **108**, 6717 (1998).

[39] K. P. Huber and G. Herzberg, *Molecular Spectra and Molecular Structure IV: Constants of Diatomic Molecules*. (Van Nostrand Reinhold, New York, 1979).

[40] I. M. B. Nielsen and E. T. Seidl, J. Comp. Chem. **16**, 1301 (1995).

[41] C. L. Janssen, I. B. Nielson, M. L. Leininger, E. T. Seidl, and M. E. Colvin, MPQC 2.1.4 (Sandia National Laboratories, Livermore, California, 2002).

[42] M. W. Schmidt, K. K. Baldridge, J. A. Boatz, S. T. Elbert, M. S. Gordon, J. H. Jensen, S. Koseki, N. NMatsunaga, K. A. Nguyen, S. J. Su, T. L. Windus, M. Dupuis, and J. A. Montgomery, J. Comp. Chem. **14**, 1347 (1993); M. S. Gordon and M. W. Schmidt, in *Theory and Applications of Computational Chemistry*, edited by C. E. Dykstra, G. Frenking, K. S. Kim, and G. E. Scuseria (Elsevier, Amsterdam, 2005).

[43] G. D. Fletcher, M. S. Gordon, and R. S. Bell, Theor. Chem. Acc. **107**, 57 (2002).

[44] C. M. Aikens, G. D. Fletcher, M. W. Schmidt, and M. S. Gordon, J. Chem. Phys. **124**, 014107 (2006).

[45] L. A. Curtiss, K. Raghavachari, G. W. Trucks, and J. A. Pople, J. Chem. Phys. **94**, 7221 (1991); L. A. Curtiss, K. Raghavachari, P. C. Redfern, V. Rassolov, and J. A. Pople, J. Chem. Phys. **109**, 7764 (1998).

CHAPTER 3

THERMOCHEMISTRY OF DISPUTED SOOT FORMATION INTERMEDAITES

C_4H_3 AND C_4H_5[1]

[1] S. E. Wheeler, W. D. Allen, and H. F. Schaefer, J. Chem. Phys. **121**, 8800 (2004). Reprinted here with permission of the American Institute of Physics.

3.1 ABSTRACT

Accurate isomeric energy differences and standard enthalpies of formation for disputed intermediates in soot formation, C_4H_3 and C_4H_5, have been determined through systematic extrapolations of *ab initio* energies. Electron correlation has been included through second-order Z-averaged perturbation theory (ZAPT2), and spin-restricted, open-shell coupled cluster methods through triple excitations [ROCCSD, ROCCSD(T), and ROCCSDT] utilizing the correlation-consistent hierarchy of basis sets, cc-pV*X*Z (*X* = D, T, Q, 5, and 6), followed by extrapolations to the complete basis set limit via the focal point method of Allen and co-workers. Reference geometries were fully optimized at the ROCCSD(T) level with a TZ(2d1f,2p1d) basis set. Our analysis finds that the resonance-stabilized *i*-C_4H_3 and *i*-C_4H_5 isomers lie 11.8 and 10.7 kcal mol^{-1} below *E*-*n*-C_4H_3 and *E*-*n*-C_4H_5, respectively, several kcal mol^{-1} (more, less) than reported in recent (diffusion Monte Carlo, B3LYP density-functional) studies. Moreover, in these systems Gaussian-3 (G3) theory suffers from large spin contamination in electronic wavefunctions, poor reference geometries, and anomalous vibrational frequencies, but fortuitous cancellation of these sizable errors leads to isomerization energies apparently accurate to 1 kcal mol^{-1}. Using focal-point extrapolations for isodesmic reactions, we determine the enthalpies of formation ($\Delta_f H_0^\circ$) for *i*-C_4H_3, *Z*-*n*-C_4H_3, *E*-*n*-C_4H_3, *i*-C_4H_5, *Z*-*n*-C_4H_5, and *E*-*n*-C_4H_5 to be 119.0, 130.8, 130.8, 78.4, 89.7, and 89.1 kcal mol^{-1}, respectively. These definitive values remove any remaining uncertainty surrounding the thermochemistry of these isomers in combustion models, allowing for better assessment of whether even-carbon pathways contribute to soot formation.

3.2 INTRODUCTION

Unraveling the complex processes involved in the pyrolysis of aliphatic fuels and the formation of soot is imperative for the development of more efficient internal combustion

technologies and the reduction of harmful emissions. The elucidation of the mechanism and associated kinetics of the formation of soot, and more specifically polycyclic aromatic hydrocarbon (PAH) intermediates,[1-3] has been a primary focus of combustion research in recent years. Some PAHs have been shown to be mutagenic and carcinogenic,[4,5] elevating the need to minimize their emission into the environment. Vital to the understanding of PAH formation is the mechanism for formation of the first aromatic ring, commonly believed to be the rate-limiting step in the production of larger aromatics.[2,3]

There has been much debate regarding even-carbon-atom reactions[6-21] for assembling the first aromatic ring, with particular focus on the addition of acetylene to *n*-C_4H_3 and *n*-C_4H_5 radicals:

$$n\text{-}C_4H_3 + C_2H_2 \rightarrow \text{phenyl} \qquad (3.1)$$

$$n\text{-}C_4H_5 + C_2H_2 \rightarrow \text{benzene} + H \qquad (3.2)$$

In 1984, Cole, Bittner, Longwell, and Howard[10] concluded, based on rates of benzene production above a 1,3-butadiene flame, that the reaction of 1,3-butadienyl radical with acetylene followed by ring closure and hydrogen abstraction was the dominant pathway toward soot formation. In 1987, modeling studies of Frenklach and Warnatz[13] suggested that the reaction of acetylene and *n*-C_4H_3 was responsible for benzene formation at higher flame temperatures, while in 1989 Westmoreland *et al.*[17] supported the role of both *n*-C_4H_3 and *n*-C_4H_5 reactions with acetylene to account for aromatic formation in acetylene flames. In a combined experimental and modeling study in 1989, Bastin and co-workers[18] identified the reaction of C_2H_2 with C_4H_3 and C_4H_5 as the source of single-ring aromatics in acetylene flames. They did not, however, differentiate between *i*- and *n*-isomers of C_4H_3 and C_4H_5.

In 1992, Miller and Melius[22] re-examined the work of Bastin *et al.*,[18] this time distinguishing between isomers of C_4H_3 and C_4H_5, as depicted in Figs. 3.1 and 3.2. They dismissed the previously proposed even-carbon-atom pathways, arguing that neither *n*-C_4H_3 nor *n*-C_4H_5 would be present under typical flame conditions in sufficiently high concentrations due to rapid isomerization to the more stable *i*-C_4H_3 and *i*-C_4H_5 isomers, which form only weakly bound complexes with acetylene.[22,23] This conclusion resulted from BAC-MP4 computations that predicted much lower stabilities for the *n*-isomers, giving *n–i* energy differences of 12 kcal mol^{-1} for C_4H_5 and 19 kcal mol^{-1} for C_4H_3. It is notable that the combustion models of Miller and Melius predicted even-carbon-atom pathways to be inoperative even for much lower *n–i* energy separations, at least under the conditions of lightly sooting, low-pressure acetylene flames. Instead, the principal route to form C_6H_5 was the self-reaction of propargyl radicals, an odd-carbon-atom pathway.[24,25] In the last decade odd-carbon-atom pathways have continued to gain support, with numerous recent studies[26-41] supporting the role of propargyl radical recombination.

Recent experimental evidence of even-atom reactions contributing to formation of aromatics and soot[42-44] has spurred renewed interest in these potential routes. Additionally, reasonable pathways have been computed[19,45] for both *n*- and *i*-isomers of C_4H_3 reacting with acetylene to form benzene. Wang and Frenklach[20] have suggested that contributions from both even- and odd-carbon-atom paths are significant in different flame regions and that precise thermodynamic characterization of these species is necessary for a full description of these combustion processes. In a recent modeling study from 2002, Richter and Howard[3] examined a range of fuel mixtures and flame conditions, concluding that the propargyl self-reaction is the dominant pathway to benzene formation under typical flame conditions and that the reactions of

C_4H_3 and C_4H_5 play no significant role. However, Richter and Howard[3] were unable to definitively exclude these even-carbon-atom pathways, specifically citing remaining uncertainties in the thermodynamic properties of C_4H_3 and C_4H_5, particularly the relative energies of the *i*- and *n*-isomers.

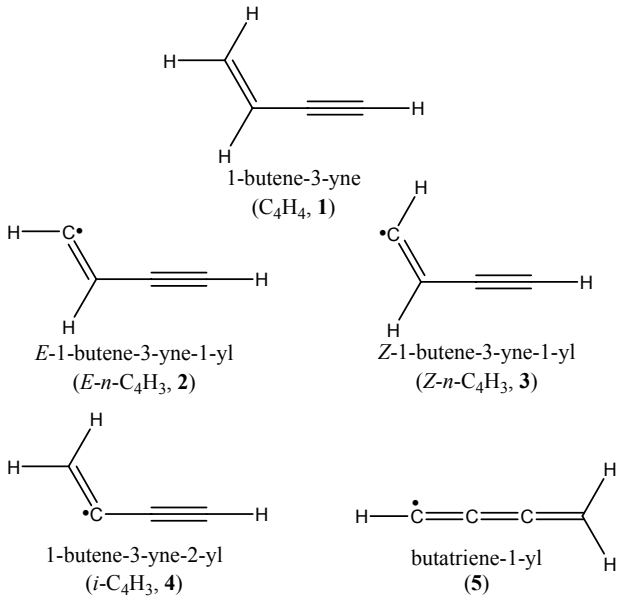

Figure 3.1 Canonical structures for C_4H_4 and isomers of C_4H_3.

While there have been numerous efforts[22,46-63] to characterize the isomers of C_4H_5 and C_4H_3, the relative stabilities and thermodynamics are still under dispute. Two isomers of *n*-C_4H_3, *E*-1-butene-3-yne-1-yl (*E*-*n*-C_4H_3, **2**) and *Z*-1-butene-3-yne-1-yl (*Z*-*n*-C_4H_3, **3**), and two isomers of *i*-C_4H_3, 1-butene-3-yne-2-yl (**4**) and butatriene-1-yl (**5**), are regularly considered, as are the corresponding isomers of *n*-C_4H_5, *E*-1,3-butadiene-1-yl (*E*-*n*-C_4H_5, **7**) and *Z*-1,3-butadiene-1-yl (*Z*-*n*-C_4H_5, **8**), and *i*-C_4H_5, 1,2-butadiene-4-yl (**9**) and 1,3-butadiene-2-yl (**10**). Canonical structures for these isomers are shown in Figs. 3.1 and 3.2.

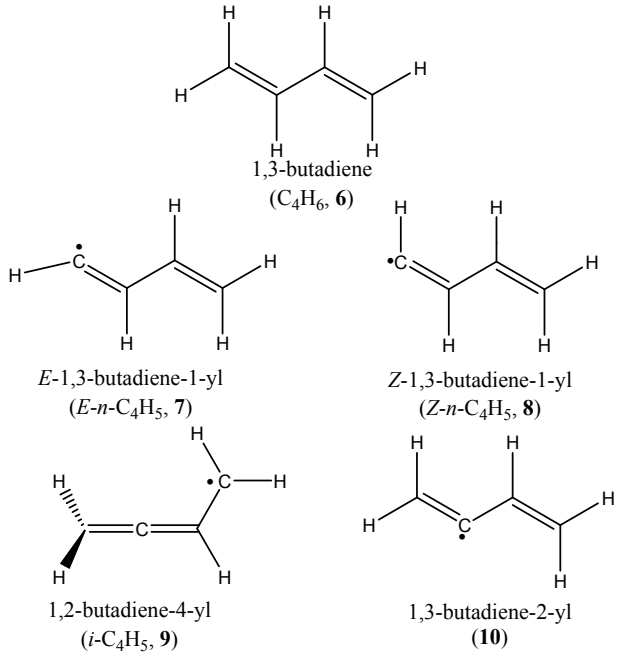

Figure 3.2 Canonical structures for C_4H_6 and isomers of C_4H_5.

All of these species have been shown to be minima in C_s symmetry, with the exception of structure **5**, which is a transition state of C_{2v} symmetry separating equivalent forms of **4**.[46,47,59,64] Parker and Cooksy[48,49] found structure **10** to be a first-order saddle point at the 6-311G(d,p) UHF, B3LYP, CISD, and QCISD levels of theory, but not at the 6-311G(d,p) UMP2, CASSCF(9,9), and MRCISD(7,7) levels, leaving a degree of uncertainty as to the nature of this species. In the literature, the precise relationship of structures **9** and **10** is somewhat muddled: as depicted in Fig. 3.2, structures **9** and **10** are distinct configurational isomers, with $^2A''$ and $^2A'$ ground states, respectively, rather than resonance forms representing a single electronic state at a fixed geometry. Parker and Cooksy[48] have shown the fully planar species **10** to be higher in energy than the twisted isomer **9** by roughly 10 kcal mol^{-1}. An alternative resonance form of **9** (Fig. 3.3) does exist that should not be confused with structure **10**. The two resonance forms of **9** depicted in Fig. 3.3 are at a fixed geometry and have the same ground electronic state ($^2A''$).

Since **10** is significantly destabilized relative to **9**, general discussion of isomeric energy differences between *n*- and *i*-C_4H_5 should involve the relative stabilities of structure **9** (equivalently represented by either resonance form) and either *E*- or *Z*-*n*-C_4H_5 (**7** or **8**). In this work, *i*-C_4H_5 will refer exclusively to 1,2-butadiene-4-yl (**9**), while *n*-C_4H_5 will signify either *E*- or *Z*-1,3-butadiene-1-yl (**7** or **8**), which are roughly isoenergetic. Similarly, *i*-C_4H_3 will denote 1-butene-3-yne-2-yl (**4**) alone, because butatriene-1-yl (**5**) is merely a transition state for interconversion of equivalent forms of **4**,[46,47,59,64] whereas *n*-C_4H_3 will refer to either **2** or **3**.

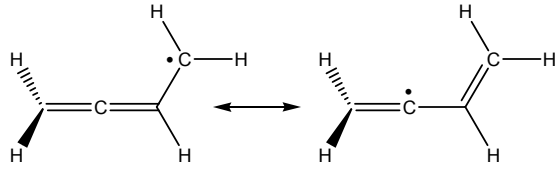

Figure 3.3 Resonance forms of *i*-C_4H_5 (**9**).

The work of Parker and Cooksy[48,49] included geometry optimizations of isomers of *n*-C_4H_5 and *i*-C_4H_5 using the 6-311G(d,p) QCISD method, giving the most reliable structures heretofore available in the literature for these species. Recent computations by Kaiser and co-workers[46,50] included an optimization at the 6-311G(d,p) CCSD(T) (coupled-cluster singles and doubles with perturbative triples) level for *i*-C_4H_3; however, the best previous systematic series of optimizations for all C_4H_3 isomers of concern were performed by Krokidis *et al.*[51] at the cc-pVQZ B3LYP level, although the actual optimized geometrical parameters were not reported in their article.

Despite a flurry of recent theoretical work on the relative energies of C_4H_5 and C_4H_3, there still remains a striking lack of consensus for these quantities, as is clear from Tables 3.1 and 3.2, including some discrepancies between papers employing the same methods. Previously

reported energies for *n*-C_4H_3, relative to *i*-C_4H_3, span over 10 kcal mol^{-1} with the majority of traditional wavefunction-based results falling within 11 ± 1 kcal mol^{-1}. There is somewhat less variation in reported energy separations for isomers of C_4H_5; the span is 7 kcal mol^{-1}, with traditional, non-DFT methods yielding results between 8 and 12 kcal mol^{-1}.

Table 3.1 Representative computed isomeric energy differences (ΔE_0, kcal mol^{-1}) for *n*-C_4H_3, relative to *i*-C_4H_3.

Z-*n*-C_4H_3	*E*-*n*-C_4H_3	Method	Reference
18.7	–	BAC-MP4	22
17 ± 1	17 ± 1	B3LYP (various basis sets)	50,51
–	6.8	DMC	51
10.39	10.38	6-31G(d) QCISD(T)[a]	51
10.76	11.84	6-31G(d) CASPT2[b]	51
10.76	10.36	ANO CASPT2[b]	51
11.19	10.88	G3(298 K)	51
10.9	10.8	G2M(RCC,MP2)	46,53
11.6	11.9	G2M(RCC,MP2)	50
11.0	11.0	6-311++G(d,p) CCSD(T)[c]	52
11.12	11.08	G3(0 K)	d
10.64	10.56	G3(0 K) at TZ(2d1f,2p1d) ROCCSD(T) geometries[e]	d
11.86	11.80	focal point extrapolation	d

[a] QCISD(T) energy computed at a QCISD geometry.
[b] CASPT2 energy computed at a CASSCF geometry.
[c] CCSD(T) energy evaluated at 6-311++G(d,p) B3LYP geometry, with scaled B3LYP ZPVE correction.
[d] This work.
[e] With cc-pVDZ ROCCSD(T) ZPVE correction.

Krokidis *et al.*[51] utilized cc-pVQZ B3LYP geometries in diffusion Monte Carlo (DMC) energy computations and obtained an energy difference[65] of 6.6 ± 1.2 kcal mol^{-1} for the isomers of C_4H_3 and 7.2 ± 1.2 kcal mol^{-1} for those of C_4H_5, in stark contrast to the BAC-MP4 results of Miller and Melius[22] (12 and 19 kcal mol^{-1}, respectively) and the majority of previous *ab initio* and DFT separations presented in Tables 3.1 and 3.2. The G3 method,[66] which is based on all-electron 6-31G(d) unrestricted MP2 geometries, yields a relative energy of 10.88 kcal mol^{-1} for *E*-*n*-C_4H_3 vs. *i*-C_4H_3, while that for the C_4H_5 isomers is 11.50 kcal mol^{-1}. Greater

disagreement is found between the DMC isomeric energy differences of Krokidis *et al.* and computed DFT values,[48-51,54-56] which fall in the range of 17 ± 1 kcal mol^{-1} and 14 ± 1 kcal mol^{-1} for *n*-C_4H_3 and *n*-C_4H_5, respectively, for a series of basis sets with the B3LYP functional.

Table 3.2 Representative computed isomeric energy differences (kcal mol^{-1}) for *n*-C_4H_5, relative to *i*-C_4H_5.[a]

Z-*n*-C_4H_5	*E*-*n*-C_4H_5	Method	Reference
–	12.4	BAC-MP4	22
14 ± 1	14 ± 1	B3LYP (various basis sets)	48,49,51,54-56
–	7.4	DMC	51
11.55	11.06	6-31G(d) QCISD(T)[b]	51
11.7	11.1	6-311G(d,p) QCISD	48,49
10.3	9.8	6-311G(d,p) CCSD(T)[c]	48,49
8.6	8.3	6-311G(d,p) CASSCF(9,9)[c,d]	48,49
–	9.1	6-311G(d,p) MRCISD(7,7)[e]	48,49
12.06	11.50	G3(298 K)	51
11.2	–	G2M(MP2)	55
–	11.04	G2M(RCC,MP2)	56
–	11.25	G2-like	54
–	10.3[e]	6-311G(d,p) CCSD(T)[f]	56
12.08	11.51	G3(0 K)	g
12.54	11.90	G3(0 K) at TZ(2d1f,2p1d) ROCCSD(T) geometries[h]	g
11.31	10.69	focal point extrapolation	g

[a] Zero-point corrected, unless otherwise noted.
[b] QCISD(T) energy computed at a QCISD geometry.
[c] Not ZPVE corrected.
[d] ZPVE corrected value for *E*-*n*-C_4H_5 was 8.9 kcal mol^{-1} using CASSCF(9,9).
[e] ZPVE correction computed at the CASSCF(7,7) level.
[f] CCSD(T) energies evaluated at B3LYP geometries. No ZPVE correction.
[g] This work.
[h] With cc-pVDZ ROCCSD(T) ZPVE correction.

The DMC results of Krokidis *et al.* are a clarion for further investigation, due to their striking discrepancy with other model chemistries, and also their relevance to proposed mechanisms of incipient soot formation. We have undertaken an aggressive computational characterization of C_4H_3 and C_4H_5 isomers, utilizing large triple-ζ quality basis sets and coupled cluster methods to obtain high-quality optimized geometries, and then executing focal point analyses to pinpoint the complete basis set (CBS) limits for the isomeric energy differences and

enthalpies of formation. The results are reliable, *ab initio* energy separations and enthalpies of formation lacking the uncertainty inherent in the DFT computations that have been predominant in the combustion literature.

3.3 THEORETICAL METHODS

Precise standard enthalpies of formation and relative energies have been computed via the focal-point extrapolation scheme of Allen and co-workers.[67-72] Geometries were optimized using coupled cluster singles and doubles theory (CCSD)[73-76] appended with perturbative inclusion of connected triple excitations [CCSD(T)],[77-80] freezing the carbon 1*s* orbitals. Semicanonical orbitals were utilized in all CCSD(T) computations.[81] Our reference electronic wave functions were determined by single-configuration spin-restricted open-shell Hartree-Fock theory (ROHF), eschewing the possibility of spurious energetic predictions resulting from a spin-contaminated reference. The geometry optimizations utilized a TZ(2d1f,2p1d) basis,[82] consisting of the Dunning C(10s6p/5s3p) and unscaled H(5s/3s) triple-ζ segmented *sp* contractions[83] augmented with correlation optimized[84] polarization functions [α_d(C) = 0.318, 1.097; α_f(C) = 0.761; α_p(H) = 0.388, 1.407; α_d(H) = 1.057]. All polarization manifolds contained only pure spherical harmonics. The geometry optimizations were carried out via finite differences of energy points utilizing a local version of the ACESII program package.[85]

In the focal point scheme, the correlation-consistent basis sets of Dunning[84] are utilized to achieve systematic dual one- and *n*-particle extrapolations to the complete basis set limit. Electron correlation is treated through second-order perturbation theory, and primarily by coupled cluster theory including single and double excitations (CCSD)[73-76] and either perturbative [CCSD(T)][77-80] or full treatments (CCSDT)[86-89] of triple excitations. Preliminary exploratory computations indicated extensive spin contamination for the open-shell species when

utilizing unrestricted MP2 theory (UMP2). The expectation values of S^2 exceeded 1.4 in some cases, as opposed to 0.75 for a pure doublet, indicating the deficiencies of an unrestricted Hartree-Fock (UHF) reference for these species. As such, the first component of the energy for the focal point procedure was obtained using spin restricted Hartree-Fock theory. Likewise, spin restricted analogs[76,81] of CCSD, CCSD(T), and CCSDT were employed, denoted by ROCCSD, ROCCSD(T), and ROCCSDT, respectively. Core-valence correlation contributions were evaluated through a second set of focal point extrapolations, available as supplementary material,[90] utilizing the cc-pCV*X*Z basis sets.[91] All energies for the focal point analyses were computed at the TZ(2d1f,2p1d) ROCCSD(T) optimized geometries described above. We report open-shell T_1-diagnostics[92] and maximum T_1 and T_2 amplitudes for the *i*- and *n*-isomers of C_4H_3 and C_4H_5 in supplementary Table A1. While the T_1-diagnostics are higher for the resonance-stabilized *i*-isomers than for the *n*-isomers, all are below 0.025, justifying the use of single-reference methods for all isomers considered.

For spin-restricted open-shell perturbation theory there exist several viable partitionings of the electronic Hamiltonian, resulting in a number of unique formulations in the literature. For the leading contribution to the correlation energy we employed the ROHF-MBPT theory of Lauderdale *et al.*[93] [which is equivalent to the restricted Møller-Plesset theory (RMP) of Knowles *et al.*[94]], the open-shell perturbation theory method 2 (OPT2) of Murray and Davidson,[95] or the Z-averaged perturbation theory (ZAPT) of Lee and Jayatilaka,[96] none of which exhibits effects due to spin contamination in the second-order energy. The parallel, direct implementation of the latter two methods in the Massively Parallel Quantum Chemistry package (MPQC)[97] allowed explicit computation of energies utilizing the cc-pV5Z basis set for all open-shell species, while the disk-based implementation of ROHF-MBPT in ACESII allowed

computations up to the cc-pVQZ basis. Given the ability to compute energies up to the cc-pV5Z basis, coupled with an expected accelerated convergence with respect to perturbation order for ZAPT, we have elected to present focal point analyses utilizing only ZAPT2 for the leading correlation contribution. In notable cases the results obtained using OPT2 and ROHF-MBPT are also reported.

All correlated energy computations involved the freezing of the carbon 1*s* orbitals, except where noted otherwise for the explicit evaluation of the core correlation contribution. The functional form for the basis set extrapolation of the Hartree-Fock energies was that of Feller,[98]

$$E_{HF} = a + be^{-cX}, \tag{3.3}$$

while the correlation energies were extrapolated via[99]

$$E_{corr} = a + bX^{-3}. \tag{3.4}$$

The focal point scheme was utilized to evaluate isomeric energy differences between *i*-C_4H_n and *E*- and *Z*-*n*-C_4H_n, defined by the following reaction:

$$i\text{-}C_4H_n \rightarrow n\text{-}C_4H_n \tag{3.5}$$

Standard enthalpies of formation for the C_4H_3 and C_4H_5 isomers were determined through the following isodesmic[100] reactions:

$$i\text{-}C_4H_3 + CH_4 \rightarrow C_4H_4 + CH_3 \tag{3.6}$$

and

$$i\text{-}C_4H_5 + CH_4 \rightarrow C_4H_6 + CH_3. \tag{3.7}$$

The necessary enthalpies of formation for C_4H_4 and C_4H_6 at 0 K were accurately determined here via additional isodesmic transformations:

$$C_4H_4 + C_2H_6 \rightarrow CH_3CCH + CH_3CHCH_2 \tag{3.8}$$

and

$$C_4H_6 + C_2H_6 \rightarrow CH_3CHCH_2 + CH_3CHCH_2. \quad (3.9)$$

Experimental enthalpies of formation were adopted for CH_3, CH_4, ethane, propene, and propyne, as given in Table 3.3. An experimental r_e bond length was employed for CH_4 (1.085 Å),[101] while an equilibrium bond length of 1.0763 Å, obtained at the all-electron cc-pCVQZ ROCCSD(T) level of theory, was utilized for CH_3. Optimizations were carried out for C_4H_4, C_4H_6, ethane, propene, and propyne at the frozen-core TZ(2d1f,2p1d) ROCCSD(T) level of theory, as before.

Table 3.3 Standard enthalpies of formation ($\Delta_f H_0^\circ$, kcal mol^{-1}) for relevant species.

Species	$\Delta_f H_0^\circ$	Uncertainty	Reference
H(^2S)	51.634	0.002	129,130
C($^3P_0$)	169.98	0.11	129,130
CH_3	35.62	0.19	129
CH_4	–15.99	0.08	129
C_2H_6	–16.34	0.10	131
C_3H_6 (propene)	8.29	0.26	132
C_3H_4 (propyne)	45.79	0.21	132
C_4H_4 (1-butene-3-yne)	70.54	–	a
C_4H_6 (1,3-butadiene)	29.98	–	a

[a] Focal-point extrapolated value, this work.

Extrapolated energies were further corrected via inclusion of the diagonal Born-Oppenheimer correction (DBOC),[102-105] the first-order correction to the energy of the Born-Oppenheimer approximation, and the one-electron mass-velocity and Darwin scalar relativistic terms.[106-110] The DBOC was evaluated at the cc-pVTZ ROHF level of theory using PSI3,[111] while the relativistic effects were computed at the cc-pCVTZ ROCCSD(T) level using ACES II.[85] Harmonic vibrational frequencies were evaluated at the cc-pVDZ ROCCSD(T) level of theory by finite differences of gradients,[81,112] with frequencies and IR intensities

provided as supplementary material.[90] These unscaled frequencies were utilized to compute zero-point vibrational energy (ZPVE) corrections.

All coupled cluster computations were carried out using a local version of ACES II,[85] while the ZAPT2 energies were evaluated using MPQC 2.1.[97] The ROHF energies evaluated with the cc-pV6Z basis were carried out using PSI3[111] or MPQC. For comparison, isomeric energy differences and enthalpies of formation were computed using the G3 model chemistry[66] for the species in Eqs. (3.5)-(3.9). The G3(0 K) energies (with 'tight' geometry convergence criteria) were computed using Gaussian 98[113] at the National Energy Research Scientific Computing Center (NERSC) at Lawrence Berkeley National Laboratory.

3.4 Geometric Structures

Optimized structures for all species considered here are given in Figs. 3.4-3.8. Geometries for *E*- and *Z*-*n*-C_4H_3 (**2** and **3**), *i*-C_4H_3 (**4**), *E*- and *Z*-*n*-C_4H_5 (**7** and **8**), and *i*-C_4H_5 (**9**) have been fully optimized at the frozen-core TZ(2d1f,2p1d) ROCCSD(T) level of theory, with optimized parameters given in Figs. 3.4 and 3.5. Structures **2**, **3**, **4**, **7**, **8**, and **9** are all minima of C_s symmetry, as confirmed by computed vibrational frequencies. Geometry optimization followed by the evaluation of harmonic vibrational frequencies at the cc-pVDZ ROCCSD(T) level of theory confirmed earlier assertions[46,47,53,59,64] that the C_{2v}-symmetry butatriene-1-yl (**5**) is indeed a first-order saddle point. A valence focal point extrapolation (supplementary Table A2) including core-correlation corrections, performed at the frozen-core TZ(2d1f,2p1d) ROCCSD(T) structures, yields an energy of 0.17 kcal mol^{-1} for structure **5** relative to **4**, representing a miniscule barrier to interconversion of equivalent forms of **4**.

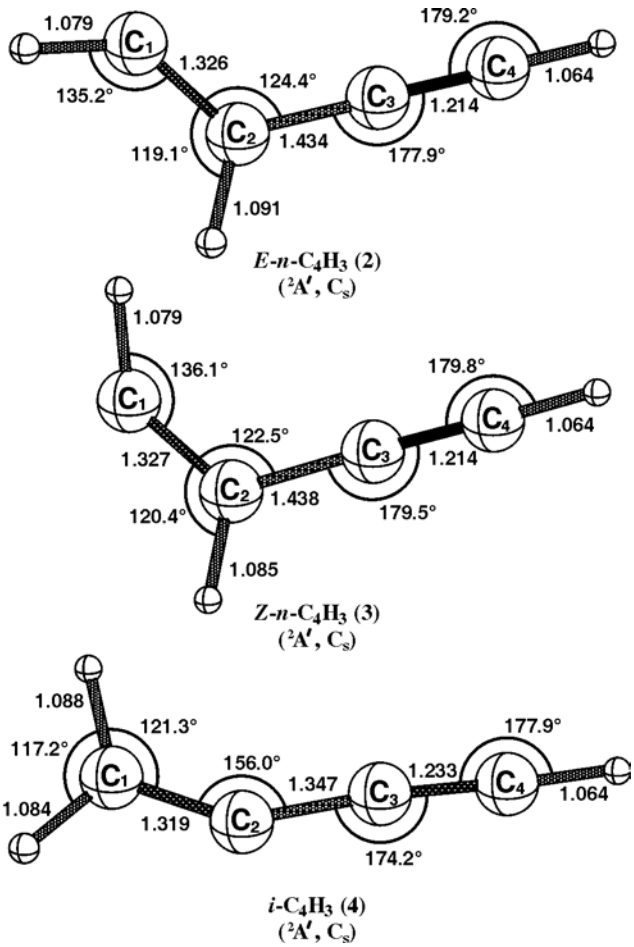

Figure 3.4 Optimized geometries for isomers of C_4H_3, computed at the frozen-core TZ(2d1f,2p1d) ROCCSD(T) level of theory.

Density functional theory, utilizing the B3LYP functional, identifies structure **5** as a minimum, not a transition state. In fact, there is no stationary point corresponding to **4** using B3LYP with a series of basis sets.[51,53] Since **4** and **5** are nearly isoenergetic, energies computed at this erroneous DFT minimum for *i*-C_4H_3 are expected to result in only a slight decrease in the energy separation between *i*-C_4H_3 and *n*-C_4H_3.

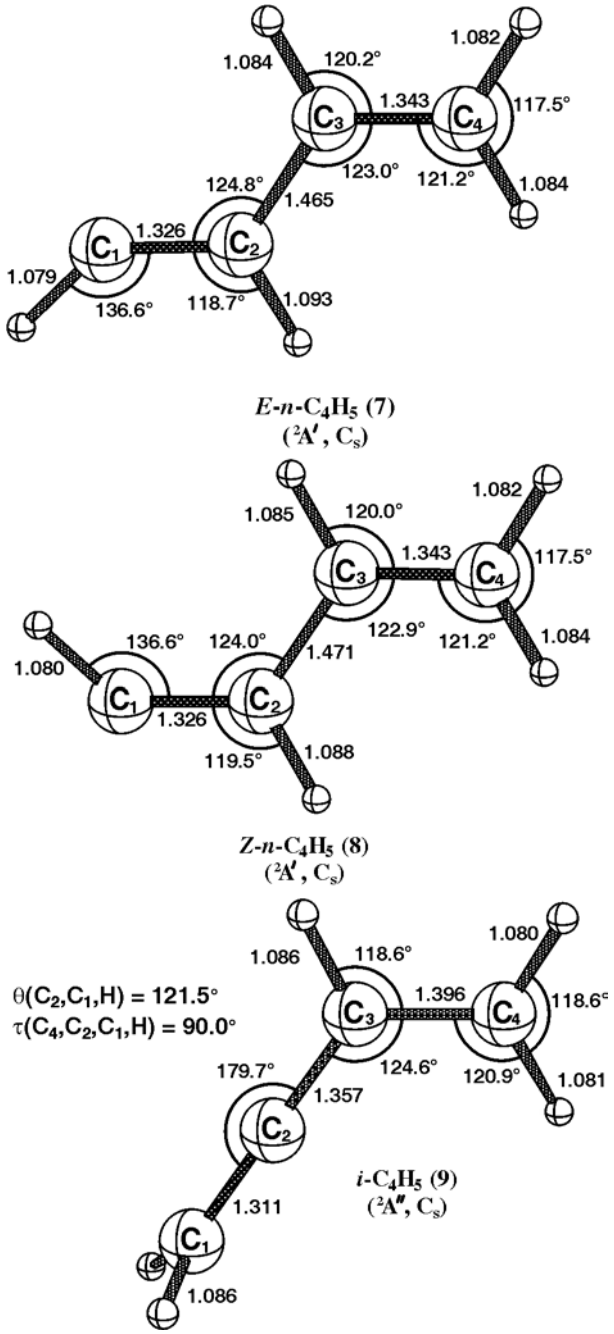

Figure 3.5 Optimized geometries for isomers of C_4H_5, computed at the frozen-core TZ(2d1f,2p1d) ROCCSD(T) level of theory.

Geometries for both forms of *n*-C_4H_3 exhibited only modest dependence on method, with our results agreeing with published DFT optimized bond lengths to within 0.02 Å. Angles differed by less than 1.5˚, with the largest deviation occurring for the C_1–C_2–C_3 bond angle.

This should be contrasted to the sensitivity to method in the case of *i*-C_4H_3, which exhibited variations of over 5° for the C_1–C_2–C_3 bond angle between our computed TZ(2d1f,2p1d) ROCCSD(T) geometries and the 6-311G(d,p) UCCSD(T) values of Kaiser *et al.*[46,50,53] Geometries optimized at the 6-31G(d) UMP2(full) level of theory have a C_1–C_2–C_3 bond angle of 143.7°, which is over 12° smaller than our computed value. For all three isomers, the use of UMP2 theory results in an increase in localization of π bonds, giving smaller bond lengths for the multiple bonds depicted in Fig. 3.1 and longer bond lengths for single bonds, as compared to our CCSD(T) geometries. The differences in bond lengths between the TZ(2d1f,2p1d) ROCCSD(T) and the 6-31G(d) UMP2 geometries were between 0.03 and 0.05 Å.

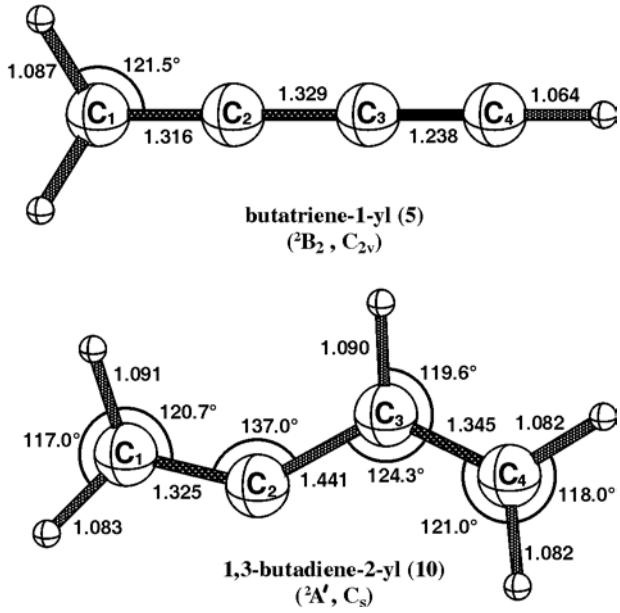

Figure 3.6 Optimized geometries for butatriene-1-yl (**5**) and 1,3-butadien-2-yl (**10**), computed at the frozen-core TZ(2d1f,2p1d) ROCCSD(T) level of theory.

Compared to the parent compound, vinylacetylene (Fig. 3.7), the structural changes accompanying formation of C_4H_3 via hydrogen abstraction are indicative of the expected

resonance and hyperconjugative effects. For *i*-C_4H_3, there is a shortening of the C_2–C_3 bond and lengthening of the C_3–C_4 bond compared to C_4H_4, eliciting traditional explanations regarding stabilization of this species through delocalization of the radical in the π system. Such delocalization is expected to decrease the acetylenic character of the C_3–C_4 bond and increase the double-bond character between C_2 and C_3. This is in contrast to *Z*-*n*-C_4H_3 and *E*-*n*-C_4H_3, for which geometric alterations are highly localized within the ethylenic subunit, as expected given the orthogonality of the σ-radical and the π system. For these two isomers, stabilization occurs primarily through hyperconjugative effects, as evinced by the slight lengthening of the C_2–C_3 and C_2–H bonds *trans* to the radical in *Z*-*n*-C_4H_3 and *E*-*n*-C_4H_3, respectively.

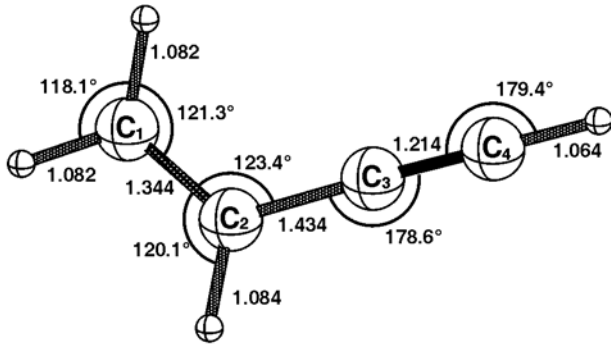

C_4H_4 (vinylacetylene, 1)
($^1A'$, C_s)

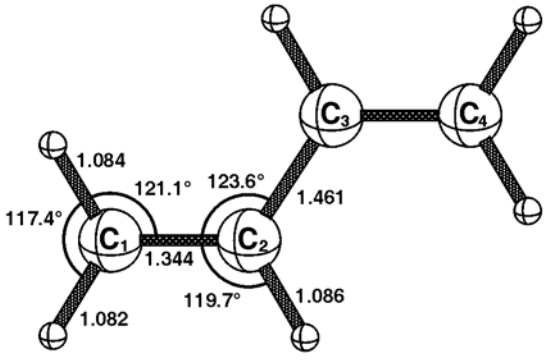

C_4H_6 (1,3-butadiene, 6)
(^1A_g, C_{2h})

Figure 3.7 Optimized geometries for C_4H_4 and C_4H_6, computed at the frozen-core TZ(2d1f,2p1d) ROCCSD(T) level of theory.

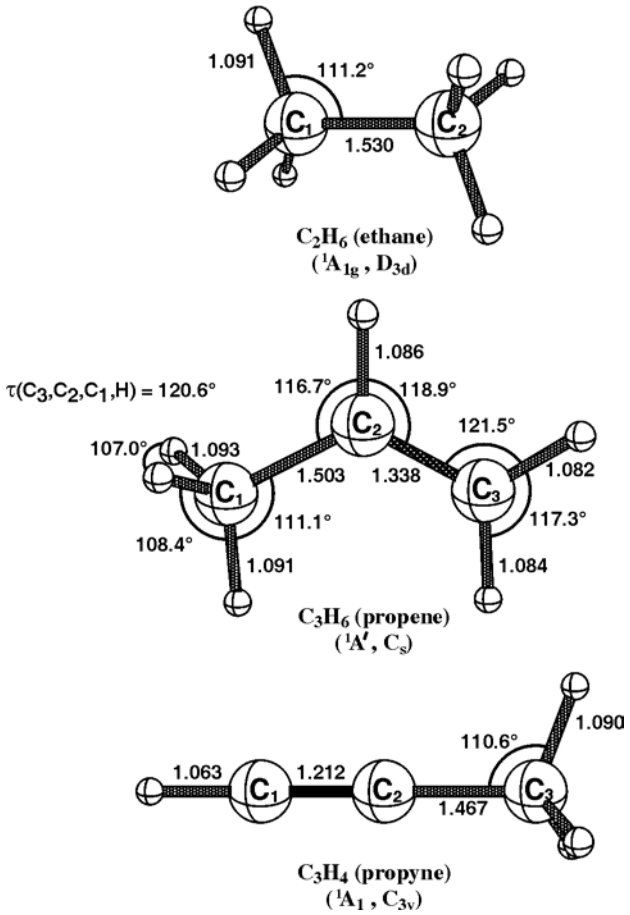

Figure 3.8 Optimized geometries for C_2H_6 (ethane), C_3H_6 (propene), and C_3H_4 (propyne), computed at the frozen-core TZ(2d1f,2p1d) ROCCSD(T) level of theory.

Comparison of optimized C_4H_5 structures with the 6-311G(d,p) QCISD results of Parker and Cooksy[48] reveals only minor differences in bond distances and valence angles, with the largest discrepancy in angles on the order of half-degrees, while bond distances agree to within 0.01 Å. At the UMP2 level there is again a contraction of interatomic distances in the *n*-C_4H_5 isomers corresponding to canonical multiple bonds as well as a lengthening of the single C–C bonds, when compared to our ROCCSD(T) structures. While the double bonds are shortened at the UMP2 level for *i*-C_4H_5, the C_3–C_4 bond is unaffected. As with the isomers of C_4H_3, comparison of optimized geometries for isomers of C_4H_5 with the parent compound,

1,3-butadiene (Fig. 3.7), is instructive in demonstrating the dominant stabilizing features of these compounds. Again, *i*-C_4H_5 exhibits considerable geometric changes, indicative of a large degree of delocalization of the radical and subsequent rehybridization at C_2, in contrast to *Z*-*n*-C_4H_5 and *E*-*n*-C_4H_5, for which the only noticeable geometric perturbations are localized at the hydrogen abstraction site.

In contrast to the unrestricted single reference results [6-311G(d,p) UHF, B3LYP, CISD, and QCISD] of Parker and Cooksy[48] for 1,3-butadiene-2-yl (**10**), harmonic vibrational frequencies computed at the cc-pVDZ ROCCSD(T) level characterize this structure as a minimum, not a first-order saddle point. However, this structure is still destabilized by 7.5 kcal mol^{-1} at the frozen-core cc-pVTZ ROCCSD(T) level of theory compared to *i*-C_4H_5, and thus was not considered further in our focal point analyses. Structure **9** (*i*-C_4H_5, $^2A''$) is preferentially stabilized, relative to *E*-*n*-C_4H_5 (**7**), *Z*-*n*-C_4H_5 (**8**), and structure **10,** due to delocalization of the radical over the C_2–C_3–C_4 framework by π-conjugation. Structures **7**, **8**, and **10** are all $^2A'$ states, misaligned for such conjugation and stabilizing delocalization.

3.5 Isomerization Energies

The relative population of the *i*- and *n*-isomers of C_4H_3 and C_4H_5 in combustion systems should depend primarily on the respective isomerization energies, provided that efficient interconversion pathways exist to aid in thermal equilibration. Reaction paths connecting these isomers have been explored extensively,[19,46,50,53-56,63] revealing a number of possible interconversion routes.

For the isomerization of *Z*-*n*-C_4H_3 to *i*-C_4H_3, promising pathways include direct conversion through a 1,2-hydrogen shift,[50,52,63] as well as isomerization through successive H-atom addition and elimination steps passing through isomers of C_4H_4 (*n*-C_4H_3 → C_4H_4 →

i-C_4H_3),[46,53] with both pathways presenting barriers on the order of 40 kcal mol^{-1}. The presence of another species to participate in reciprocal hydrogen abstraction could significantly promote the second pathway. The barrier for interconversion of *E*- and *Z*-*n*-C_4H_3 has been shown[52] to be less than 5 kcal mol^{-1}, and hydrogen tunneling is expected to lead to a smaller effective barrier.

The isomerization of *n*-C_4H_5 to *i*-C_4H_5 is somewhat more complicated, however, since these two isomers are of different ground electronic states. Possible routes include a hydrogen abstraction to form vinylacetylene followed by addition of hydrogen,[55] with a barrier of about 40 kcal mol^{-1}, as well as an alternative path[56] through C_4H_6 involving hydrogen addition first and subsequent abstraction. Miller *et al.*[54] have reported, in the context of the reaction of vinyl and acetylene, two computed transition states connecting *E*-*n*-C_4H_5 with *i*-C_4H_5, corresponding to 1,2- and 1,3-hydrogen shifts. However, unless these transition states involved out-of-plane transfer of hydrogen, they should correspond to a saddle point connecting *E*-*n*-C_4H_5 with structure **10**. Structure **10**, however, can easily isomerize to *i*-C_4H_5 with a small barrier.[48] The computed paths had barriers of 44-46 kcal mol^{-1} using a G2-like method, and this isomerization was shown to play a negligible role in the product distribution of the reaction of vinyl with acetylene for the temperature ranges considered. Previous semi-empirical work by Wang *et al.*[19] yielded a similar barrier for the isomerization of *n*-C_4H_5 to *i*-C_4H_5 via a 1,2-H shift. The key point of concern here is that effective mechanisms do exist for the facile interconversion of *i*- and *n*-isomers of C_4H_3 and C_4H_5 at elevated temperatures and under soot formation conditions, allowing our analysis to focus on thermodynamic stabilities alone.

The incremental valence focal point tables for the energy difference between *i*-C_4H_3 and *Z*- and *E*-*n*-C_4H_3 are included as Table 3.4. For both isomerization reactions there is rapid convergence with respect to one- and many-particle basis. For example, all of the individual

coupled-cluster correlation increments are less than 1.5 kcal mol^{-1} in magnitude, and the composite post-MP2 corrections are less than 1 kcal mol^{-1}. Neglecting electron correlation, the *i*- and *n*-isomers are seen to be roughly isoenergetic, with the *Z*- and *E*-*n*-C_4H_3 extrapolated ROHF energies lying 1.38 and 1.52 kcal mol^{-1} above that for *i*-C_4H_3, respectively. However, the inclusion of electron correlation preferentially stabilizes the *i*-isomer relative to the *n*-isomers by about 10 kcal mol^{-1}.

Table 3.4 Incremental valence focal point tables (kcal mol^{-1}) for isomerization reactions of C_4H_3.[a]

Basis Set	ΔE_e[ROHF]	+δ[ZAPT2]	+δ[CCSD]	+δ[CCSD(T)]	+δ[CCSDT]	ΔE_e[CCSDT]
i-C_4H_3 → *Z*-*n*-C_4H_3						
cc-pVDZ	1.146	+7.981	–0.451	+1.136	+0.014	9.826
cc-pVTZ	1.402	+8.738	–0.626	+1.298	[+0.014]	[10.827]
cc-pVQZ	1.360	+8.887	–0.698	+1.344	[+0.014]	[10.907]
cc-pV5Z	1.372	+8.876	[–0.660]	[+1.360]	[+0.014]	[10.963]
cc-pV6Z	1.382	[+8.872]	[–0.660]	[+1.360]	[+0.014]	[10.967]
CBS limit	[1.384]	[+8.865]	[–0.660]	[+1.360]	[+0.014]	**[10.964]**
i-C_4H_3 → *E*-*n*-C_4H_3						
cc-pVDZ	1.310	+7.818	–0.345	+1.180	+0.011	9.973
cc-pVTZ	1.556	+8.552	–0.528	+1.342	[+0.011]	[10.932]
cc-pVQZ	1.494	+8.715	–0.604	+1.386	[+0.011]	[11.001]
cc-pV5Z	1.494	+8.715	[–0.573]	[+1.402]	[+0.011]	[11.048]
cc-pV6Z	1.515	[+8.715]	[–0.573]	[+1.402]	[+0.011]	[11.068]
CBS limit	[1.521]	[+8.714]	[–0.573]	[+1.402]	[+0.011]	**[11.075]**
Fit	$a+be^{-cX}$	$a+bX^{-3}$	$a+bX^{-3}$	$a+bX^{-3}$	additive	
Points (X=)	4,5,6	4,5	3,4	3,4		
Cut-off	none	none	5	5		

[a]The symbol δ denotes the increment in the energy difference (ΔE) with respect to the previous level of theory. Bracketed numbers are the result of basis set extrapolations (using the fits denoted in the table), while unbracketed numbers were explicitly computed. Extrapolations for CCSD and CCSD(T) increments were cut off at the cc-pV5Z level, after which additivity was assumed.

The explicitly computed cc-pV5Z ZAPT2 values are within 0.009 and 0.001 kcal mol^{-1} of the extrapolated ZAPT2 CBS limit. It is worth noting that in each case the CCSD(T) increment overshadows the relatively small CCSD increment, a characteristic that was not observed when including ROHF-MBPT or OPT2 energies for the second order contribution.[114] This suggests a

more rapid convergence of ZAPT*n* towards the full configuration interaction (FCI) limit relative to ROHF-MBPT and OPT2.

The extrapolated core correlation contribution (Tables A3 and A4) comprises a mere 1.5% of the energy difference in both cases. After inclusion of core correlation, as well as the contribution due to harmonic zero-point vibrational energy differences, DBOC, and relativistic effects, *Z*-*n*-C_4H_3 and *E*-*n*-C_4H_3 are predicted to be higher in energy than *i*-C_4H_3 by 11.86 and 11.80 kcal mol^{-1}, respectively, as detailed in Table 3.5.

Table 3.5 Determination of isomerization energies for C_4H_3 and C_4H_5, in kcal mol^{-1}.[a]

Reaction	ΔE_{fp}(V)	Δ_{fp}(core)	ΔZPVE	ΔDBOC	ΔRel	ΔE_0(final)
i-$C_4H_3 \rightarrow$ *Z*-*n*-C_4H_3	10.96	+0.14	+0.81	–0.04	–0.01	11.86
i-$C_4H_3 \rightarrow$ *E*-*n*-C_4H_3	11.08	+0.13	+0.63	–0.03	–0.01	11.80
i-$C_4H_5 \rightarrow$ *Z*-*n*-C_4H_5	10.36	+0.19	+0.81	–0.04	–0.01	11.31
i-$C_4H_5 \rightarrow$ *E*-*n*-C_4H_5	9.86	+0.18	+0.69	–0.03	–0.01	10.69

[a] ΔE_{fp}(V) = valence focal point energy difference from Tables 3.4 and 3.6; Δ_{fp}(core) = focal-point core correlation correction from Tables A3 and A4; ΔZPVE = zero-point vibrational energy correction [cc-pVDZ ROCCSD(T)]; ΔDBOC = diagonal Born-Oppenheimer correction (cc-pVTZ ROHF); ΔRel = scalar relativistic corrections [cc-pCVTZ ROCCSD(T)]; ΔE_0(final) = sum of previous five columns.

Relative energies of *Z*-*n*-C_4H_5 and *E*-*n*-C_4H_5 were treated in an analogous manner, with the valence focal point tables included as Table 3.6. The resulting estimates for the complete basis set limit CCSDT isomeric energy difference, including ZPVE, DBOC, relativistic, and core correlation effects, are 11.31 and 10.69 kcal mol^{-1} for *Z*-*n*-C_4H_5 and *E*-*n*-C_4H_5, respectively.

For C_4H_5, in the ROHF CBS limit the *i*- and *n*-isomers are even closer in energy than for the corresponding C_4H_3 isomers, with ROHF energy separations of 1.207 and 0.718 kcal mol^{-1} for *Z*-*n*-C_4H_3 and *E*-*n*-C_4H_3, respectively. Electron correlation once again greatly stabilizes the *i*-isomer, in this case by about 9 kcal mol^{-1}. This trend is in accord with previous findings in our group[115] that relative energies of isomeric cumulenes and poly-ynes are exceptionally sensitive to inclusion of correlation. The magnitude of the composite post-MP2 correlation corrections is

less than 0.5 kcal mol^{-1}, even smaller than in the C_4H_3 case. The same trend is observed for C_4H_5 as was seen with C_4H_3 regarding the CCSD(T) increment overshadowing the CCSD increment when utilizing ZAPT2 for the leading electron correlation contribution.

Table 3.6 Incremental valence focal point tables (kcal mol^{-1}) for isomerization reactions of C_4H_5.[a]

Basis Set	ΔE_e[ROHF]	+δ[ZAPT2]	+δ[CCSD]	+δ[CCSD(T)]	+δ[CCSDT]	ΔE_e[CCSDT]
i-C_4H_5 → *Z*-*n*-C_4H_5						
cc-pVDZ	0.974	+7.766	–0.283	+0.341	–0.061	8.736
cc-pVTZ	1.246	+9.027	–0.667	+0.469	[–0.061]	[10.014]
cc-pVQZ	1.209	+9.390	–0.838	+0.516	[–0.061]	[10.216]
cc-pV5Z	1.211	+9.452	[–0.832]	[+0.533]	[–0.061]	[10.303]
cc-pV6Z	1.208	[+9.479]	[–0.832]	[+0.533]	[–0.061]	[10.327]
CBS limit	[1.207]	[+9.517]	[–0.832]	[+0.533]	[–0.061]	**[10.364]**
i-C_4H_5 → *E*-*n*-C_4H_5						
cc-pVDZ	0.502	+7.620	–0.135	+0.373	–0.058	8.302
cc-pVTZ	0.763	+8.838	–0.535	+0.498	[–0.058]	[9.507]
cc-pVQZ	0.729	+9.205	–0.708	+0.545	[–0.058]	[9.712]
cc-pV5Z	0.723	+9.273	[–0.707]	[+0.561]	[–0.058]	[9.792]
cc-pV6Z	0.719	[+9.303]	[–0.707]	[+0.561]	[–0.058]	[9.818]
CBS limit	[0.718]	[+9.344]	[–0.707]	[+0.561]	[–0.058]	**[9.858]**
Fit	$a+be^{-cX}$	$a+bX^{-3}$	$a+bX^{-3}$	$a+bX^{-3}$	additive	
Points (X=)	4,5,6	4,5	3,4	3,4		
Cut-off	none	none	5	5		

[a] See footnote *a* of Table 3.4.

For the isomerization energies of (*E*-*n*-C_4H_3, *E*-*n*-C_4H_5) relative to (*i*-C_4H_3, *i*-C_4H_5), our focal point extrapolations give final values of (11.8, 10.7) kcal mol^{-1} (Table 3.5), significantly larger than the DMC energy separations of (6.8 ± 1.2, 7.4 ± 1.2) kcal mol^{-1} recently reported by Krokidis *et al.*[51] However, our computed energy differences are also noticeably smaller than the (19, 12) kcal mol^{-1} BAC-MP4 values of Miller and Melius,[22] with the most significant discrepancy arising for C_4H_3.

The DMC results of Krokidis *et al.*[51] employed the fixed-node approximation,[116-119] in which the nodal structure of a trial wave function is imposed onto the DMC wave function. For

the C_4H_3 and C_4H_5 species, an MCSCF trial function was used, which, lacking dynamical correlation, is expected to result in exiguous nodal surfaces. While it has been shown[120] that even modestly accurate trial wave functions (and therefore nodal hypersurfaces) generally yield satisfactory results, relative energies computed via DMC would suffer in cases where the quality of the trial function is noticeably deficient for one of the species under consideration. Moreover, errors associated with the fixed-node-approximation are not reflected in the reported error estimates.

The G3 model ostensibly yields accurate thermochemistry for both C_4H_3 and C_4H_5. As seen in Tables 3.1 and 3.2, the standard G3 procedure gives isomerization energies within 1 kcal mol^{-1} of our more rigorous focal-point extrapolations. However, this comparison is quite misleading.

First, the G3 method suffers from spin contamination in its UHF-based electronic wave functions, leading to unbalanced errors because the extent of contamination is significantly different in the *i*- vs. *n*-isomers. In order to isolate intrinsic errors, we re-evaluated G3 electronic energies at the frozen-core TZ(2d1f,2p1d) ROCCSD(T) geometries employed in our focal-point analyses. The resulting G3 separations (also listed in Tables 3.1 and 3.2) between *n*- and *i*-isomers showed discrepancies with respect to our focal-point values of –1.2 and +1.2 kcal mol^{-1} for C_4H_3 and C_4H_5, respectively.

Second, the G3 approach utilizes 6-31G(d) UMP2 geometries for its single-point computations, which proves problematic in these systems. As discussed in Section 3.4, 6-31G(d) UMP2 theory generally yields too much carbon-carbon bond alternation when compared to TZ(2d1f,2p1d) ROCCSD(T), and in the case of *i*-C_4H_3 the C_1–C_2–C_3 bond angle is over 12° too

small. Accordingly, the use of 6-31G(d) UMP2 reference geometries engenders respective errors of –0.7 and –0.2 kcal mol^{-1} in the isomerization energies of C_4H_3 and C_4H_5.

Third, the G3 scheme evaluates ZPVE corrections on the basis of scaled 6-31G(d) UHF vibrational frequencies, an insidious pitfall for the unusual C_4H_3 species. For *i*-C_4H_3 there are two multiple-bond C-C stretching modes and several large-amplitude chain bending modes for which the unscaled 6-31G(d) UHF frequencies are much *smaller* than their cc-pVDZ ROCCSD(T) counterparts. Scaling these frequencies by the standard factor of 0.8929 thus exacerbates the errors in the zero-point vibrational energies. For *n*-C_4H_3 the 6-31G(d) UHF frequency underestimations are not present for the chain bending modes and are less severe for the multiple-bond C–C stretches. Consequently, the evaluation of ZPVEs using scaled 6-31G(d) UHF frequencies, as opposed to unscaled cc-pVDZ ROCCSD(T) values, gives rise to an unusually large error of +1.2 kcal mol^{-1} in the vibrational contribution to the C_4H_3 isomerization energy. The corresponding error for C_4H_5 is only –0.2 kcal mol^{-1}.

Summing the intrinsic electronic structure, reference geometry, and ZPVE disparities of the G3 method, as compared to our focal-point procedure, gives G3 isomerization energy errors of –1.2 – 0.7 + 1.2 = –0.7 kcal mol^{-1} for C_4H_3 and +1.2 – 0.2 – 0.2 = +0.8 kcal mol^{-1} for C_4H_5. Therefore, the final G3 values for the energy separation between *i*- and *n*-isomers are quite accurate, but due to fortuitous cancellations of more substantial errors.

In recent theoretical work on the reaction of vinyl and acetylene, Miller and Klippenstein[54] solved the time-dependent master equation for three wells on a C_4H_5 surface computed using a G2-like method to yield product distributions as a function of temperature and pressure. This potential featured an *E*-*n*-C_4H_5 energy of 11.2 kcal mol^{-1} relative to *i*-C_4H_5, close

to our extrapolated result of 10.69 kcal mol^{-1}. Thus, their conclusions should remain unaltered by our thermochemical refinements.

The 2002 modeling study of Richter and Howard[3], which concluded that the even-carbon-atom pathways play no significant role in benzene formation under typical flame conditions, utilized enthalpies of formation of the isomers of C_4H_3 and C_4H_5 that corresponded to energy differences of 18.6 and 11.6 kcal mol^{-1} for *n*-C_4H_3 and *n*-C_4H_5 relative to *i*-C_4H_3 and *i*-C_4H_5, respectively. While their energy separation for C_4H_5 is within 1 kcal mol^{-1} of our result, their value for C_4H_3 is almost 7 kcal mol^{-1} larger than our value, raising some doubt over the conclusion that even-carbon-atom pathways play no role. The kinetic model of Pope and Miller,[36] which leads to similar conclusions regarding the role of even-carbon-atom pathways, includes the original BAC-MP4 energy separations of Miller and Melius[22] of 18.7 and 12.4 kcal mol^{-1} for C_4H_3 and C_4H_5, respectively. Again, the relative energies of *n*-isomers of C_4H_3 in this model are considerably higher than our extrapolated results. On the other hand, Wang and Frenklach[20] modeled premixed acetylene and ethylene flames, concluding that even-carbon-atom pathways are as important as the propargyl recombination path in aromatic formation. They used an energy separation of 8 kcal mol^{-1} for both C_4H_3 and C_4H_5, several kcal mol^{-1} lower than our extrapolated results. While there have been conflicting reports regarding the sensitivity of the combustion models to the $n - i$ isomerization energies, it is clear that a re-evaluation of even-carbon-atom pathways is warranted based on the definitive energetics reported here. In the very least, all models should now be updated to be consistent on the thermochemistry of C_4H_3 and C_4H_5 species.

There are considerable differences between our extrapolated energy separations and representative DFT values, which fall in the range of 17 ± 1 kcal mol^{-1} and 14 ± 1 kcal mol^{-1} for

both isomers of *n*-C_4H_3 and *n*-C_4H_5, respectively. This failure of DFT (specifically the B3LYP functional) to accurately treat highly unsaturated hydrocarbons is established in the literature, particularly for relative energies of isomeric cumulenes and poly-ynes[115] and of isomers of C_{20},[121-123] and should serve as a further warning about the blind application of DFT to these classes of systems.

Table 3.7 Incremental valence focal point tables (kcal mol^{-1}) for decomposition of C_4H_4 and C_4H_6.[a]

Basis Set	ΔE_e[RHF]	+δ[MP2]	+δ[CCSD]	+δ[CCSD(T)]	+δ[CCSDT]	ΔE_e[CCSDT]
$C_4H_4 + C_2H_6 \rightarrow C_3H_6 + C_3H_4$						
cc-pVDZ	–0.334	+1.495	–0.782	+0.460	–0.024	0.815
cc-pVTZ	–0.542	+1.452	–0.822	+0.469	[–0.024]	[0.533]
cc-pVQZ	–0.687	+1.358	–0.831	+0.461	[–0.024]	[0.277]
cc-pV5Z	–0.742	+1.334	[–0.843]	[+0.458]	[–0.024]	[0.182]
cc-pV6Z	–0.747	[+1.323]	[–0.843]	[+0.458]	[–0.024]	[0.167]
CBS limit	[–0.747]	[+1.309]	[–0.843]	[+0.458]	[–0.024]	**[0.152]**
$C_4H_6 + C_2H_6 \rightarrow C_3H_6 + C_3H_6$						
cc-pVDZ	3.061	+0.955	–0.780	+0.429	+0.016	3.681
cc-pVTZ	2.962	+0.845	–0.805	+0.413	[+0.016]	[3.431]
cc-pVQZ	2.879	+0.806	–0.807	+0.412	[+0.016]	[3.306]
cc-pV5Z	2.839	+0.813	[–0.828]	[+0.412]	[+0.016]	[3.252]
cc-pV6Z	2.838	[+0.817]	[–0.828]	[+0.412]	[+0.016]	[3.256]
CBS limit	[2.839]	[+0.821]	[–0.828]	[+0.412]	[+0.016]	**[3.259]**
Fit	$a + be^{-cX}$	$a + bX^{-3}$	$a + bX^{-3}$	$a + bX^{-3}$	additive	
Points (X=)	4,5,6	4,5	3,4	3,4		
Cut-off	none	none	5	5		

[a] See footnote *a* of Table 3.4.

3.6 Enthalpies of Formation of C_4H_4 and C_4H_6

Enthalpies of formation of C_4H_4 (vinylacetylene, **1**) and C_4H_6 (1,3-butatdiene, **6**) were determined through isodesmic reactions (3.8) and (3.9), respectively, which minimize differential errors in electronic structure computations by matching formal bond types in reactants and products.[100] Geometries of all pertinent species were computed at the TZ(2d1f,2p1d) RCCSD(T) level of theory, with optimized structures given in Figs. 3.7 and 3.8. Valence focal point tables are included as Table 3.7. The agreement of RHF and CCSDT reaction energies to better than 1

kcal mol^{-1} is a clear indication of the isodesmic balancing in reactions (3.8) and (3.9). At all levels of theory for both reactions, the largest explicitly computed increment is within 0.025 kcal mol^{-1} of the extrapolated CBS value. The extrapolated valence energies were further corrected for core-correlation, DBOC, zero-point vibrational, and relativistic effects, as detailed in Table 3.8 and supplementary Table A5. The resulting enthalpies of formation are $\Delta H^{\circ}_{f,0}(C_4H_4)$ = 70.5 and $\Delta H^{\circ}_{f,0}(C_4H_6)$ = 30.0 kcal mol^{-1}. Standard G3 model chemistry applied to atomization reactions yields similar values of 71.0 and 30.2 kcal mol^{-1} for C_4H_4 and C_4H_6, respectively. Our computed enthalpy of formation of C_4H_6 at 0 K is in nice agreement with the experimental value[124] of 29.76 kcal mol^{-1}.

Table 3.8 Determination of standard enthalpies of formation for C_4H_4, C_4H_6, *i*-C_4H_3, and *i*-C_4H_5, in kcal mol^{-1}.[a]

Reaction	ΔE_{fp}(V)	Δ_{fp}(core)	ΔZPVE	ΔDBOC	ΔRel	ΔE_0(final)	Target	$\Delta_f H_0^\circ$	$\Delta_f H_0^\circ$ (G3)[b]
(3.8)	0.15	–0.05	–0.21	–0.01	+0.00	–0.12	C_4H_4 (**1**)	**70.54**	71.0
(3.9)	3.26	–0.03	–0.29	+0.00	+0.00	+2.94	C_4H_6 (**6**)	**29.98**	30.2
(3.6)	3.39	+0.13	–0.29	–0.02	–0.01	+3.20	*i*-C_4H_3 (**4**)	**118.95**	120.1
(3.7)	3.37	+0.17	–0.29	–0.02	–0.01	+3.22	*i*-C_4H_5 (**9**)	**78.37**	77.5
$CH_4 \rightarrow CH_3 + H$	112.55	+0.17	–9.58	–0.12	–0.02	102.99 (103.24, expt.)[c]			

[a] Enthalpies of formation for C_4H_3 and C_4H_5 are given relative to the corresponding computed values for C_4H_4 and C_4H_6. See footnote *a* of Table 3.5 for notation.
[b] Standard results from computed atomization energies and atomic enthalpies of formation.
[c] From experimental enthalpies of formation in Table 3.3.

3.7 Enthalpies of Formation of C_4H_3 and C_4H_5

The enthalpies of formation of *i*-C_4H_3 and *i*-C_4H_5 were determined through hydrogen-exchange reactions (3.6) and (3.7), relative to our computed enthalpies of formation for C_4H_4 and C_4H_6. Very similar results would be obtained without invoking the isodesmic balancing provided in these reactions, because our focal-point approach already yields $D_0(CH_3–H)$ within 0.25 kcal mol^{-1} of experiment (see Table 3.8). Incremental focal point tables for the formation of *i*-C_4H_3 and *i*-C_4H_5 are included as Table 3.9. Core-correlation effects were again incorporated via secondary focal point extrapolations, included as supplementary material (Table A6). While the convergence behavior in the focal-point grids of Table 3.9 is good, it is notable that the composite post-MP2 contributions of +3.0 and +1.9 kcal mol^{-1} for reactions (3.6) and (3.7), respectively, are larger than those observed in the other reactions considered here. As shown in Table 3.8, our final prediction is that the *iso* C–H bonds of both vinylacetylene (**1**) and 1,3-butadiene (**6**) have dissociation energies 3.2 kcal mol^{-1} less than in methane. From this result we obtain enthalpies of formation for *i*-C_4H_3 (**4**) and *i*-C_4H_5 (**9**) of 119.0 and 78.4 kcal mol^{-1}, respectively. By adding the final isomerization energies from the focal-point analyses of Section 3.5 to the enthalpies of formation of the *i*-isomers deduced here, we find that $\Delta_f H_0^\circ$ (*Z*-*n*-C_4H_3, *E*-*n*-C_4H_3) = (130.8, 130.8) kcal mol^{-1} and $\Delta_f H_0^\circ$ (*Z*-*n*-C_4H_5, *E*-*n*-C_4H_5) = (89.7, 89.1) kcal mol^{-1}.

By comparison, the G3 scheme yields for the *i*-isomers $\Delta_f H_0^\circ$ (**4**) = 120.1 and $\Delta_f H_0^\circ$ (**9**) = 77.5 kcal mol^{-1} from atomization energies. The level of agreement with our values is in accord with the mean accuracy (1.02 kcal mol^{-1}) of the G3 method within the G2/97 test set.[66] However, once again there is embedded error cancellation among the deficiencies discussed in Section 3.6 with the G3 treatment of the *i*-isomers of C_4H_3 and C_4H_5. In particular,

for *i*-C_4H_3, if the more reliable TZ(2d1f,2p1d) ROCCSD(T) reference geometry and cc-pVDZ ROCCSD(T) zero-point vibrational energy are employed for the G3 electronic structure computations, then $\Delta_f H_0^\circ$(**4**) is lowered by 2.1 kcal mol^{-1}.

Table 3.9 Incremental valence focal point tables (kcal mol^{-1}) for reaction (3.6) and (3.7).[a]

Basis Set	ΔE_e[ROHF]	+δ[ZAPT2]	+δ[CCSD]	+δ[CCSD(T)]	+δ[CCSDT]	ΔE_e[CCSDT]
i-C_4H_3 + CH_4 → C_4H_4 + CH_3						
cc-pVDZ	–7.219	+7.285	+1.860	+1.386	+0.202	2.840
cc-pVTZ	–7.303	+7.885	+1.025	+1.588	[+0.202]	[3.396]
cc-pVQZ	–7.431	+7.987	+1.035	+1.640	[+0.202]	[3.433]
cc-pV5Z	–7.478	+7.940	[+1.123]	[+1.658]	[+0.202]	[3.445]
cc-pV6Z	–7.484	[+7.919]	[+1.123]	[+1.658]	[+0.202]	[3.418]
CBS limit	[–7.485]	[+7.891]	[+1.123]	[+1.658]	[+0.202]	**[3.388]**
i-C_4H_5 + CH_4 → C_4H_6 + CH_3						
cc-pVDZ	–7.081	+7.226	+1.345	+0.595	+0.133	2.218
cc-pVTZ	–7.121	+8.372	+0.982	+0.768	[+0.133]	[3.133]
cc-pVQZ	–7.243	+8.706	+0.891	+0.825	[+0.133]	[3.313]
cc-pV5Z	–7.300	+8.746	[+0.938]	[+0.846]	[+0.133]	[3.362]
cc-pV6Z	[–7.322]	[+8.764]	[+0.938]	[+0.846]	[+0.133]	[3.359]
CBS limit	[–7.332]	[+8.788]	[+0.938]	[+0.846]	[+0.133]	**[3.373]**
Fit	$a + be^{-cX}$	$a + bX^{-3}$	$a + bX^{-3}$	$a + bX^{-3}$	additive	
Points (X=)	3,4,5	4,5	3,4	3,4		
Cut-off	none	none	5	5		

[a] See footnote *a* of Table 3.4.

3.8 SUMMARY

Improved, fully optimized geometries for species **1-10** have been obtained at the frozen-core TZ(2d1f,2p1d) ROCCSD(T) level of theory. Rigorous series of single-point energies were then computed and extrapolated within the focal point scheme of Allen and co-workers[67-72] to yield highly-accurate isomeric energy differences and enthalpies of formation for isomers of C_4H_3 and C_4H_5. Corrections were made for core correlation via secondary focal point extrapolations, and ZPVEs were obtained from reliable harmonic vibrational frequencies evaluated at the cc-pVDZ ROCCSD(T) level of theory. With further inclusion of non-Born-Oppenheimer and relativistic effects, *Z*-*n*-C_4H_3 and *E*-*n*-C_4H_3 are found to be higher in

energy by 11.86 and 11.80 kcal mol^{-1} relative to *i*-C_4H_3, while *Z*-*n*-C_4H_5 and *E*-*n*-C_4H_5 are computed to be higher relative to *i*-C_4H_5 by 11.31 and 10.69 kcal mol^{-1}, respectively.

These isomerization energies are significantly lower than B3LYP density-functional results, which overestimate the relative stability of *i*-C_4H_3 and *i*-C_4H_5 by 7 and 5 kcal mol^{-1}, respectively. Furthermore, the popular B3LYP hybrid functional does not yield a stationary point corresponding to *i*-C_4H_3. Instead, the B3LYP potential energy surface features a minimum at the symmetric, C_{2v} structure **5**, shown to be a transition state at the cc-pVDZ ROCCSD(T) level of theory. These deficiencies of DFT in describing highly unsaturated hydrocarbons are in accord with previously documented shortcomings.[115,121-123]

Our computed isomeric energy differences are several kcal mol^{-1} larger than the recent diffusion Monte Carlo results of Krokidis *et al*.,[51] especially for the C_4H_3 species. While the DMC results were computed at a qualitatively incorrect, C_{2v} geometry for *i*-C_4H_3, we expect this error to be small because the potential surface for bending of the carbon framework is very flat. Instead, the errors in the DMC relative energies are more likely due to the use of exiguous trial wave functions within the fixed-node approximation.

In the C_4H_3 and C_4H_5 systems, G3 theory suffers from large and unbalanced spin-contamination in electronic wave functions, poor UMP2 reference geometries with excessive carbon-carbon bond alternation and framework bending, and numerous UHF vibrational frequencies that are anomalously lower than their CCSD(T) counterparts. Our focal-point approach has none of these deficiencies. Fortuitously, the problems with G3 theory in large part cancel to give thermochemistry within 1-2 kcal mol^{-1} of our final proposals.

By performing focal-point analyses of isodesmic reactions and using known thermochemistry for C_1-C_3 hydrocarbons, the following enthalpies of formation ($\Delta_f H_0^\circ$, kcal

mol^{-1}) are determined: vinylacetylene (**1**), 70.5; *E*-*n*-C_4H_3 (**2**), 130.8; *Z*-*n*-C_4H_3 (**3**), 130.8; *i*-C_4H_3 (**4**), 119.0; 1,3-butadiene (**6**), 30.0; *E*-*n*-C_4H_5 (**7**), 89.1; *Z*-*n*-C_4H_5 (**8**), 89.7; and *i*-C_4H_5 (**9**), 78.4 kcal mol^{-1}. Any changes in our $\Delta_f H_0^\circ$ values necessitated by future thermochemical revisions for reference compounds can be readily computed by means of the pure theoretical results[125] underlying our conclusions. The errors in our proposed enthalpies are expected to be ≤ 1 kcal mol^{-1}. In contrast, some of the enthalpies of formation contained in a standard database[126] for chemical kinetic modeling have errors in the 10 kcal mol^{-1} range. For example, after accounting for thermal effects, our enthalpies of formation for *i*-C_4H_3 and *i*-C_4H_5 are 7-8 kcal mol^{-1} higher than the $\Delta_f H_{298}^\circ$ values reported from the database.[3] Fortunately, the continuing advances in electronic structure theory are allowing such lacunae in thermochemical knowledge to be steadily rectified, thus providing a solid foundation for unraveling the complexities of combustion in general and soot formation in particular.

Recent modeling studies[3,36] that have ruled out even-carbon-atom pathways for a significant role in benzene formation under typical flame conditions have employed enthalpies of formation corresponding to an energy difference between *i*- and *n*-C_4H_3 isomers that is 7 kcal mol^{-1} higher than our extrapolated value. The modeling study of Wang and Frenklach,[20] which concluded that even- and odd-carbon-pathways play comparable roles in aromatic formation during combustion, utilized enthalpies of formation corresponding to an *n*–*i* isomeric energy difference of 8 kcal mol^{-1} for both C_4H_3 and C_4H_5, *i.e.*, values approximately 3 kcal mol^{-1} lower than our final predictions. On closer scrutiny, the disparity between the Miller-Melius[22] and Wang-Frenklach[2,19,20,127] analyses may be attributed[128] to large differences in three primary parameters in these combustion models: the rate coefficient for propargyl recombination, the rate coefficient for the formation of *n*-C_4H_3 from diacetylene, and the enthalpy of formation of

n-C_4H_3. The definitive $\Delta_f H_0^\circ$ values advanced here remove persisting uncertainty in the thermochemistry of the C_4H_3 and C_4H_5 intermediates, allowing improved modeling studies aimed at resolving current disputes on the significance of even-carbon-atom pathways in the initial steps of soot formation.

3.9 ACKNOWLEDGEMENTS

This research was supported by the U. S. Department of Energy, Office of Basic Energy Sciences, Combustion Program (Grant No. DE-FG02-00ER14748) and the SciDAC Computational Chemistry Program (Grant No. DE-FG02-01ER15226). Computer resources were supplied in part by the National Energy Research Scientific Computing Center (NERSC), in support of the Department of Energy's Combustion and SciDAC programs. SEW is supported by a UGA Presidential Fellowship, and would like to thank Dr. C. J. Pope for providing a reprint of Ref. 36 and Professors A. G. Császár and P. R. Westmoreland for helpful suggestions regarding the manuscript.

REFERENCES

1 B. S. Haynes and H. G. Wagner, Prog. Energy Combust. Sci. **7**, 229 (1981).

2 M. Frenklach, Phys. Chem. Chem. Phys. **4**, 2028 (2002).

3 H. Richter and J. B. Howard, Phys. Chem. Chem. Phys. **4**, 2038 (2002).

4 J. L. Durant, W. F. Busby, A. L. Lafleur, B. W. Penman, and C. L. Crespi, Mutat. Res. **371**, 123 (1996).

5 M. F. Denissenko, A. Pao, M. S. Tang, and G. P. Pfeifer, Science **274**, 430 (1996).

6 R. E. Kinney and D. J. Crowley, Ind. Eng. Chem. **46**, 258 (1954).

7 F. C. Stehling, J. D. Frazee, and R. C. Anderson, Proc. Combust. Inst. **6**, 247 (1956).

[8] J. D. Bittner and J. B. Howard, Proc. Combust. Inst. **18**, 1105 (1981).

[9] M. Weissman and S. W. Benson, Int. J. Chem. Kinet. **16**, 307 (1984).

[10] J. A. Cole, J. D. Bittner, J. P. Longwell, and J. B. Howard, Combust. Flame **56**, 51 (1984).

[11] M. Frenklach, D. W. Clary, W. C. Gardiner Jr., and S. E. Stein, Proc. Combust. Inst. **20**, 887 (1984).

[12] M. Frenklach, D. W. Clary, T. Yuan, W. C. Gardiner Jr., and S. E. Stein, Combust. Sci. Tech. **50**, 79 (1986).

[13] M. Frenklach and J. Warnatz, Combust. Sci. Tech. **51**, 265 (1987).

[14] M. B. Colket, Proc. Combust. Inst. **21**, 851 (1987).

[15] S. J. Harris, A. M. Weiner, and R. J. Blint, Combust. Flame **72**, 91 (1988).

[16] I. Glassman, Proc. Combust. Inst. **22**, 295 (1989).

[17] P. R. Westmoreland, A. M. Dean, J. B. Howard, and J. P. Longwell, J. Phys. Chem. **93**, 8171 (1989).

[18] E. Bastin, J.-L. Delfau, M. Reuillon, C. Vovelle, and J. Warnatz, Proc. Combust. Inst. **22**, 313 (1989).

[19] H. Wang and M. Frenklach, J. Phys. Chem. **98**, 11465 (1994).

[20] H. Wang and M. Frenklach, Combust. Flame **110**, 173 (1997).

[21] H. Anderson, C. S. McEnally, and L. D. Pfefferle, Proc. Combust. Inst. **28**, 2577 (2000).

[22] J. A. Miller and C. F. Melius, Combust. Flame **91**, 21 (1992).

[23] J. D. Adamson, C. L. Morter, J. D. DeSain, G. P. Glass, and R. F. Curl, J. Phys. Chem. **100**, 2125 (1996).

[24] R. D. Kern, H. J. Singh, and C. H. Wu, Int. J. Chem. Kinet. **20**, 731 (1988).

[25] C. H. Wu and R. D. Kern, J. Phys. Chem. **91**, 6291 (1987).

[26] K. M. Leung and R. P. Lingstedt, Combust. Sci. Tech. **102**, 129 (1995).

[27] N. M. Marinov, W. J. Pitz, C. K. Westbrook, M. J. Castaldi, and S. M. Senkan, Combust. Sci. Tech. **116-117**, 211 (1996).

[28] J. A. Miller, Proc. Combust. Inst. **26**, 461 (1996).

[29] M. J. Castaldi, N. M. Marinov, C. F. Melius, J. Huang, S. M. Senkan, W. J. Pitz, and C. K. Westbrook, Proc. Combust. Inst. **26**, 693 (1996).

[30] R. P. Lindstedt and G. Skevis, Combust. Sci. Tech. **125**, 73 (1997).

[31] N. M. Marinov, M. J. Castaldi, C. F. Melius, and W. Tsang, Combust. Sci. Tech. **128**, 295 (1997).

[32] A. D'Anna and A. Violi, Proc. Combust. Inst. **27**, 423 (1998).

[33] N. M. Marinov, W. J. Pitz, C. K. Westbrook, A. E. Lutz, A. M. Vincitore, and S. M. Senkan, Proc. Combust. Inst. **27**, 605 (1998).

[34] N. M. Marinov, W. J. Pitz, C. K. Westbrook, A. M. Vincitore, M. J. Castaldi, S. M. Senkan, and C. F. Melius, Combust. Flame **114**, 192 (1998).

[35] A. Violi, A. D'Anna, and A. D'Alessio, Chem. Eng. Sci. **54**, 3439 (1999).

[36] C. J. Pope and J. A. Miller, Proc. Combust. Inst. **28**, 1519 (2000).

[37] J. A. Miller, Faraday Discuss. **119**, 461 (2001).

[38] J. A. Miller and S. J. Klippenstein, J. Phys. Chem. A **105**, 7254 (2001).

[39] A. D'Anna, A. D'Alessio, and J. Kent, Combust. Flame **125**, 1196 (2001).

[40] A. D'Anna and J. H. Kent, Combust. Flame **132**, 715 (2003).

[41] J. A. Miller and S. J. Klippenstein, J. Phys. Chem. A **107**, 2680 (2003).

[42] C. S. McEnally, L. D. Pfefferle, A. G. Robinson, and T. S. Zwier, Combust. Flame **123**, 344 (2000).

[43] N. Olten and S. M. Senkan, Combust. Flame **125**, 1032 (2001).

[44] B. Atakan, A. Lamprecht, and K. Kohse-Hoinghaus, Combust. Flame **133**, 431 (2003).

[45] S. P. Walch, J. Chem. Phys. **103**, 8544 (1995).

[46] R. I. Kaiser, A. M. Mebel, A. H. H. Chang, S. H. Lin, and Y. T. Lee, J. Chem. Phys. **110**, 10330 (1999).

[47] A. L. Cooksy, J. Am. Chem. Soc. **117**, 1098 (1995).

[48] C. L. Parker and A. L. Cooksy, J. Phys. Chem. A **102**, 6186 (1998).

[49] C. L. Parker and A. L. Cooksy, J. Phys. Chem. A **103**, 2160 (1999).

[50] T. N. Le, A. M. Mebel, and R. I. Kaiser, J. Comp. Chem. **22**, 1522 (2001).

[51] X. Krokidis, N. W. Moriarty, W. A. Lester Jr., and M. Frenklach, Int. J. Chem. Kinet. **33**, 808 (2001).

[52] B. Ceursters, H. M. T. Nguyen, J. Peeters, and M. T. Nguyen, Chem. Phys. **262**, 243 (2000).

[53] A. M. Mebel, R. I. Kaiser, and Y. T. Lee, J. Am. Chem. Soc. **122**, 1776 (2000).

[54] J. A. Miller, S. J. Klippenstein, and S. H. Robertson, J. Phys. Chem. A **104**, 7525 (2000).

[55] T. L. Nguyen, A. M. Mebel, and R. I. Kaiser, J. Phys. Chem. A **107**, 2990 (2003).

[56] H.-Y. Lee, V. V. Kislov, S.-H. Lin, A. M. Mebel, and D. M. Neumark, Chem. Eur. J. **9**, 726 (2003).

[57] E. Gey, S. Wiegratz, W. Kühnel, B. Ondruschka, W. Saffert, and G. Zimmermann, J. Mol. Struct. (THEOCHEM) **53**, 69 (1989).

[58] E. Gey, S. Wiegratz, and B. Ondruschka, Z. Phys. Chem.-Leipzig **270**, 1067 (1989).

[59] T.-K. Ha and E. Gey, J. Mol. Struct. (THEOCHEM) **306**, 197 (1994).

[60] L. K. Madden, L. V. Moskaleva, S. Kristyan, and M. C. Lin, J. Phys. Chem. A **101**, 6790 (1997).

[61] J. Cioslowski, G. Liu, and D. Moncrieff, J. Phys. Chem. A **103**, 11465 (1999).

[62] C. Cavallotti, R. Rota, and S. Carrà, J. Phys. Chem. A **106**, 7769 (2002).

[63] H. Yang, H. Wang, X. Ran, Q. Shi, and Z. Wen, J. Mol. Struct. (THEOCHEM) **618**, 209 (2002).

[64] H. Wang and A. L. Cooksy, Chem. Phys. **213**, 139 (1996).

[65] These DMC computations only considered relative energies of the *E*-*n*- and *i*-isomers.

[66] L. A. Curtiss, K. Raghavachari, P. C. Redfern, V. Rassolov, and J. A. Pople, J. Chem. Phys. **109**, 7764 (1998).

[67] W. D. Allen, A. L. L. East, and A. G. Császár, in *Structures and Conformations of Non-Rigid Molecules*, edited by J. Laane, M. Dakkouri, B. van der Vecken, and H. Oberhammer (Kluwer, Dordrecht, 1993), pp. 343.

[68] A. G. Császár, W. D. Allen, and H. F. Schaefer, J. Chem. Phys. **108**, 9751 (1998).

[69] A. G. Császár, G. Tarczay, M. L. Leininger, O. L. Polyansky, and W. D. Allen, in *Spectroscopy from Space*, edited by J. Demaison and K. Sarka (Kluwer, Dordrecht, 2001), pp. 317.

[70] A. L. L. East and W. D. Allen, J. Chem. Phys. **99**, 4638 (1993).

[71] J. M. Gonzales, C. Pak, R. S. Cox, W. D. Allen, G. Tarczay, and A. G. Császár, Chem. Eur. J. **9**, 2173 (2003).

[72] J. P. Kenny, W. D. Allen, and H. F. Schaefer, J. Chem. Phys. **118**, 7353 (2003).

[73] G. D. Purvis and R. J. Bartlett., J. Chem. Phys. **76**, 1910 (1982).

[74] G. E. Scuseria, A. C. Scheiner, T. J. Lee, J. E. Rice, and H. F. Schaefer, J. Chem. Phys. **86**, 2881 (1987).

[75] G. E. Scuseria, C. L. Janssen, and H. F. Schaefer, J. Chem. Phys. **89**, 7382 (1988).

[76] M. Rittby and R. J. Bartlett, J. Phys. Chem. **92**, 3033 (1988).

[77] K. Raghavachari, G. W. Trucks, J. A. Pople, and M. Head-Gordon, Chem. Phys. Lett. **157**, 479 (1989).

[78] J. Gauss, W. J. Lauderdale, J. F. Stanton, J. D. Watts, and R. J. Bartlett, Chem. Phys. Lett. **182**, 207 (1991).

[79] R. J. Bartlett, J. D. Watts, S. A. Kucharski, and J. Noga, Chem. Phys. Lett. **167**, 609 (1990).

[80] R. J. Bartlett, J. D. Watts, S. A. Kucharski, and J. Noga, Chem. Phys. Lett. **165**, 513 (1990).

[81] J. D. Watts, J. Gauss, and R. J. Bartlett, J. Chem. Phys. **98**, 8718 (1993).

[82] R. A. King, W. D. Allen, B. Ma, and H. F. Schaefer, Faraday Discuss. **110**, 23 (1998).

[83] T. H. Dunning, J. Chem. Phys. **55**, 716 (1971).

[84] T. H. Dunning, J. Chem. Phys. **90**, 1007 (1989).

[85] ACES II; J. F. Stanton, J. Gauss, W. J. Lauderdale, J. D. Watts, R. J. Bartlett. The package also contains modified versions of the MOLECULE Gaussian integral program of J. Almlöf and P. R. Taylor, the ABACUS integral derivative program written by T. U. Helgaker, H. J. Aa. Jensen, P. Jørgensen, and P. R. Taylor, and the PROPS property evaluation integral code of P. R. Taylor.

[86] J. Noga and R. J. Bartlett, J. Chem. Phys. **86**, 7041 (1987).

[87] J. Noga and R. J. Bartlett, J. Chem. Phys. **89**, 3401 (1988).

[88] J. D. Watts and R. J. Bartlett, J. Chem. Phys. **93**, 6104 (1990).

[89] G. E. Scuseria and H. F. Schaefer, Chem. Phys. Lett. **152**, 382 (1988).

[90] See Appendix A for supplementary coupled-cluster diagnostics, focal point tables, vibrational frequencies, and IR intensities.

[91] D. E. Woon and T. H. Dunning, J. Chem. Phys. **103**, 4572 (1995).

[92] D. Jayatilaka and T. J. Lee, J. Chem. Phys. **98**, 9734 (1993).

[93] W. J. Lauderdale, J. F. Stanton, J. Gauss, J. D. Watts, and R. J. Bartlett, Chem. Phys. Lett. **187**, 21 (1991).

[94] P. J. Knowles, J. S. Andrews, R. D. Amos, N. C. Handy, and J. A. Pople, Chem. Phys. Lett. **186**, 130 (1991).

[95] C. Murray and E. R. Davidson, Chem. Phys. Lett. **187**, 451 (1991).

[96] T. J. Lee and D. Jayatilaka, Chem. Phys. Lett. **201**, 1 (1993).

[97] C. L. Janssen, I. B. Nielson, M. L. Leininger, E. T. Seidl, and M. E. Colvin, MPQC 2.1.4 (Sandia National Laboratories, Livermore, California, 2002).

[98] D. Feller, J. Chem. Phys. **98**, 7059 (1993).

[99] T. Helgaker, W. Klopper, H. Koch, and J. Noga, J. Chem. Phys. **106**, 9639 (1997).

[100] W. J. Hehre, R. Ditchfield, L. Radom, and J. A. Pople, J. Am. Chem. Soc. **92**, 4796 (1970).

[101] D. L. Gray and A. G. Robiette, Mol. Phys. **37**, 1901 (1979).

[102] N. C. Handy, Y. Yamaguchi, and H. F. Schaefer, J. Chem. Phys. **84**, 4481 (1986).

[103] A. G. Ioannou, R. D. Amos, and N. C. Handy, Chem. Phys. Lett. **251**, 52 (1996).

[104] N. C. Handy and A. M. Lee, Chem. Phys. Lett. **252**, 425 (1996).

[105] W. Kutzelnigg, Mol. Phys. **90**, 909 (1997).

[106] S. A. Perera and R. J. Bartlett, Chem. Phys. Lett. **216**, 606 (1993).

[107] K. Balasubramanian, *Relativistic Effects in Chemistry: Part A, Theory and Techniques*. (Wiley, New York, 1997).

[108] K. Balasubramanian, *Relativistic Effects in Chemistry: Part B, Applications*. (Wiley, New York, 1997).

[109] R. D. Cowan and D. C. Griffin, J. Opt. Soc. Am. **66**, 1010 (1976).

[110] G. Tarczay, A. G. Császár, W. Klopper, and H. M. Quiney, Mol. Phys. **99**, 1769 (2001).

[111] T. D. Crawford, C. D. Sherrill, E. F. Valeev, J. T. Fermann, M. L. Leininger, R. A. King, S. T. Brown, C. L. Janssen, E. T. Seidl, Y. Yamaguchi, W. D. Allen, B. Kellogg, and H. F. Schaefer, PSI 3 (2002).

[112] J. D. Watts, J. Gauss, and R. J. Bartlett, Chem. Phys. Lett. **200**, 1 (1992).

[113] Gaussian 98, Revision A.9, M. J. Frisch, G. W. Trucks, H. B. Schlegel, G. E. Scuseria, M. A. Robb, J. R. Cheeseman, V. G. Zakrzewski, J. A. Montgomery, Jr., R. E. Stratmann, J. C. Burant, S. Dapprich, J. M. Millam, A. D. Daniels, K. N. Kudin, M. C. Strain, O. Farkas, J. Tomasi, V. Barone, M. Cossi, R. Cammi, B. Mennucci, C. Pomelli, C. Adamo, S. Clifford, J. Ochterski, G. A. Petersson, P. Y. Ayala, Q. Cui, K. Morokuma, D. K. Malick, A. D. Rabuck, K. Raghavachari, J. B. Foresman, J. Cioslowski, J. V. Ortiz, A. G. Baboul, B. B. Stefanov, G. Liu, A. Liashenko, P. Piskorz, I. Komaromi, R. Gomperts, R. L. Martin, D. J. Fox, T. Keith, M. A. Al-Laham, C. Y. Peng, A. Nanayakkara, M. Challacombe, P. M. W. Gill, B. Johnson, W. Chen, M. W. Wong, J. L. Andres, C. Gonzalez, M. Head-Gordon, E. S. Replogle, and J. A. Pople, Gaussian, Inc., Pittsburgh PA, 1998.

[114] The CBS extrapolated CCSD contributions when utilizing ROHF-MBPT and OPT2 energies were –1.821 and –1.469 kcal/mol for *Z*-*n*-C_4H_3, respectively, and –1.913 and –1.367 kcal mol^{-1} for *E*-*n*-C_4H_3, respectively.

[115] H. L. Woodcock, H. F. Schaefer, and P. R. Schreiner, J. Phys. Chem. A **106**, 11923 (2002).

[116] D. M. Ceperley and B. J. Alder, Phys. Rev. Lett. **45**, 566 (1980).

[117] D. M. Ceperley, in *Recent Progress in Many-Body Theories*, edited by J. G. Zabolitzky, M. de Llano, M. Fortes, and J. W. Clark (Springer, Berlin, 1981), pp. 262.

[118] B. J. Alder, D. M. Ceperley, and P. J. Reynolds, J. Phys. Chem. **86**, 1200 (1982).

[119] P. J. Reynolds, D. M. Ceperley, B. J. Alder, and W. A. Lester Jr., J. Chem. Phys. **77**, 5593 (1982).

[120] J. B. Anderson, in *Reviews in Computational Chemistry*, edited by K. B. Lipkowitz and D. B. Boyd (Wiley, New York, 1999), Vol. 13, pp. 119.

[121] K. Raghavachari, D. L. Strout, G. K. Odom, G. E. Scuseria, J. A. Pople, B. G. Johnson, and P. M. W. Gill, Chem. Phys. Lett. **214**, 357 (1993).

[122] S. Sokolova, A. Lüchow, and J. B. Anderson, Chem. Phys. Lett. **323**, 229 (2000).

[123] S. Grimme and C. Mück-Lichtenfeld, ChemPhysChem **2**, 207 (2002).

[124] J. D. Cox and G. Pilcher, *Thermochemistry of Organic and Organometallic Compounds*. (Academic Press, London, 1970).

125 The fundamental relationships, devoid of embedded empirical data, determined in our theoretical study are as follows: $\Delta_f H_0^\circ$(**1**) = $\Delta_f H_0^\circ$(propene) + $\Delta_f H_0^\circ$(propyne) – $\Delta_f H_0^\circ$(ethane) + 0.12 kcal mol^{-1}; $\Delta_f H_0^\circ$(**6**) = 2 $\Delta_f H_0^\circ$(propene) – $\Delta_f H_0^\circ$(ethane) – 2.94 kcal mol^{-1}; $\Delta_f H_0^\circ$(**4**) = $\Delta_f H_0^\circ$(1-butene-3-yne) + $\Delta_f H_0^\circ$(methyl) – $\Delta_f H_0^\circ$(methane) – 3.20 kcal mol^{-1}; $\Delta_f H_0^\circ$(**9**) = $\Delta_f H_0^\circ$(1,3-butadiene) + $\Delta_f H_0^\circ$(methyl) – $\Delta_f H_0^\circ$(methane) – 3.22 kcal mol^{-1}; $\Delta_f H_0^\circ$(**2**) = $\Delta_f H_0^\circ$(**4**) + 11.80 kcal mol^{-1}; $\Delta_f H_0^\circ$(**3**) = $\Delta_f H_0^\circ$(**4**) + 11.86 kcal mol^{-1}; $\Delta_f H_0^\circ$(**7**) = $\Delta_f H_0^\circ$(**9**) + 10.69 kcal mol^{-1}; $\Delta_f H_0^\circ$(**8**) = $\Delta_f H_0^\circ$(**9**) + 11.31 kcal mol^{-1}.

126 R. J. Kee, F. M. Rupley, and J. A. Miller, The Chemkin Thermodynamic Data Base, Sandia Technical Report SAND87-8215B, UC-4, Sandia National Laboratories, Livermore, CA (1994).

127 M. Frenklach and H. Wang, *Soot Formation in Combustion: Mechanisms and Models*. (Springer-Verlag, Heidelberg, 1994).

128 J. A. Miller, M. J. Pilling, and J. Troe, Proc. Combust. Inst. **30**, in press (2004).

129 M. W. Chase, *NIST-JANAF Thermochemical Tables*, 4th ed. (1998).

130 J. D. Cox, D. D. Wagman, and V. A. Medvedev, *CODATA Key Values for Thermodynamics*. (Hemisphere Publishing Corp., New York, 1989).

131 L. V. Gurvich, I. V. Veyts, and C. B. Alcock, *Thermodynamic Properties of Individual Substances*, Fourth ed. (Hemisphere Pub. Co., New York, 1989).

132 M. Frenkel, K. N. Marsh, R. C. Wilhoit, G. J. Kabo, and G. N. Roganov, *Thermodynamics of Organic Compounds in the Gas State*. (Thermodynamics Research Center, College Station, TX, 1994).

CHAPTER 4

THERMOCHEMISTRY OF KEY SOOT FORMATION INTERMEDIATES: ISOMERS OF C_3H_3[1]

[1] S. E. Wheeler, K. A. Robertson, W. D. Allen, H. F. Schaefer, Y. J. Bomble, and J. F. Stanton. To be submitted to the Journal of Chemical Physics.

4.1 ABSTRACT

Accurate standard enthalpies of formation for allene, propyne, and four C_3H_3 isomers important in the formation of soot during combustion have been determined through systematic extrapolations of *ab initio* energies within the focal point method of Allen and co-workers. Further corrections have been applied for zero-point vibrational energy and core-valence correlation, non-Born-Oppenheimer, and relativistic effects. Electron correlation has been accounted for through second-order Z-averaged perturbation theory (ZAPT2) and restricted open-shell coupled cluster theory through full triple excitations [ROCCSD, ROCCSD(T), and ROCCSDT] utilizing the correlation-consistent hierarchy of basis sets, cc-pV*X*Z (*X* = D,T,Q,5,6). All geometries were fully optimized using ROCCSD(T) with the TZ(2d1f,2p1d) basis set. Our recommended values for the enthalpies of formation are as follows: $\Delta_f H_0^\circ$(propargyl) = 84.7, $\Delta_f H_0^\circ$(1-propynyl) = 126.6, $\Delta_f H_0^\circ$(cycloprop-1-enyl) = 125.7, $\Delta_f H_0^\circ$(cycloprop-2-enyl) = 117.3, $\Delta_f H_0^\circ$(allene) = 47.2, and $\Delta_f H_0^\circ$(propyne) = 46.2 kcal mol^{-1}. The corresponding energies for C_3H_3 isomers 1-propynyl, cycloprop-1-enyl, and cycloprop-2-enyl, relative to propargyl radical, are 41.9, 41.0, and 32.7 kcal mol^{-1}. These isomerization energies are roughly 1 kcal mol^{-1} larger than previous coupled cluster predictions and several kcal mol^{-1} below those previously predicted using density functional theory.

4.2 INTRODUCTION

Unraveling the complex mechanism of soot formation during pyrolysis stands at the forefront of current combustion research. A primary focus concerns the formation and growth of polycyclic aromatic hydrocarbons (PAHs), which are the primary precursors to soot particles. The rate-limiting step in PAH formation is thought to be the formation of the first aromatic ring (benzene or naphthalene) from smaller precursors.[1-3] Although both C3 and C4 species have

been hypothesized to play important roles (via the so-called odd- and even-carbon-atom pathways),[3] it is now generally accepted that the dominant reaction leading to the formation of benzene during combustion is the self-reaction of the propargyl radical (2-propynyl, **1)**.[1]

Several other isomeric forms of C_3H_3 are also energetically accessible during combustion (see Fig. 4.1), including the 1-propynyl (**2**), cycloprop-1-enyl (**3**), and cycloprop-2-enyl (**4**) radicals, though propargyl is universally accepted to be the lowest energy isomer. Pathways connecting these C_3H_3 isomers have been explored extensively using density functional theory (DFT),[4-6] and details of the associated isomerization energy surface is thought to play a vital role in the lifetime and kinetics of the formation of propargyl radical during combustion. Additional C_3H_3 isomers can also be formed (2-propen-1-yl-3-ylidene and 1-propen-1-yl-3-ylidene), though these alternative isomers are kinetically unstable with respect to isomerization to structures **1** – **4**.[4,6]

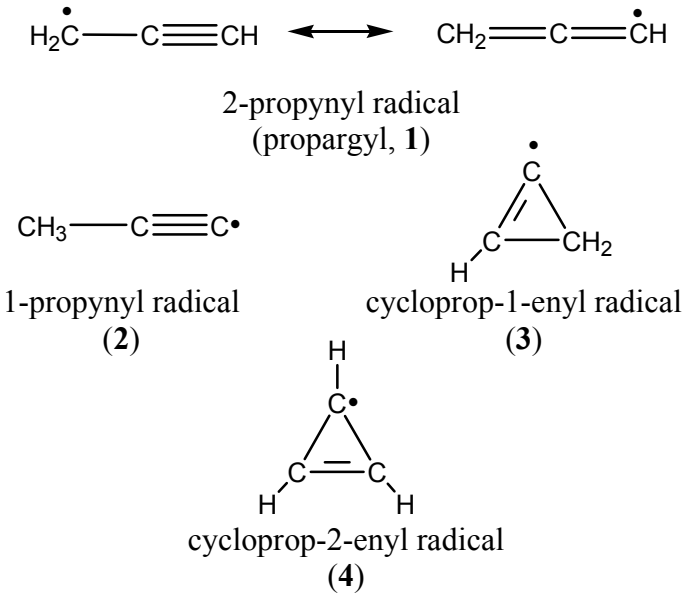

Figure 4.1 Canonical Lewis structures for the four C_3H_3 isomers considered.

Despite the central role these C_3H_3 isomers play in the formation of benzene during combustion, there are few purely *ab initio* predictions of their relative energies available in the literature. While there have been numerous attempts to pinpoint these energies using theory, previous studies have almost universally relied on DFT for the optimization of geometries. However, DFT, and in particular the popular B3LYP functional, is known to sometimes perform poorly for unsaturated hydrocarbon radicals and was shown to yield qualitatively incorrect geometries for the closely related *i*-C_4H_3 radical in previous work from our group.[7]

In a series of papers based on 6-311+G(3df,2p) RCCSD(T) (restricted coupled cluster theory including single, double, and perturbative triple excitations)[8] energies computed at 6-311G(d,p) B3LYP optimized geometries, Mebel and co-workers[5,6] predicted energies of 40.1, 40.1, and 31.3 kcal mol^{-1} for 1-propynyl (**2**), cycloprop-1-enyl (**3**), and cycloprop-2-enyl (**4**) radicals relative to propargyl, respectively. This predicted energy for 1-propynyl radical was in excellent agreement with the experimentally determined value of 40 ± 3 kcal mol^{-1} due to Robinson, Polak, Bierbaum, DePuy, and Lineberger.[9] Energies were also computed using 6-311G(d,p) B3LYP, resulting in separations consistently several kcal mol^{-1}, higher than the RCCSD(T) values: 1-propynyl at 46.0, cycloprop-1-enyl at 44.2, and cycloprop-2-enyl at 34.5 kcal mol^{-1}. Previously, Vereecken, Pierloot, and Peters[4] had reported similar work including energies computed using both 6-31G(d,p) B3LYP and complete active space second-order perturbation theory (CASPT2) with an ANO-type basis set. The CASPT2 predicted relative energies, computed at the B3LYP optimized geometries, were 41.3, 43.7, and 35.7 kcal mol^{-1} for **2**, **3**, and **4**, respectively.

Given the prominent role of propargyl radicals in the formation of benzene in most models of PAH formation,[1,3] any effort to fully characterize soot formation pathways must

include reliable enthalpies of formation of these low-lying C_3H_3 radicals. A representative list of previously determined enthalpies of formation for propargyl radical is included in Table 4.1 A review by Tsang[10] in 1996 of single-pulse shock-tube[11,12] and very low-pressure pyrolysis[13,14] studies led to an estimation of $\Delta_f H^\circ_{298}$ (propargyl) = 81.0 ± 1 kcal mol^{-1}. A previous review of the literature by McMillen and Golden[15] yielded an estimate of $\Delta_f H^\circ_{298}$ (propargyl) = 81.5 ± 2 kcal mol^{-1}. In a more recent experimental study, Robinson *et al.*[9] derived the enthalpy of formation of the propargyl radical using negative ion photoelectron spectroscopy, gas phase acidity measurements, and a negative ion thermochemical cycle. Although this technique bears little resemblance to the earlier studies, the estimated value of 82.5 ± 3 kcal mol^{-1} at 298 K is in reasonable agreement with the earlier experiments. In 1994, Roth, Hopf, and Horn[16] determined an enthalpy of formation at 0 K of 85.2 kcal mol^{-1} based on a single-pulse shock-tube study. While this value is within the error bars of the results of Robinson *et al.*,[9] it is considerably higher than and outside of the error estimates of the older experimental results, even accounting for thermal corrections.

Harkless and Lester[17] predicted the enthalpy of formation for propargyl radical via an atomization reaction using diffusion Monte Carlo (DMC), predicting values of 81.5 ± 1.3 and 82.5 ± 0.6 kcal mol^{-1} at 298 K using two different effective core potentials. Harkless and Lester also used the B3LYP and B3PW91 DFT functionals, paired with the 6-311G** basis set and atomization reactions, to predict enthalpies of formation (298 K) of 84.0 and 79.9 kcal mol^{-1}, respectively. Likewise, Saeys, Reyniers, Marin, Speybroeck, and Waroquier assessed[18] the accuracy of the CBS-QB3 method and the B3LYP functional in predicting enthalpies of formation via atomization reactions for a large set of test systems, including propargyl radical. Both methods were seen to overshoot previous theoretical and experimental values, yielding

enthalpies of formation (298 K) of 85.3, 86.8, and 85.9 kcal mol^{-1} at the CBS-QB3, 6-31G(d) B3LYP, and 6-311G(d,p) B3LYP levels of theory, respectively. Melius reported an estimate of $\Delta_f H^\circ_{298}$ (propargyl) = 83.6 ± 5.8 kcal mol^{-1} based on the bond-additivity-corrected fourth-order Møller-Plesset (BAC-MP4) method.

Table 4.1 Representative enthalpies of formation ($\Delta_f H^\circ_0$, kcal mol^{-1}) for propargyl radical.

$\Delta_f H^\circ_0$	Method	Reference
80.7[a]	Single-pulse shock-tube study	11
82.7[a]	Single-pulse shock-tube study	12
86[a]	Iodine catalyzed isomerization	19
82[a]	Positive ion thermochemical cycle	20
81.5 ± 1.0[a]	Very low-pressure pyrolysis	13,14
81.5 ± 2.0[a]	Review of previous experiments	15
81.0 ± 1.0[a]	Review of previous experiments	10
85.2	Single-pulse shock-tube study	16
82.5 ± 3.0[a]	Negative ion thermochemical cycle	9
83.6 ± 5.8[a]	BAC-MP4	21
81.5 ± 1.3[a,c]	DMC	17
82.5 ± 0.6[a,c]	DMC	17
84.0[a]	6-311G** B3LYP via atomization energy	17
79.9[a]	6-311G** B3PW91 via atomization energy	17
85.3[a]	CBS-QB3	18
86.8[a]	6-31G(d) B3LYP	18
85.9[a]	6-311G(d,p) B3LYP	18
83.8[a,b]	G3 theory	6
84.9[a,b]	ROCCSD(T)	6
84.3[a,b]	UCCSD(T)	6
84.1	G3 theory via atomization energy	6
84.7	Focal point extrapolation	d

[a] Enthalpy of formation at 298 K.
[b] Average enthalpy obtained using six isodesmic reactions.
[c] DMC results are computed using two different effective core potentials.
[d] Present work, averaged enthalpy determined from three formation reactions.

The most thorough theoretical investigation of the enthalpy of formation of C_3H_3 isomers is due to Nguyen, Mebel, and Kaiser,[6] who employed a series of isodesmic reactions coupled with G3 theory and coupled-cluster energies computed at B3LYP geometries to predict the enthalpies of formation for all four low-lying C_3H_3 isomers. The result was a consistent set of

enthalpies, with average recommended values for propargyl (298 K) of 83.8, 84.9, and 84.3 kcal mol^{-1} from G3 theory, RCCSD(T), and ROCCSD(T), respectively.

In the present work we seek to dispel any lingering uncertainties in C_3H_3 isomerization energies and enthalpies of formation utilizing large triple-ζ quality basis sets and coupled cluster methods to compute reliable geometries, paired with focal point extrapolations to predict accurate relative energies and enthalpies of formation at the complete basis set (CBS) limit. Along the way, we also predict accurate enthalpies of formation for allene and propyne.

4.3. Theoretical Methods

Precise standard enthalpies of formation and relative energies have been computed via the focal-point extrapolation scheme of Allen and co-workers.[22-27] Geometries were optimized using coupled cluster singles and doubles theory (CCSD)[28-31] appended with perturbative inclusion of connected triple excitations [CCSD(T)],[32-35] freezing the carbon 1*s* orbitals. Semicanonical orbitals were utilized in all open-shell CCSD(T) computations.[36] Reference electronic wave functions were determined using spin-restricted open-shell Hartree-Fock theory (ROHF), eschewing the possibility of spurious energetic predictions resulting from a spin-contaminated reference. The geometry optimizations utilized a TZ(2d1f,2p1d) basis,[7,37] comprising the Dunning C(10s6p/5s3p) and unscaled H(5s/3s) triple-ζ segmented *sp* contractions[38] augmented with correlation optimized[39] polarization functions [α_d(C) = 0.318, 1.097; α_f(C) = 0.761; α_p(H) = 0.388, 1.407; α_d(H) = 1.057]. All polarization manifolds contained only pure spherical harmonics. The geometry optimizations were carried out by analytic gradients using the ACES II program package.[40]

In the focal point scheme, the correlation-consistent basis sets of Dunning[39] are utilized to achieve systematic dual one- and *n*-particle expansions. Electron correlation is treated through

second-order perturbation theory, and primarily by coupled cluster theory including single and double excitations (CCSD)[28-31] and either perturbative [CCSD(T)][32-35] or full treatments (CCSDT)[41-44] of triple excitations. The first component of the energy for the focal point procedure was obtained using spin restricted Hartree-Fock theory. Likewise, spin restricted analogs[31,36] of CCSD, CCSD(T), and CCSDT, were employed, denoted by ROCCSD, ROCCSD(T), and ROCCSDT, respectively. Core-valence correlation contributions were evaluated through a second set of focal point extrapolations, available as supplementary material,[45] utilizing the cc-pCV*X*Z family of basis sets.[46] All energies for the focal point analyses were computed at the frozen-core TZ(2d1f,2p1d) ROCCSD(T) optimized geometries described above. Examination of the T_1 and T_2 amplitudes for the converged CCSD wave functions for all structures considered did not reveal any lurking multireference character, providing justification for the use of single-reference methods.

For spin-restricted open-shell Møller-Plesset perturbation theory there is some ambiguity in the choice of partitioning of the electronic Hamiltonian, resulting in a number of unique formulations in the literature. An analysis[47] of results from Z-averaged perturbation theory (ZAPT)[48] has suggested that the convergence properties of ZAPT*n* energies are similar to the popular restricted Møller-Plesset (RMP)[49,50] theory, but without the added computational expense associated with the use of different orbitals for different spins. Furthermore, comparison of predicted equilibrium bond lengths and harmonic vibrational frequencies has indicated that at second and fourth order, ZAPT performs at least as well as RMP theory. In light of the computational advantages offered by ZAPT theory and the availability of the efficient, parallel implementation in MPQC,[51] ZAPT2 energies were utilized for the leading contribution to the correlation energy in all focal point analyses involving open-shell species.

All correlated energy computations involved the freezing of the carbon 1*s* orbitals, except where noted otherwise for the explicit evaluation of the core correlation contribution. The functional form for the basis set extrapolation of the Hartree-Fock energies was that of Feller,[52]

$$E_{HF} = a + be^{-cX}, \tag{4.1}$$

while the correlation energies were extrapolated via[53]

$$E_{corr} = a + bX^{-3}. \tag{4.2}$$

The focal point scheme was utilized to evaluate relative energies of three low-lying C_3H_3 isomers, relative to propargyl radical, and the energy of allene relative to propyne. The enthalpy of formation (0 K) for the propargyl radical was determined through the reactions

$$H_2CCCH_2 + CH_3 \rightarrow HCCCH_2 + CH_4, \tag{4.3}$$

$$H_2CCCH_2 \rightarrow HCCCH_2 + H, \tag{4.4}$$

and

$$CH\ (^2\Pi) + HCCH \rightarrow HCCCH_2, \tag{4.5}$$

of which (4.3) is isodesmic.[54] Enthalpies of formation of allene and propyne were also predicted, using the focal point procedure paired with the isodesmic reactions

$$H_2C{=}CH_2 + H_2C{=}CH_2 \rightarrow H_2CCCH_2 + CH_4 \tag{4.6}$$

and

$$HC{\equiv}CH + H_3C{-}CH_3 \rightarrow HCCCH_3 + CH_4. \tag{4.7}$$

Experimental enthalpies of formation were adopted for $^2\Pi$ CH, CH_3, CH_4, acetylene, ethane, and ethene, as given in Table 4.2. Enthalpies of formation from the Active Thermochemical Tables (ATcT) of Ruscic *et al.*[55] have been utilized, as these constitute the most comprehensive, consistent set of experimental enthalpies available. An experimental r_e bond length was employed for CH_4 (1.085 Å),[56] while an equilibrium bond length of 1.0763 Å,

obtained at the all-electron cc-pCVQZ ROCCSD(T) level of theory, was utilized for CH_3. Geometric structures for acetylene, ethene, and ethane are included in Fig. 4.2, optimized at the frozen-core TZ(2d1f,2p1d) CCSD(T) level of theory. Likewise, an optimized bondlength of 1.1213 Å was used for CH ($^2\Pi$).

Table 4.2 Standard enthalpies of formation ($\Delta_f H_0^\circ$, kcal mol^{-1}) for relevant species.[a]

Species	$\Delta_f H_0^\circ$	Uncertainty
H(^2S)	51.63	0.00
CH ($^2\Pi$)	141.78	0.09
CH_3	35.84	0.03
CH_4	–15.91	0.01
C_2H_2 (acetylene)	56.54	0.15
C_2H_4 (ethene)	14.64	0.05
C_2H_6 (ethane)	–16.24	0.05
C_3H_4 (allene)[b]	47.15	–
C_3H_4 (propyne)[b]	46.23	–

[a] Reference enthalpies of formation are from the ATcT.[57]
[b] Focal-point extrapolated value, this work.

Extrapolated energies were further corrected via inclusion of the diagonal Born-Oppenheimer correction (DBOC),[58-61] which constitutes the first-order perturbative correction to the Born-Oppenheimer energy, and the mass-velocity and one-electron Darwin scalar relativistic terms.[62-66] The DBOC was evaluated at the cc-pVTZ ROHF level of theory using PSI3,[67] while the relativistic effects were computed at the cc-pCVTZ ROCCSD(T) level of theory using ACES II.[40] Harmonic vibrational frequencies were evaluated at the TZ(2d1f,2p1d) ROCCSD(T) level of theory by finite differences of gradients[36,68] using ACES II, with frequencies and IR intensities provided as supplementary material. The HF, CCSD, and CCSD(T) energies were computed using MOLPRO,[69] while the ZAPT2 and CCSDT energies were evaluated using MPQC 2.1[51] and ACES II,[40] respectively.

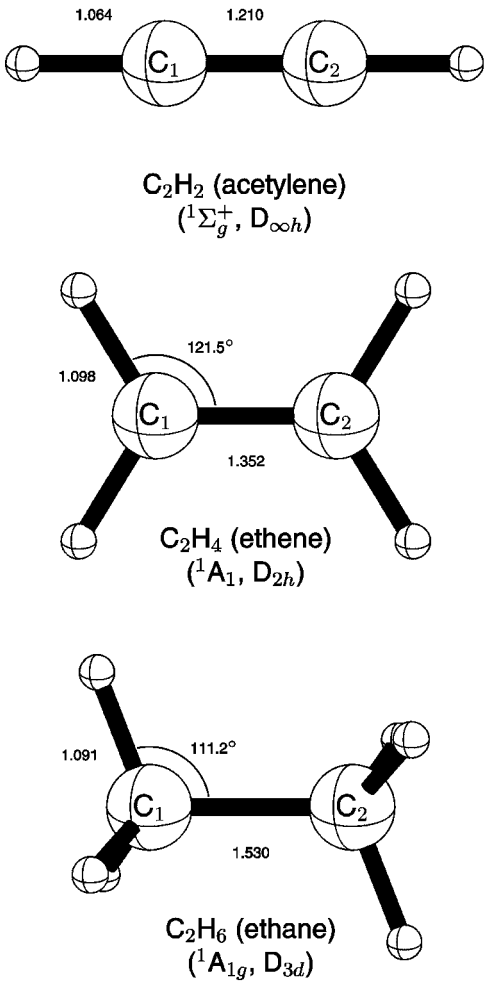

Figure 4.2 Optimized geometries of acetylene, ethene, and ethane, computed at the TZ(2d1f,2p1d) CCSD(T) level of theory.

4.4 GEOMETRIC STRUCTURES

Optimized structures for allene, propyne, and the four C_3H_3 isomers considered are included in Figs. 4.3 and 4.4, obtained at the frozen-core TZ(2d1f,2p1d) ROCCSD(T) level of theory. The propargyl radical (**1**) exhibits C_{2v} symmetry, with a $^2B_1$ electronic state (with the *z*-axis along the C–C–C framework and the molecule in the *yz*-plane). Compared to the CCSD(T) optimized structures (Fig. 4.4), previously reported[4-6] B3LYP geometries for propargyl are seen

to underestimate the length of the C_1–C_2 bond by between 0.02 and 0.04 Å, with the extent of underestimation depending on the basis set employed. The contraction of the C_1–C_2 distance in the B3LYP geometry corresponds to an enhanced contribution from the cumulenic resonance form of propargyl (see Fig. 4.1) relative to the acetylenic form, reflective of known shortcomings of some DFT functionals for describing acetylenic and cumulenic systems.[70] Moreover, this bond-length contraction in the B3LYP optimized structure will artificially increase any *ab initio* energy computed at this geometry, potentially altering predicted relative energies and enthalpies of formation. The B3LYP functional reproduces the TZ(2d1f,2p1d) ROCCSD(T) optimized C_2–C_3 bond length, fortuitously giving agreement to within 0.001 Å when paired with the 6-31G(d,p) basis set. Comparison of the propargyl radical structure with the parent allene structure (Fig. 4.3) reveals a lengthening of the C_1–C_2 bond length by 0.07 Å and contraction of the C_2–C_3 distance by 0.09 Å. Alternatively, viewing propargyl radical as arising from the abstraction of a methyl hydrogen from propyne (Fig. 4.3), the C_1–C_2 bond length exhibits a decrease of 0.09 Å accompanied by a much smaller increase in the C_2–C_3 bond length of 0.02 Å.

For the C_{3v}-symmetric 1-propynyl radical (**2**), there are two low-lying doublet electronic states, resulting from electron configurations in which the unpaired electron occupies either a π-type orbital or a non-bonding orbital of a_1 symmetry. Single occupation of one of the degenerate C–C π-orbitals yields a ^{2}E electronic state, so this structure will distort due to the Jahn-Teller effect to yield bent ^{2}A′ and ^{2}A″ structures. Indeed, Vereeken *et al.* reported[4] a bent ^{2}A′ ground state for 1-propynyl radical at the 6-31G(d,p) B3LYP level of theory. However, Mebel *et al.* write[5] that at the 6-311+G(3df,2p) CCSD(T) level of theory the C_s structure is 1.8 kcal mol^{-1} higher in energy than the $^2A_1$ C_{3v} structure. Previously, Bauschlicher and Langhoff[71] reported

that the ^2E state was some 9.7 kcal mol^{-1} lower than the $^2A_1$ state using Hartree-Fock theory with a double-ζ basis set, though they did not report any structures distorted from C_{3v} symmetry.

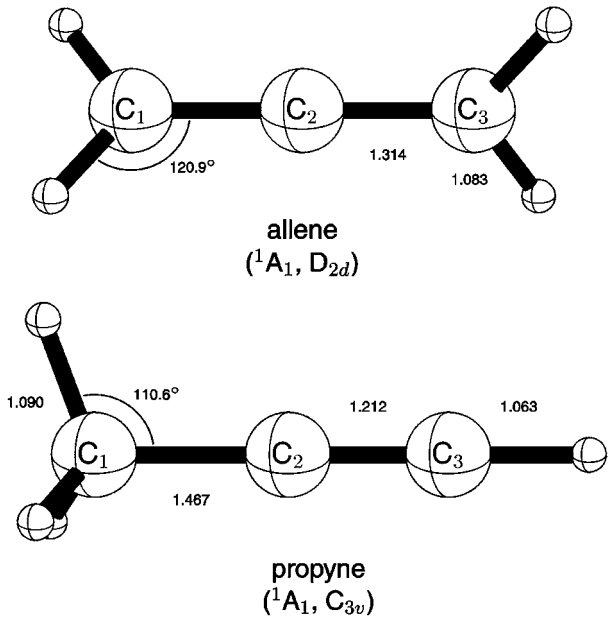

Figure 4.3 Optimized geometries of allene and propyne, computed at the TZ(2d1f,2p1d) ROCCSD(T) level of theory.

The C_{3v}-symmetric 1-propynyl radical poses a difficulty for typical electronic structure theory packages, in which molecular orbitals are constructed to transform as irreducible representations of the largest Abelian subgroup of the full molecular point-group [C_s symmetry in the case of structure **2**]. The problem is that the a_1-symmetric non-bonding orbital and in-plane π-orbital transform as the same irreducible representation of the C_s point group (a′), and some mixing of the two can occur during the SCF procedure, resulting in a non-degeneracy of the in-plane and out-of-plane π-orbitals and an artifactual lowering of the Hartree-Fock energy. However, in ACES II one can constrain the ROHF orbitals to transform as irreducible representations of the full point group (C_{3v}), resulting in orbitals that exhibit the proper degeneracies and full symmetry of the molecular framework. Geometries have been optimized

using CCSD for the $^2A_1$ state and equation of motion CCSD (EOM-CCSD)[72] for the ^2E state, with the cc-pVDZ basis set[39] and based on Hartree-Fock orbitals possessing C_{3v} symmetry. The results indicate that the $^2A_1$ equilibrium geometry is 7.2 kcal mol^{-1} *below* the ^2E C_{3v} stationary point. This is analogous to the $^2\Sigma^+$ ground electronic state of C_2H, though it conflicts with the Hartree-Fock results of Bauschlicher and Langhoff.[71] The Jahn-Teller distortion of the ^2E state will result in a lowering of energy upon bending of the C–C–C framework, resulting in a $^2A'$ state possibly lying below the $^2A_1$ state. Preliminary results[73] indicate that this is not the case, and that the C_{3v}-symmetric $^2A_1$ structure (Fig. 4.4) is indeed the global minimum. As such, the TZ(2d1f,2p1d) ROCCSD(T) $^2A_1$ geometry was used in all subsequent computations. Comparison of this optimized structure to the parent compound (propyne), we see that there is negligible change in geometry upon removal of the acetylenic hydrogen, indicative of the non-bonding nature of the singly occupied a_1 orbital.

The optimized CCSD(T) structures for cyclic isomers **3** and **4** are quite similar to previously reported B3LYP geometries,[4-6] with all deviations in bond lengths less than 0.01 Å. Cycloprop-1-enyl radical (**3**) exhibits a remarkably long C_1–C_3 bond length of 1.61 Å, presumably an indication of the large degree of strain in this unconventional cyclic radical. The C_1–C_3–C_2 bond angle of 48.9° is also quite notable. The cycloprop-2-enyl radical distorts to from D_{3h} symmetry due to the Jahn-Teller effect,[74,75] yielding a $^2A'$ electronic state and the C_s global minimum geometry (**4**) displayed in Fig. 4.4. At the frozen-core TZ(2d1f,2p1d) ROCCSD(T) level of theory, the relaxation from D_{3h} to C_s symmetry results in an energy lowering of 14.5 kcal mol^{-1}. Previous theoretical results indicate a small (3–4 kcal mol^{-1}) barrier to pseudorotation, passing through an allylic transition state.[75]

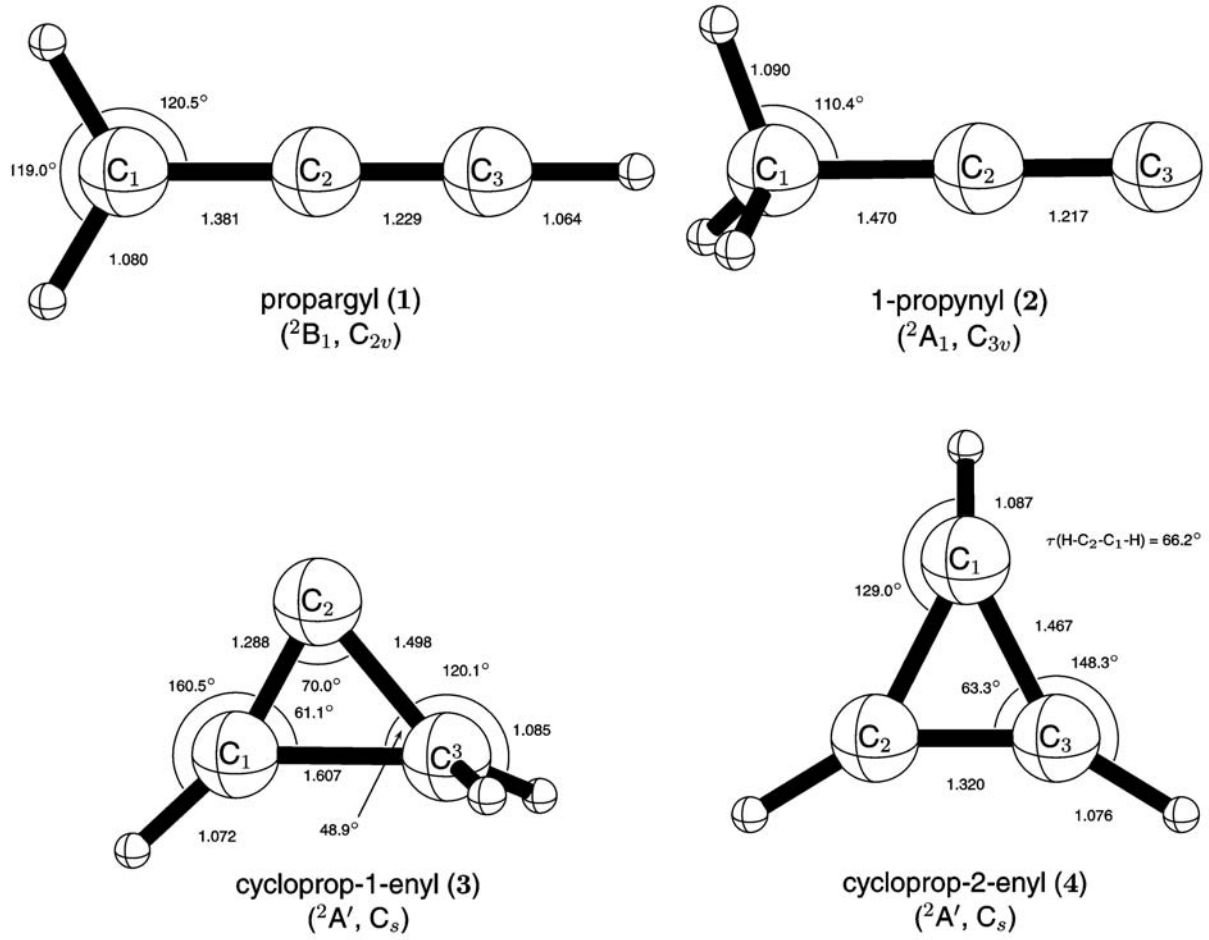

Figure 4.4 Optimized geometries of C_3H_3 isomers, computed at the TZ(2d1f,2p1d) ROCCSD(T) level of theory.

4.5 Isomerization Energies

The valence focal point table for the energy of allene relative to propyne is provided in Table 4.3. The computed energy exhibits excellent convergence with respect to completeness of the one-particle basis for Hartree-Fock and coupled-cluster methods: the cc-pV6Z HF relative energy is within 0.002 kcal mol^{-1} of the extrapolated limit (1.534 kcal mol^{-1}), while the cc-pV5Z CCSD(T) relative energy is within 0.02 kcal mol^{-1} of the extrapolated CCSD(T) limit. The leading contribution to the correlation energy, computed using MP2 theory, exhibits somewhat poorer convergence, with the cc-pV6Z value remaining 0.07 kcal mol^{-1} above the extrapolated

CBS value. Furthermore, the CBS limit MP2 contribution raises the relative energy of allene by nearly 3.4 kcal mol^{-1} to 4.9 kcal mol^{-1}. This effect is cancelled out by the coupled cluster contributions to yield a final valence relative energy of 1.20 kcal mol^{-1}. This failure of MP2 to predict the relative energy of allene and propyne has previously been documented,[70] and is a testament to the importance of the more complete treatment of dynamic correlation provided by coupled cluster methods. The isomerization energy is seen to converge rather slowly with respect to completeness of the *n*-particle basis: at the CBS limit, the correction to the CCSD energy due to the inclusion of connected triple excitations (–0.55 kcal mol^{-1}) is nearly half the size of the final extrapolated valence energy. In light of this slow convergence, the precise determination of the energy of allene relative to propyne will require at least partial inclusion of contributions from connected quadruple excitations via the perturbative CCSDT(Q) method recently introduced by Bomble, Stanton, Kállay, and Gauss.[76]

Table 4.3 Incremental valence focal point table (kcal mol^{-1}) for isomerization of propyne to allene.[a]

Basis Set	ΔE_e[RHF]	+δ[MP2]	+δ[CCSD]	+δ[CCSD(T)]	+δ[CCSDT]	ΔE_e[CCSDT]
Propyne → Allene						
cc-pVDZ	1.081	+3.180	–3.499	–0.271	–0.170	0.320
cc-pVTZ	1.573	+3.139	–3.262	–0.286	[–0.170]	[0.995]
cc-pVQZ	1.571	+3.208	–3.168	–0.309	[–0.170]	[1.133]
cc-pV5Z	1.543	+3.274	–3.148	[–0.345]	[–0.170]	[1.153]
cc-pV6Z	1.536	+3.322	[–3.158]	[–0.361]	[–0.170]	[1.169]
CBS limit	[1.534]	[+3.387]	[–3.172]	[–0.383]	[–0.170]	**[1.197]**
Fit	$a+be^{-cX}$	$a+bX^{-3}$	$a+bX^{-3}$	$a+bX^{-3}$	additive	
Points (X=)	4,5,6	5,6	4,5	3,4		

[a]The symbol δ denotes the increment in the energy difference (ΔE) with respect to the previous level of theory. Bracketed numbers are the result of basis set extrapolations (using the fits denoted in the table), while unbracketed numbers were explicitly computed.

Upon further corrections (see Table 4.4) for zero-point vibrational energy (ZPVE) and non-Born-Oppenheimer, core-valence correlation, and scalar relativistic effects, the final recommended propyne to allene isomerization energy is 0.92 kcal mol^{-1}, with the largest

correction arising from the inclusion of ZPVE effects. The computed harmonic vibrational frequencies are in good agreement with experimental fundamental frequencies for both C_3H_4 isomers with the exception of the C–H stretches.[77] Expectedly, CCSD(T) harmonic frequencies overestimate the experimental C–H stretching fundamentals by 140 ± 10 cm^{-1} for both systems. However, these errors are balanced in propyne and allene and the ZPVE correction to the relative energy calculated from CCSD(T) frequencies (–0.39 kcal mol^{-1}) is only 0.09 kcal mol^{-1} from that derived directly from the experimental frequencies (–0.48 kcal mol^{-1}). As such, the use of a ZPVE derived from the presently computed harmonic frequencies is expected to have only a minor effect on the predicted energy separation.

Table 4.4 Determination of isomerization energies for C_3H_4 and C_3H_3, in kcal mol^{-1}.[a]

Reaction	ΔE_{fp}(V)	Δ_{fp}(core)	ΔZPVE	ΔDBOC	ΔRel	ΔE_0(final)
propyne → allene	1.20	+0.10	–0.39	+0.02	–0.01	**0.92**
propargyl → **2**	39.86	+0.26	+1.78	–0.02	+0.01	**41.88**
propargyl → **3**	39.76	+0.51	+0.76	+0.02	–0.05	**41.00**
propargyl → **4**	31.30	+0.22	+1.10	–0.01	+0.04	**32.65**

[a] ΔE_{fp}(V) = focal point energy difference from Tables 4.3 and 4.5; Δ_{fp}(core) = focal-point core correlation correction from Tables B1 and B2; ΔZPVE = zero-point vibrational energy correction [TZ(2d1f,2p1d) ROCCSD(T)]; ΔDBOC = diagonal Born-Oppenheimer correction (cc-pVTZ ROHF); ΔRel = scalar relativistic corrections [cc-pCVTZ ROCCSD(T)]; ΔE_0(final) = sum of previous five columns.

The most robust theoretical prediction of the energy of allene relative to propyne in the literature is that of Feller and Dixon,[78] who provided extrapolated CCSD(T) atomization energies appended with corrections for core-valence correlation, scalar relativistic effects, and a 'high order' correction designed to account for shortcomings in the CCSD(T) method relative to full configuration interaction. The highest-level results in that work, arising from an aug-cc-pV(T,Q,5)Z CCSD(T) extrapolation for allene and an aug-cc-pV(D,T,Q)Z extrapolation for propyne, yield an energy splitting of 1.6 kcal mol^{-1}, significantly higher than the present result. However, comparing atomization energies on a more equal footing [using the aug-cc-

pV(D,T,Q)Z CCSD(T) extrapolated values for both allene and propargyl] gives an isomerization energy of 0.8 kcal mol^{-1}, in agreement with our recommended value of 0.92 kcal mol^{-1}. This agreement is perhaps due in part to fortuitous cancellations, however, since the extrapolated valence isomerization energy of Feller and Dixon (1.4 kcal mol^{-1}) is 0.2 kcal mol^{-1} larger than that resulting from the present focal point extrapolation. This difference is largely compensated for by differing ZPVE corrections. Feller and Dixon rely on the average of experimental fundamental frequencies and aug-cc-pVDZ CCSD(T) computed harmonic frequencies to derive a ZPVE correction. However, there is an imbalance of errors relative to experimental frequencies in the aug-cc-pVDZ CCSD(T) predicted frequencies for propyne and allene. The result is that the ZPVE correction for the isomerization energy arising purely from the aug-cc-pVDZ CCSD(T) frequencies is +0.03 kcal mol^{-1}, which, when averaged with the experimental ZPVE correction of –0.48 kcal mol^{-1}, yields a ZPVE correction of only –0.22 kcal mol^{-1}.

More recently, Kobychev *et al*. predicted[79] the energy of allene relative to propyne at a number of levels of theory. Most notably, this isomerization energy was computed using the Gaussian-1 (G1) and G2 composite methods, yielding energies for allene relative to propyne of 0.79 and 0.77 kcal mol^{-1}, respectively. The agreement with the present results is remarkable, given the extensive reliance of the G*n* methods on MP2 energies, since at the CBS limit MP2 theory yields an anomalous isomerization energy of 4.9 kcal mol^{-1}. Very recently, Yu and Muckerman presented[80] results from extrapolated CCSD(T) energies, arriving at a final energy of 1.09 kcal mol^{-1} for allene relative to propyne, in agreement with the present results.

Table 4.5 Incremental valence focal point tables (kcal mol^{-1}) for three isomerization reactions of propargyl radical (**1**).[a]

Basis Set	ΔE_e[ROHF]	+δ[ZAPT2]	+δ[CCSD]	+δ[CCSD(T)]	+δ[CCSDT]	ΔE_e[CCSDT]
Propargyl → 1-propynyl (**2**)[b]						
cc-pVDZ	34.134	–	+2.082	+0.284	–0.103	36.398
cc-pVTZ	35.240	–	+3.575	+0.419	[–0.103]	[39.132]
cc-pVQZ	35.206	–	+3.908	+0.482	[–0.103]	[39.493]
cc-pV5Z	35.249	–	[+4.026]	[+0.504]	[–0.103]	[39.676]
cc-pV6Z	[35.277]	–	[+4.079]	[+0.514]	[–0.103]	[39.759]
CBS limit	[35.280]	–	[+4.151]	[+0.527]	[–0.103]	**[39.855]**
Propargyl → cycloprop-1-enyl (**3**)						
cc-pVDZ	42.552	–5.010	+1.360	–0.912	+0.116	38.106
cc-pVTZ	43.968	–4.996	+1.580	–1.062	[+0.116]	[39.606]
cc-pVQZ	43.985	–4.869	+1.523	–1.068	[+0.116]	[39.687]
cc-pV5Z	44.018	–5.002	[+1.681]	[–1.070	[+0.116]	[39.743]
cc-pV6Z	44.012	[–5.061]	[+1.751]	[–1.071]	[+0.116]	[39.747]
CBS limit	[44.009]	[–5.142]	[+1.847]	[–1.073]	[+0.116]	**[39.758]**
Propargyl → cycloprop-2-enyl (**4**)						
cc-pVDZ	27.704	+1.819	+1.150	+0.221	+0.140	31.035
cc-pVTZ	28.812	+1.630	+0.988	+0.182	[+0.140]	[31.753]
cc-pVQZ	28.747	+1.577	+0.826	+0.199	[+0.140]	[31.489]
cc-pV5Z	28.722	+1.423	[+0.905]	[+0.205]	[+0.140]	[31.394]
cc-pV6Z	28.702	[+1.354]	[+0.939]	[+0.208]	[+0.140]	[31.343]
CBS limit	[28.696]	[+1.260]	[+0.987]	[+0.212]	[+0.140]	**[31.295]**
Fit	$a+be^{-cX}$	$a+bX^{-3}$	$a+bX^{-3}$	$a+bX^{-3}$	additive	
Points (X=)	4,5,6	4,5	3,4	3,4		

[a] See footnote a from Table 4.3 for notation.
[b] For 1-propynyl radical (**2**), the necessity of restricting the molecular orbitals to posses C_{3v} symmetry to properly describe the ground state prohibits us from computing ZAPT2 energies, so they are excluded form the focal point table in this instance. Additionally, we were unable to compute a cc-pV6Z ROHF energy for (**2**), so the points used in this fit were (3,4,5), rather than (4,5,6).

Valence focal point tables for the energies of structures **2**, **3**, and **4** relative to propargyl radical (**1**) are provided in Table 4.5. Due to the unavailability of programs capable of computing ZAPT2 energies that are also capable of straightforwardly restricting the Hartree-Fock orbitals to transform as irreducible representations of the C_{3v} point group (see Sec. 4.4), the leading correlation contribution in the focal point extrapolation for the energy of 1-propynyl radical comes from CCSD energies. However, the omission of ZAPT2 energies in this case should have a negligible effect on the final extrapolated value, since we were able to compute CCSD energies with up to the cc-pVQZ basis, providing a sound basis for extrapolation to the

CBS limit without relying on larger-basis corrections from ZAPT2 energies. Similarly, in this case the CBS limit Hartree-Fock relative energy was extrapolated from cc-pVTZ, cc-pVQZ, and cc-pV5Z ROHF energies, since we were unable to compute an ROHF energy using the cc-pV6Z basis set for 1-propynyl radical. Again, however, this should have little bearing on the final predicted relative energy, since the explicitly computed cc-pV5Z ROHF energy difference is within 0.03 kcal mol^{-1} of the extrapolated CBS value. The final focal point extrapolated valence energy of 1-propynyl radical (**2**), relative to propargyl, is 39.86 kcal mol^{-1}. The isomerization energy of propargyl to structure **3** exhibits somewhat slow convergence with respect to the inclusion of electron correlation, similar to that observed for allene and propyne. In this case, the CBS limit correction due to the inclusion of triple excitations amounts to 0.957 kcal mol^{-1}, contributing to a total valence isomerization energy of 39.76 kcal mol^{-1}. For structure **4**, we arrive at a well-converged valence energy separation of 31.30 kcal mol^{-1}.

Correcting these extrapolated energies for higher-order effects (see Table 4.4), we arrive at final recommended isomerization energies of 41.88, 41.00, and 32.65 kcal mol^{-1} for 1-propynyl (**2**), cycloprop-1-enyl (**3**), and cycloprop-2-enyl (**4**), respectively. While these final relative energies are on par with the CCSD(T) predictions of Nguyen and co-workers,[6] the present results are 1.8, 0.9, and 1.3 kcal mol^{-1} larger. To discern the sources of these differences, we first compare the 6-311+G(3df,2p) RCCSD(T) energies of Nguyen *et al.*[6] with the extrapolated valence energies from Table 4.4 [$\Delta E_{fp}(V)$], revealing that for each isomer the RCCSD(T) energies of Nguyen *et al.*,[6] computed at B3LYP geometries, underestimate $\Delta E_{fp}(V)$ by 0.85 ± 0.05 kcal mol^{-1}. This difference could be a result of the use of B3LYP geometries [compared to explicitly optimized TZ(2d1f,2p1d) ROCCSD(T) structures], the use of RCCSD(T) [as opposed to ROCCSD(T), as in this work] or through the use of the 6-311+G(3df,2p) basis

set. However, examining the convergence of the ROCCSD(T) energies in Table 4.5, we see that in the worst case (1-propynyl radical), the ROCCSD(T) increment is within 0.1 kcal mol^{-1} of the extrapolated CBS limit even with the moderately-sized cc-pVTZ basis set. This suggests that the major source of difference in valence energies arises from the former two causes, with the use of B3LYP geometries expected to have a far greater impact than the use of RCCSD(T). Examination of the B3LYP ZPVE corrections included in the work of Nguyen *et al*. reveals differences of 0.7, –0.5, and 0.2 kcal mol^{-1} relative to the ZPVE corrections used in the present work. The final remaining errors in the results of Nguyen *et al*. (0.3, 0.5, and 0.3 kcal mol^{-1}), relative to the present values, arise from core-valence correlation, relativistic, and non-Born-Oppenheimer effects, with the inclusion of core-valence correlation the major contributor. The present results are 2-4 kcal mol^{-1} below previously reported B3LYP results.[4-6]

While these predicted isomerization energies do not change any conclusions from previous studies regarding general features of the C_3H_3 isomerization surface, they do provide theoretically sound energetics for the C_3H_3 isomerization surface. Additionally, the predicted relative energies will allow for the accurate determination of enthalpies of formation of these isomers relative to $\Delta_f H_0^\circ$(propargyl).

4.6 Enthalpies of Formation of Allene and Propyne

Valence focal point tables for the energies of reactions (4.6) and (4.7) are provided in Table 4.6. While the energy of reaction (4.7) converges rapidly with respect to inclusion of electron correlation, this convergence is protracted in the case of reaction (4.6). Indeed, at the CBS limit the correction to the CCSD energy splitting arising from the inclusion of triple excitations is +0.53 kcal mol^{-1}, which constitutes nearly 10% of the final reaction energy and is more than twice the analogous increment in the case of the propyne formation reaction (–0.24).

This imparts a larger degree of uncertainty onto the predicted energy of reaction (4.6) and enthalpy of formation of allene, and is a clarion for the importance of connected quadruple excitations in high-accuracy predictions of thermochemical values

Table 4.6 Incremental valence focal point tables (kcal mol^{-1}) for formation of allene and propyne via isodesmic reactions (4.6) and (4.7).[a]

Basis Set	ΔE_e[RHF]	+δ[MP2]	+δ[CCSD]	+δ[CCSD(T)]	+δ[CCSDT]	ΔE_e[CCSDT]
$H_2C{=}CH_2 + H_2C{=}CH_2 \rightarrow$ allene + CH_4 (4.6)						
cc-pVDZ	5.577	–2.001	+1.350	–0.253	+0.031	4.704
cc-pVTZ	5.501	–2.809	+1.327	–0.297	[+0.031]	[3.754]
cc-pVQZ	5.666	–2.996	+1.305	–0.323	[+0.031]	[3.684]
cc-pV5Z	5.767	–2.945	+1.285	[–0.438]	[+0.031]	[3.700]
cc-pV6Z	5.781	[–2.922]	[+1.276]	[–0.489]	[+0.031]	[3.677]
CBS limit	[5.783]	[–2.891]	[+1.264]	[–0.559]	[+0.031]	**[3.628]**
$HC{\equiv}CH + H_3C{-}CH_3 \rightarrow$ propyne + CH_4 (4.7)						
cc-pVDZ	–7.694	+0.169	+0.820	–0.088	+0.048	–6.744
cc-pVTZ	–7.828	–0.138	+0.837	–0.048	[+0.048]	[–7.130]
cc-pVQZ	–7.872	–0.231	+0.827	–0.071	[+0.048]	[–7.298]
cc-pV5Z	–7.886	–0.150	+0.798	[–0.176]	[+0.048]	[–7.356]
cc-pV6Z	–7.887	[–0.114]	[+0.794]	[–0.222]	[+0.048]	[–7.377]
CBS limit	[–7.888]	[–0.065]	[+0.786]	[–0.286]	[+0.048]	**[–7.404]**
Fit	$a + be^{-cX}$	$a + bX^{-3}$	$a + bX^{-3}$	$a + bX^{-3}$	additive	
Points (X=)	4,5,6	4,5	3,4	3,4		

[a] See footnote a from Table 4.3 for notation.

Appending corrections for core-correlation, zero-point vibrational, non-Born-Oppenheimer, and scalar relativistic effects (see Table 4.7) to these reaction energies, we arrive at enthalpies of formation (0 K) of 47.7 and 46.2 kcal mol^{-1} for allene and propyne, respectively. These computed enthalpies are within the error bars of tabulated experimental values (47.4 ± 0.3 and 46.0 ± 0.2 kcal mol^{-1})[81] and slightly lower than the results of Feller and Dixon (48.1 ± 0.5 and 46.5 ± 1.5 kcal mol^{-1}).[78] However, the energy difference between propyne and allene derived from these independently computed enthalpies of formation is 1.5 kcal mol^{-1}, which is nearly 0.6 kcal mol^{-1} higher than the directly computed isomerization energy of 0.92 kcal mol^{-1}. This discrepancy arises at least in part from inconsistencies and uncertainties in the underlying

reference enthalpies of formation in Table 4.2. However, given the slow convergence of the energy of reaction (4.6) with respect to the inclusion of electron correlation, the computed enthalpy of formation of propyne should be considered more reliable. So, discounting the effects of any underlying inconsistencies in the reference enthalpies of formation, we take the enthalpy of formation of propyne as 46.1 kcal mol^{-1}, and derive a recommended value of 47.1 kcal mol^{-1} for allene based on the computed isomeric energy splitting of 0.92 kcal mol^{-1}.

Table 4.7 Determination of enthalpies of formation energies for allene, propyne, and propargyl (**1**), in kcal mol^{-1}.[a]

Reaction	ΔE_{fp}(V)	Δ_{fp}(core)	ΔZPVE	ΔDBOC	ΔRel	ΔE_0(final)	Target	$\Delta_f H^\circ_0$
(4.6)	3.63	–0.20	–0.97	–0.02	+0.01	2.45	allene	**47.65**[b]
(4.7)	–7.40	–0.13	–0.40	–0.05	+0.00	–7.99	propyne	**46.23**
(4.3)	–14.43	–0.18	+0.73	+0.00	+0.01	–13.86	propargyl	**85.03**
(4.4)	98.12	+0.01	–8.85	+0.54	–0.01	89.32	propargyl	**84.83**
(4.5)	–115.75	–1.01	+4.53	–0.02	+0.14	–112.11	propargyl	**84.21**

[a] Enthalpy of formation for propargyl (**1**) given relative to the a value of 47.31 kcal mol^{-1} for the enthalpy of formation (0 K) of allene. See footnote a from Table 4.4 for notation.
[b] The recommended value is **47.05** kcal mol^{-1}, derived from the computed enthalpy of formation (0 K) for propyne and an isomerization energy of 0.92 kcal mol^{-1}.

4.7 Enthalpy of Formation of Propargyl Radical

The enthalpy of formation for propargyl radical has been predicted using reactions (4.3), (4.4), and (4.5), with the valence focal point tables shown in Table 4.8. While the computed energy for reaction (4.3) is rapidly convergent with respect to one-particle basis set completeness, the correction arising from the inclusion of triple excitations is still –0.68 at the CBS limit, yielding a final extrapolated valence reaction energy of –14.43 kcal mol^{-1}. Similarly, for reaction (4.5) the correction from triple excitations contributes –2.68 kcal mol^{-1} to the total reaction energy of –115.75 kcal mol^{-1}. While this triples correction is actually smaller when expressed as a portion of the total reaction energy than in the case of reaction (4.3), it leads to an overall greater degree of uncertainty in the computed reaction energy. An accurate prediction of

the energy of reactions (4.3) and (4.5) will require at least partial inclusion of the effects of quadruple excitations, through CCSDT(Q) computations. This is in contrast to the energy for reaction (4.4), for which triple excitations contribute a mere +0.31 kcal mol^{-1} to the total valence energy of 98.12 kcal mol^{-1}. It is remarkable that reaction (4.4), which is not isodesmic, appears to converge more rapidly than isodesmic reaction (4.3), despite the balancing of bond types in reaction (4.3).

Upon further corrections for higher-order effects (see Table 4.7), the final predictions for the enthalpy of formation for propargyl from reactions (4.3), (4.4), and (4.5) are 85.0, 84.8, and 84.2 kcal mol^{-1}, respectively, relative to the reference enthalpies provided in Table 4.2. That the predicted enthalpy arising from reaction (4.5) is somewhat removed from the other two values is not unexpected, given the lack of convergence with respect to completeness of the *n*-particle basis set for this particular reaction energy. Taking the average of these three computed values, we arrive at a final recommended enthalpy of formation for propargyl of 84.7 kcal mol^{-1}.

From Table 4.1 we see that previous experimental work has resulted in a relatively wide range of predicted enthalpies of formation. From the work of Nguyen *et al.*,[6] the thermal correction from 0 to 298 K should be on the order of –0.6 kcal mol^{-1}, in which case the Tsang[10] and McMillan and Golden[15] values (81.0 ± 1.0 and 81.5 ± 2.0, respectively) appear to be too low. The two modern experimental values from Roth *et al.*[16] and Robinson *et al.*[9] (85.2 kcal mol^{-1} at 0K and 82.5 ± 3.0 kcal mol^{-1} at 298 K, respectively) are in far better agreement with the present results. The agreement with the 0 K results of Roth *et al.* is quite good, while our recommended value falls well within the upper limit of the experimental uncertainty in the latter case.

Table 4.8 Incremental valence focal point tables (kcal mol^{-1}) for formation of propargyl radical (**1**).[a]

Basis Set	ΔE_e[ROHF]	+δ[ZAPT2]	+δ[CCSD]	+δ[CCSD(T)]	+δ[CCSDT]	ΔE_e[CCSDT]
$H_2CCCH_2 + CH_3 \rightarrow HCCCH_2 + CH_4$ (4.3)						
cc-pVDZ	–6.762	–7.995	+2.282	–0.529	+0.030	–12.974
cc-pVTZ	–7.104	–8.523	+2.239	–0.670	[+0.030]	[–14.029]
cc-pVQZ	–7.020	–8.761	+2.181	–0.695	[+0.030]	[–14.265]
cc-pV5Z	–6.964	–8.838	[+2.154]	[–0.704]	[+0.030]	[–14.322]
cc-pV6Z	–6.956	[–8.872]	[+2.141]	[–0.708]	[+0.030]	[–14.364]
CBS limit	[–6.954]	[–8.919]	[+2.125]	[–0.713]	[+0.030]	**[–14.432]**
$H_2CCCH_2 \rightarrow HCCCH_2 + H$ (4.4)						
cc-pVDZ	80.920	+11.394	+2.362	+0.137	+0.024	94.836
cc-pVTZ	81.122	+13.981	+1.842	+0.255	[+0.024]	[97.224]
cc-pVQZ	81.166	+14.645	+1.625	+0.275	[+0.024]	[97.735]
cc-pV5Z	81.198	+14.847	[+1.582]	[+0.282]	[+0.024]	[97.933]
cc-pV6Z	81.205	[+14.937]	[+1.563]	[+0.285]	[+0.024]	[98.014]
CBS limit	[81.207]	[+15.060]	[+1.537]	[+0.290]	[+0.024]	**[98.117]**
$CH (^2\Pi) + HCCH \rightarrow HCCCH_2$ (4.5)						
cc-pVDZ	–94.022	–21.766	+7.609	–1.932	+0.075	–110.035
cc-pVTZ	–94.353	–24.688	+8.005	–2.486	[+0.075]	[–113.447]
cc-pVQZ	–94.351	–25.842	+7.971	–2.643	[+0.075]	[–114.789]
cc-pV5Z	–94.347	–26.108	[+7.814]	[–2.698]	[+0.075]	[–115.264]
cc-pV6Z	–94.332	[–26.226]	[+7.745]	[–2.723]	[+0.075]	[–115.461]
CBS limit	[–94.327]	[–26.387]	[+7.650]	[–2.757]	[+0.075]	**[–115.746]**
Fit	$a + be^{-cX}$	$a + bX^{-3}$	$a + bX^{-3}$	$a + bX^{-3}$	additive	
Points (X=)	4,5,6	4,5	3,4	3,4		

[a] See footnote a from Table 4.3 for notation.

Previous theoretically predicted enthalpies of formation for propargyl span a similar range (see Table 4.1). Nguyen *et al.*[6] report 298 K values of 84.9 and 84.3 kcal mol^{-1} based on two different formulations of open-shell coupled cluster theory applied to isodesmic reaction energies. Accounting for thermal corrections, these results are in agreement with the presently predicted value. Application of the G3 method to an atomization reaction resulted in a predicted enthalpy of formation (0 K) of 84.1 kcal mol^{-1}, just 0.6 kcal mol^{-1} below the presently predicted value. However, the diffusion Monte Carlo results of Harkless and Lester[17] (81.5 ± 1.3 and 82.5 ± 0.6 kcal mol^{-1}) appear to be too small by 1-2 kcal mol^{-1}. These DMC results seem to have been computed at DFT optimized geometries, so the observed differences could arise from deficiencies in these optimized structures, unbalanced errors due to the fixed-node

approximation, or errors resulting from the use of effective core-potentials to account for the inner-most electrons. Moreover, none of these effects would be accounted for in the determination of the reported error estimates.

Finally, combining the enthalpy of formation for propargyl with the previously computed relative energies for the three low-lying C_3H_3 isomers (see Section 4.5), we arrive at recommended enthalpies of formation of 126.6, 125.7, and 117.3 kcal mol^{-1} for 1-propynyl (**2**), cycloprop-1-enyl (**3**), and cycloprop-2-enyl (**4**) radicals, respectively.

4.8 SUMMARY

We have presented definitive optimized geometries and isomerization energies for four low-lying C_3H_3 radical isomers that play a key role in the rate limiting steps on the pathway to benzene and soot during combustion. Isomerization energies were derived through the systematic extrapolation of *ab initio* energies and then corrected for core-valence correlation, non-Born-Oppenheimer effects, relativistic effects, and zero-point vibrational energy. Energies of 41.9, 41.0, and 32.7 kcal mol^{-1} were computed for 1-propynyl, cyclopro-1-enyl, and cyclopro-2-enyl radicals, relative to propargyl radical, respectively. These computed isomerization energies are roughly 1 kcal mol^{-1} larger than the RCCSD(T) results of Nguyen *et al*.,[6] and several kcal mol^{-1} smaller than B3LYP density functional results.[4-6] The deficiencies in the results of Nguyen *et al*., compared to the present results, are due to the accumulation of errors resulting from the use of exiguous DFT geometries (particularly for propargyl radical), inaccurate ZPVE corrections, and a failure to account for basis set incompleteness, core-valence correlation, and other small effects. Our final predicted energy of allene relative to propyne is 0.92 kcal mol^{-1}, in general agreement with the extrapolated results of Feller and Dixon.[78]

In addition, enthalpies of formation have been determined for all four C_3H_3 isomers, as well as for propyne and allene. The final recommended enthalpy of formation for allene is 47.2 kcal mol^{-1}, derived from the recommended value for propyne (46.2 kcal mol^{-1}) and the directly computed isomerization energy. The final recommended enthalpies of formation (0 K) for propargyl, 1-propynyl, cycloprop-1-enyl, and cycloprop-2-enyl radicals are 84.7, 126.6, 125.7, and 117.3 kcal mol^{-1}, respectively. Accounting for thermal corrections, these are in reasonable agreement with the 298 K values reported by Nguyen *et al*[6] and the final recommended enthalpy for propargyl radical is in agreement with modern experimental determinations,[9,16] falling at the upper end of the experimental range reported by Robinson *et al*.[9]

Together, the recommended enthalpies of formation for these C_3H_3 isomers constitute the most reliable presently available, and should be incorporated into detailed kinetic models of soot formation, displacing previous values based on less rigorous theoretical results. Furthermore, the computed isomerization energies should be used to calibrate and verify more approximate treatments of the entire C_3H_3 isomerization surface to derive accurate barriers and rate constants for these important isomerization processes. A proper account of this isomerization surface will be vital to accurately model the fate of propargyl radical in combustion processes. Additionally, the computed energy of allene relative to propyne should prove useful as a suitable benchmark against which DFT functionals can be tested, since this system poses a difficulty for many popular DFT functionals.[70] The definitive isomerization energies and enthalpies of formation presented here remove lingering uncertainties in the thermochemistry of these key soot formation intermediates, allowing for more defintive conclusions to be drawn regarding the pathways to benzene, PAHs, and soot during combustion.

4.9 Acknowledgements

This research was supported by the U. S. Department of Energy, Office of Basic Energy Sciences, Combustion Program (Grant No. DE-FG02-00ER14748). S.E.W. was also supported by a University of Georgia Presidential Fellowship. K.A.R. would like to thank D. Wood for helpful discussions. Figs. 4.2-4.4 were generated using HFSmol.[82]

References

1 J. A. Miller, M. J. Pilling, and J. Troe, Proc. Combust. Inst. **30**, 43 (2005).

2 M. Frenklach, Phys. Chem. Chem. Phys. **4**, 2028 (2002).

3 H. Richter and J. B. Howard, Phys. Chem. Chem. Phys. **4**, 2038 (2002).

4 L. Vereecken, K. Pierloot, and J. Peeters, J. Chem. Phys. **108**, 1068 (1998).

5 A. M. Mebel, W. M. Jackson, A. H. H. Chang, and S. H. Lin, J. Am. Chem. Soc. **120**, 5751 (1998).

6 T. L. Nguyen, A. M. Mebel, and R. I. Kaiser, J. Phys. Chem. A **105**, 3284 (2001).

7 S. E. Wheeler, W. D. Allen, and H. F. Schaefer, J. Chem. Phys. **121**, 8800 (2004).

8 The implementation of ROHF reference CCSD(T) in Molpro allows for restrictions on the T-amplitudes to ensure that the resulting CC wave function is a spin-eigenfunction. This formulation was used by Mebel and co-workers, and will be denoted by RCCSD(T) in this work

9 M. S. Robinson, M. L. Polak, V. M. Bierbaum, C. H. DePuy, and W. C. Lineberger, J. Am. Chem. Soc. **117**, 6766 (1995).

10 W. Tsang, in *Energetics of Organic Free Radicals*, edited by J. A. Martinho Simoes, A. Greenberg, and J. F. Liebman (Blackie Academic and Profressional, London, 1996), pp. 22.

11 W. Tsang, J. Chem. Kinetics **2**, 23 (1970).

12 W. Tsang, Int. J. Chem. Kinet. **10**, 687 (1978).

13 K. D. King, Int. J. Chem. Kinet. **10**, 545 (1978).

[14] K. D. King and T. T. Nguyen, J. Phys. Chem. **83**, 1940 (1979).

[15] D. F. McMillen and D. M. Golden, Annu. Rev. Phys. Chem. **33**, 493 (1982).

[16] W. R. Roth, H. Hopf, and C. Horn, Chem. Ber. **127**, 1781 (1994).

[17] J. A. W. Harkless and A. W. Lester, J. Chem. Phys. **113**, 2680 (2000).

[18] M. Saeys, M. F. Reyniers, G. B. Marin, V. V. Speybroeck, and M. Waroquier, J. Phys. Chem. A **107**, 9147 (2003).

[19] R. Walsh, Trans. Faraday Soc. **67**, 2085 (1971).

[20] D. K. Sen Sharma and J. L. Franklin, J. Am. Chem. Soc. **95**, 6562 (1973).

[21] C. F. Melius, *BAC-MP4 Heats of Formation and Free Energies*. (Sandia National Laboratories, Livermore, CA, 1996).

[22] W. D. Allen, A. L. L. East, and A. G. Császár, in *Structures and Conformations of Non-Rigid Molecules*, edited by J. Laane, M. Dakkouri, B. van der Vecken, and H. Oberhammer (Kluwer, Dordrecht, 1993), pp. 343.

[23] A. G. Császár, W. D. Allen, and H. F. Schaefer, J. Chem. Phys. **108**, 9751 (1998).

[24] A. G. Császár, G. Tarczay, M. L. Leininger, O. L. Polyansky, and W. D. Allen, in *Spectroscopy from Space*, edited by J. Demaison and K. Sarka (Kluwer, Dordrecht, 2001), pp. 317.

[25] A. L. L. East and W. D. Allen, J. Chem. Phys. **99**, 4638 (1993).

[26] J. M. Gonzales, C. Pak, R. S. Cox, W. D. Allen, G. Tarczay, and A. G. Császár, Chem. Eur. J. **9**, 2173 (2003).

[27] J. P. Kenny, W. D. Allen, and H. F. Schaefer, J. Chem. Phys. **118**, 7353 (2003).

[28] G. D. Purvis and R. J. Bartlett, J. Chem. Phys. **76**, 1910 (1982).

[29] G. E. Scuseria, A. C. Scheiner, T. J. Lee, J. E. Rice, and H. F. Schaefer, J. Chem. Phys. **86**, 2881 (1987).

[30] G. E. Scuseria, C. L. Janssen, and H. F. Schaefer, J. Chem. Phys. **89**, 7382 (1988).

[31] M. Rittby and R. J. Bartlett, J. Phys. Chem. **92**, 3033 (1988).

[32] K. Raghavachari, G. W. Trucks, J. A. Pople, and M. Head-Gordon, Chem. Phys. Lett. **157**, 479 (1989).

[33] J. Gauss, W. J. Lauderdale, J. F. Stanton, J. D. Watts, and R. J. Bartlett, Chem. Phys. Lett. **182**, 207 (1991).

[34] R. J. Bartlett, J. D. Watts, S. A. Kucharski, and J. Noga, Chem. Phys. Lett. **167**, 609 (1990).

[35] R. J. Bartlett, J. D. Watts, S. A. Kucharski, and J. Noga, Chem. Phys. Lett. **165**, 513 (1990).

[36] J. D. Watts, J. Gauss, and R. J. Bartlett, J. Chem. Phys. **98**, 8718 (1993).

[37] R. A. King, W. D. Allen, B. Ma, and H. F. Schaefer, Faraday Discuss. **110**, 23 (1998).

[38] T. H. Dunning, J. Chem. Phys. **55**, 716 (1971).

[39] T. H. Dunning, J. Chem. Phys. **90**, 1007 (1989).

[40] ACES II; J. F. Stanton, J. Gauss, W. J. Lauderdale, J. D. Watts, and R. J. Bartlett. The package also contains modified versions of the MOLECULE Gaussian integral program of J. Almlöf and P. R. Taylor, the ABACUS integral derivative program written by T. U. Helgaker, H. J. Aa Jensen, P. Jørgensen, and P. R. Taylor, and the PROPS property evaluation integral code of P. R. Taylor.

[41] J. Noga and R. J. Bartlett, J. Chem. Phys. **86**, 7041 (1987).

[42] J. Noga and R. J. Bartlett, J. Chem. Phys. **89**, 3401 (1988).

[43] J. D. Watts and R. J. Bartlett, J. Chem. Phys. **93**, 6104 (1990).

[44] G. E. Scuseria and H. F. Schaefer, Chem. Phys. Lett. **152**, 382 (1988).

[45] See Appendix B for supplementary core-valence focal point tables, vibrational frequencies, and IR intensities.

[46] D. E. Woon and T. H. Dunning, J. Chem. Phys. **103**, 4572 (1995).

[47] See Chapter 2.

[48] T. J. Lee and D. Jayatilaka, Chem. Phys. Lett. **201**, 1 (1993).

[49] P. J. Knowles, J. S. Andrews, R. D. Amos, N. C. Handy, and J. A. Pople, Chem. Phys. Lett. **186**, 130 (1991).

[50] W. J. Lauderdale, J. F. Stanton, J. Gauss, J. D. Watts, and R. J. Bartlett, Chem. Phys. Lett. **187**, 21 (1991).

[51] C. L. Janssen, I. B. Nielson, M. L. Leininger, E. T. Seidl, and M. E. Colvin, MPQC 2.1.4 (Sandia National Laboratories, Livermore, California, 2002).

[52] D. Feller, J. Chem. Phys. **98**, 7059 (1993).

[53] T. Helgaker, W. Klopper, H. Koch, and J. Noga, J. Chem. Phys. **106**, 9639 (1997).

[54] W. J. Hehre, R. Ditchfield, L. Radom, and J. A. Pople, J. Am. Chem. Soc. **92**, 4796 (1970).

[55] B. Ruscic, R. E. Pinzon, M. L. Morton, G. von Laszevski, S. J. Bittner, S. G. Nijsure, K. A. Amin, M. Minkoff, and A. F. Wagner, J. Phys. Chem. A **108**, 9979 (2004).

[56] D. L. Gray and A. G. Robiette, Mol. Phys. **37**, 1901 (1979).

[57] B. Ruscic, private communication of unpublished results obtained from Active Thermochemical Tables (ATcT) ver. 1.25 using the Core (Argonne) Thermochemical Network ver. 1.056 (2006).

[58] N. C. Handy, Y. Yamaguchi, and H. F. Schaefer, J. Chem. Phys. **84**, 4481 (1986).

[59] A. G. Ioannou, R. D. Amos, and N. C. Handy, Chem. Phys. Lett. **251**, 52 (1996).

[60] N. C. Handy and A. M. Lee, Chem. Phys. Lett. **252**, 425 (1996).

[61] W. Kutzelnigg, Mol. Phys. **90**, 909 (1997).

[62] S. A. Perera and R. J. Bartlett, Chem. Phys. Lett. **216**, 606 (1993).

[63] K. Balasubramanian, *Relativistic Effects in Chemistry: Part A, Theory and Techniques*. (Wiley, New York, 1997).

[64] K. Balasubramanian, *Relativistic Effects in Chemistry: Part B, Applications*. (Wiley, New York, 1997).

[65] R. D. Cowan and D. C. Griffin, J. Opt. Soc. Am. **66**, 1010 (1976).

[66] G. Tarczay, A. G. Császár, W. Klopper, and H. M. Quiney, Mol. Phys. **99**, 1769 (2001).

[67] T. D. Crawford, C. D. Sherrill, E. F. Valeev, J. T. Fermann, M. L. Leininger, R. A. King, S. T. Brown, C. L. Janssen, E. T. Seidl, Y. Yamaguchi, W. D. Allen, B. Kellogg, and H. F. Schaefer, PSI 3 (2002).

[68] J. D. Watts, J. Gauss, and R. J. Bartlett, Chem. Phys. Lett. **200**, 1 (1992).

[69] MOLPRO, version 2002.1, a package of ab initio programs written by H.-J. Werner, P. J. Knowles, M. Schütz, R. Lindh, P. Celani, T. Korona, G. Rauhut, F. R. Manby, R. D. Amos, A. Bernhardsson, A. Berning, D. L. Cooper, M. J. O. Deegan, A. J. Dobbyn, F. Eckert, C. Hampel, G. Hetzer, A. W. Lloyd, S. J. McNicholas, W. Meyer, M. E. Mura, A. Nicklaß, P. Palmieri, R. M. Pitzer, U. Schumann, H. Stoll, A. J. Stone, R. Tarroni, and T. Thorsteinsson; Birmingham, UK, 2003.

[70] H. L. Woodcock, H. F. Schaefer, and P. R. Schreiner, J. Phys. Chem. A **106**, 11923 (2002).

[71] C. W. Bauschlicher and S. R. Langhoff, Chem. Phys. Letters **193**, 380 (1992).

[72] J. F. Stanton and R. J. Bartlett, J. Chem. Phys. **98**, 7029 (1993).

[73] S. E. Wheeler, personal speculation.

[74] M. R. Hoffmann, W. D. Laidig, K. S. Kim, D. J. Fox, and H. F. Schaefer, J. Chem. Phys. **80**, 338 (1984).

[75] D. M. Chipman and K. E. Miller, J. Am. Chem. Soc. **106**, 6236 (1984).

[76] Y. J. Bomble, J. F. Stanton, M. Kállay, and J. Gauss, J. Chem. Phys. **123**, 054101 (2005).

[77] T. Shimanouchi, *Tables of Molecular Vibrational Frequencies Consolidated*. (National Bureau of Standards, Washington, DC, 1972).

[78] D. Feller and D. A. Dixon, J. Phys. Chem. A **104**, 3048 (2000).

[79] V. B. Kobychev, N. M. Vitkovskaya, N. S. Klyba, and B. A. Trofimov, Russ. Chem. Bull., Int. Ed. **51**, 774 (2002).

[80] H.-G. Yu and J. T. Muckerman, J. Phys. Chem. A **109**, 1890 (2005).

[81] J. B. Pedley, *Thermodynamic Data and Structures of Organic Compounds*. (Thermodynamic Research Center, College Station, TX, 1994).

[82] S. E. Wheeler, HFSmol (2005).

CHAPTER 5

SUMMARY AND CONCLUDING REMARKS

Highly accurate isomerization energies and enthalpies of formation have been presented for several key intermediates in the formation of the first aromatic ring during combustion, compted through the extrapolation of *ab initio* energies using the focal point method. Within focal point analyses, the leading contribution for the effects of electron correlation arises from the use of second-order perturbation theory. We have explicitly examined the convergence properties of ZAPT*n* energies and predicted bond lengths and frequencies. Comparison of high-order ZAPT*n* energy series with ROMP, RMP, OPT1, OPT2, and UMP series from the literature suggests that ZAPT*n* energies closely parallel results from ROMP and RMP theories, though at a reduced computational cost. Furthermore, at second- and fourth-order, ZAPT predicted bond lengths and frequencies for NO, CN, and O_2 are as good as or better than those from ROMP and RMP theories, relative to experiment. These are the first published results for ZAPT computed beyond second order. Based on these findings, we recommend low-order ZAPT for applications to open-shell systems, as well as ZAPT2 for the inclusion in focal point analyses.

Using the focal point method, definitive isomerization energies were predicted for C_4H_3 and C_4H_5, whose role in combustion and soot formation has been extensively debated in the literature during the last decade, largely based on widely varying predicted energy differences.[1-3] While any definite answers regarding the fate of these even-carbon-atom species in combustion will require more complete kinetic models than are currently available, the present isomerization energies and associated enthalpies of formation will provide sound thermodynamic values for incorporation into such models and allow for more definitive conclusions to be drawn regarding the fate of these species in combustion. Moreover, the definitive results presented here refute the 2002 DMC values of Krokidis *et al.*,[4] which have been a source of a great deal of the recent debate regarding even-carbon-atom pathways to benzene and soot.

The general consensus is that the dominant pathway to benzene (and therefore soot) in combustion involves the self-reaction of the propargyl radical. Additional low-lying C_3H_3 isomers are also vital to this process, so we have presented accurate isomerization energies and enthalpies of formation for propargyl radical and three low-lying C_3H_3 isomers. Our extrapolated isomerization energies are somewhat larger than recent CCSD(T) results from the literature, with the differences arising primarily through the use of basis set extrapolations, inclusion of effects due to core-valence correlation, and the use of more accurate molecular structures and harmonic vibrational frequencies in the present work. However, the present results do suggest that at least partial treatment of quadruple excitations within the coupled-cluster framework will be necessary before truly definitive values can be predicted. The recently published CCSDT(Q) method offers a computationally efficient means towards this end.

By pushing *ab initio* methods to both the one- and *n*-particle basis set limits, we have demonstrated the feasibility of computing accurate thermochemical parameters for several key intermediates in combustion chemistry that have proven problematic for less robust theoretical techniques. The present results have allowed us to critically examine results from diffusion Monte Carlo and the ever-popular DFT and composite *ab initio* methods for the prediction of enthalpies of formation and isomerization energies for these key systems, revealing troubling deficiencies in these commonly employed methods. Inclusion of the presently predicted thermochemical values into detailed kinetic models of soot formation will allow for a more complete and theoretically sound description of the combustion of aliphatic fuels and formation of soot. While less rigorous theoretical treatments are invaluable for mapping out large swaths of complex potential energy surfaces and predicting qualitative thermochemical parameters, robust *ab initio* procedures such as those applied in this work are necessary to provide the

definitive results required to develop accurate models of combustion and soot formation. The understanding of combustion processes afforded by these models constitutes the most promising path towards reduction of soot particle emissions.

REFERENCES

1 J. A. Miller and C. F. Melius, Combust. Flame **91**, 21 (1992).

2 H. Richter and J. B. Howard, Phys. Chem. Chem. Phys. **4**, 2038 (2002).

3 M. Frenklach, Phys. Chem. Chem. Phys. **4**, 2028 (2002).

4 X. Krokidis, N. W. Moriarty, W. A. Lester Jr., and M. Frenklach, Int. J. Chem. Kinet. **33**, 808 (2001).

APPENDIX A

SUPPLEMENTARY MATERIAL FOR CHAPTER 3

Table A1. Open-shell T_1 diagnostics and maximum T_1 and T_2 amplitudes for isomers of C_4H_3 and C_4H_5 at the cc-pVTZ ROCCSD level.[a]

Species	T_1 Diagnostic	Largest T_1 Amplitude	Largest T_2 Amplitude
i-C_4H_3	0.024	0.111	0.105
Z-*n*-C_4H_3	0.015	0.050	0.092
E-*n*-C_4H_3	0.015	0.048	0.093
i-C_4H_5	0.024	0.124	0.089
Z-*n*-C_4H_5	0.014	0.039	0.107
E-*n*-C_4H_5	0.014	0.037	0.108

[a] Computed at frozen-core TZ(2d1f,2p1d) ROCCSD(T) geometries using Psi3.

Table A2. Incremental valence focal point table (kcal mol^{-1}) for the energy of the C_{2v}-symmetric structure **5** relative to *i*-C_4H_3.[a]

Basis Set	ΔE_e[ROHF]	+δ[ZAPT2]	+δ[CCSD]	+δ[CCSD(T)]	+δ[CCSDT]	ΔE_e[CCSDT]
i-C_4H_3 (**4**) → C_{2v}-C_4H_3 (**5**)						
cc-pVDZ	2.609	–3.814	+1.966	–0.200	+0.071	0.633
cc-pVTZ	2.587	–4.213	+2.122	–0.248	[+0.071]	[0.320]
cc-pVQZ	2.592	–4.344	+2.177	–0.260	[+0.071]	[0.236]
cc-pV5Z	2.599	–4.342	[+2.147]	[–0.265]	[+0.071]	[0.211]
cc-pV6Z	2.601	[–4.341]	[+2.147]	[–0.265]	[+0.071]	[0.214]
CBS limit	[2.602]	[–4.340]	[+2.147]	[–0.265]	[+0.071]	**[0.216]**
Fit	$a+be^{-cX}$	$a+bX^{-3}$	$a+bX^{-3}$	$a+bX^{-3}$	additive	
Points (X=)	4,5,6	4,5	3,4	3,4		
Cut-off	none	none	5	5		

[a] See footnote *a* of Table 3.4. The extrapolated core-correlation correction is –0.044 kcal mol^{-1}, resulting in a final extrapolated energy separation of 0.172 kcal mol^{-1}.

Table A3. Incremental core-correlation focal point tables (kcal mol^{-1}) for isomerization reactions of C_4H_3.[a]

Basis Set	Δ_{fp}(core)[ZAPT2]	+δ[CCSD]	+δ[CCSD(T)]	Δ_{fp}(core)[CCSD(T)]
i-C_4H_3 → *Z*-*n*-C_4H_3				
cc-pCVDZ	0.118	–0.015	+0.007	0.110
cc-pCVTZ	0.140	–0.028	+0.009	0.120
cc-pCVQZ	0.152	[–0.028]	[+0.009]	[0.132]
cc-pCV5Z	[0.156]	[–0.028]	[+0.009]	[0.136]
CBS limit	[0.160]	[–0.028]	[+0.009]	**[0.141]**
i-C_4H_3 → *E*-*n*-C_4H_3				
cc-pCVDZ	0.121	–0.015	+0.007	0.112
cc-pCVTZ	0.132	–0.029	+0.008	0.112
cc-pCVQZ	0.144	[–0.029]	[+0.008]	[0.124]
cc-pCV5Z	[0.148]	[–0.029]	[+0.008]	[0.128]
CBS limit	[0.152]	[–0.029]	[+0.008]	**[0.132]**
Fit	$a+bX^{-3}$	additive	additive	
Points (X=)	3,4			
Cut-off	none			

[a] See footnote *a* of Table 3.4 for notation. This table pertains to the core correlation *correction* [Δ_{fp}(core)] to the reaction energy.

Table A4. Incremental core-correlation focal point tables (kcal mol^{-1}) for isomerization reactions of C_4H_5.[a]

Basis Set	Δ_{fp}(core)[ZAPT2]	+δ[CCSD]	+δ[CCSD(T)]	Δ_{fp}(core)[CCSD(T)]
i-C_4H_5 → *Z*-*n*-C_4H_5				
cc-pCVDZ	0.161	–0.020	–0.000	0.141
cc-pCVTZ	0.182	–0.020	–0.003	0.159
cc-pCVQZ	0.198	[–0.020]	[–0.003]	[0.175]
cc-pCV5Z	[0.205]	[–0.020]	[–0.003]	[0.181]
CBS limit	[0.211]	[–0.020]	[–0.003]	**[0.188]**
i-C_4H_5 → *E*-*n*-C_4H_5				
cc-pCVDZ	0.159	–0.020	–0.000	0.139
cc-pCVTZ	0.173	–0.020	–0.003	0.150
cc-pCVQZ	0.189	[–0.020]	[–0.003]	[0.167]
cc-pCV5Z	[0.195]	[–0.020]	[–0.003]	[0.173]
CBS limit	[0.201]	[–0.020]	[–0.003]	**[0.179]**
Fit	$a+bX^{-3}$	additive	additive	
Points (X=)	3,4			
Cut-off	none			

[a] See footnote *a* of Table 3.4. This table pertains to the core correlation *correction* [Δ_{fp}(core)] to the reaction energy.

Table A5. Incremental core-correlation focal point tables (kcal mol^{-1}) for decomposition reactions of C_4H_4 and C_4H_6.[a]

Basis Set	Δ_{fp}(core)[MP2]	+δ[CCSD]	+δ[CCSD(T)]	Δ_{fp}(core)[CCSD(T)]
$C_4H_4 + C_2H_6 \rightarrow C_3H_6 + C_3H_4$				
cc-pCVDZ	–0.004	–0.000	+0.004	–0.001
cc-pCVTZ	–0.028	–0.003	+0.006	–0.025
cc-pCVQZ	–0.041	[–0.003]	[+0.006]	[–0.038]
cc-pCV5Z	[–0.045]	[–0.003]	[+0.006]	[–0.042]
CBS limit	[–0.050]	[–0.003]	[+0.006]	**[–0.047]**
$C_4H_6 + C_2H_6 \rightarrow C_3H_6 + C_3H_6$				
cc-pCVDZ	0.009	–0.000	+0.001	0.010
cc-pCVTZ	–0.009	–0.003	+0.000	–0.012
cc-pCVQZ	–0.017	[–0.003]	[+0.000]	[–0.020]
cc-pCV5Z	[–0.020]	[–0.003]	[+0.000]	[–0.022]
CBS limit	[–0.021]	[–0.003]	[+0.000]	**[–0.025]**
Fit	$a + bX^{-3}$	additive	additive	
Points (X=)	3,4			
Cut-off	none			

[a] See footnote *a* of Table 3.4. This table pertains to the core correlation *correction* [Δ_{fp}(core)] to the reaction energy.

Table A6. Incremental core-correlation focal point tables (kcal mol^{-1}) for isodesmic reaction of *i*-C_4H_3 and *i*-C_4H_5.[a]

Basis Set	Δ_{fp}(core)[ZAPT2]	+δ[CCSD]	+δ[CCSD(T)]	Δ_{fp}(core)[CCSD(T)]
i-$C_4H_3 + CH_4 \rightarrow C_4H_4 + CH_3$				
cc-pCVDZ	0.117	–0.005	+0.008	0.120
cc-pCVTZ	0.112	–0.014	+0.012	0.110
cc-pCVQZ	0.121	[–0.014]	[+0.012]	[0.119]
cc-pCV5Z	[0.125]	[–0.014]	[+0.012]	[0.123]
CBS limit	[0.129]	[–0.014]	[+0.012]	**[0.126]**
i-$C_4H_5 + CH_4 \rightarrow C_4H_6 + CH_3$				
cc-pCVDZ	0.161	–0.010	+0.002	0.152
cc-pCVTZ	0.153	–0.006	+0.001	0.148
cc-pCVQZ	0.168	[–0.006]	[+0.001]	[0.162]
cc-pCV5Z	[0.173]	[–0.006]	[+0.001]	[0.167]
CBS limit	[0.178]	[–0.006]	[+0.001]	[0.172]
Fit	$a + bX^{-3}$	additive	additive	
Points (X=)	3,4			
Cut-off	none			

[a] See footnote *a* of Table 3.4. This table pertains to the core correlation *correction* [Δ_{fp}(core)] to the reaction energy.

Table A7. Harmonic vibrational frequencies (cm^{-1}) for C_4H_4 and isomers of C_4H_3, computed at the cc-pVDZ ROCCSD(T) level of theory. IR intensities (km mol^{-1}) are in parentheses.

Species	*a′*	*a″*
C_4H_4 (vinylacetylene,**1**)	206 (2)	297 (4)
	524 (1)	670 (0)
	883 (3)	914 (25)
	1097 (4)	979 (23)
	1304 (1)	
	1432 (2)	
	1655 (6)	
	2146 (1)	
	3167 (3)	
	3186 (7)	
	3271 (8)	
	3461 (56)	
E-*n*-C_4H_3 (**2**)	209 (5)	306 (14)
	511 (3)	571 (55)
	616 (34)	662 (16)
	816 (18)	784 (0)
	1015 (8)	
	1252 (3)	
	1609 (3)	
	2148 (1)	
	3094 (5)	
	3255 (1)	
	3462 (57)	
Z-*n*-C_4H_3 (**3**)	199 (0)	314 (1)
	491 (6)	567 (33)
	613 (40)	663 (16)
	875 (11)	860 (46)
	997 (21)	
	1253 (1)	
	1594 (4)	
	2139 (0)	
	3166 (3)	
	3250 (1)	
	3461 (57)	
i-C_4H_3 (**4**)	149 (4)	245 (2)
	378 (7)	509 (9)
	435 (37)	575 (28)
	871 (1)	8501 (37)
	983 (1)	
	1428 (1)	
	1722 (5)	
	1962 (7)	
	3104 (4)	
	3209 (3)	
	3451 (74)	

Table A8. Harmonic vibrational frequencies (cm^{-1}) for 1,3-butadiene-2-yl, computed at the cc-pVDZ ROCCSD(T) level of theory. IR intensities (km mol^{-1}) are in parentheses.

Species	a_1	b_1	b_2
1,3-butadiene-2-yl (**5**)	870 (0)	118*i*	214 (4)
	1436 (0)	96 (12)	464 (6)
	1754 (1)	351 (15)	564 (31)
	1927 (2)	976 (0)	844 (40)
	3102 (5)	3158 (5)	
	3450 (82)		

Table A9. Harmonic vibrational frequencies (cm^{-1}) for C_4H_6, computed at the cc-pVDZ ROCCSD(T) level of theory. IR intensities (km mol^{-1}) are in parentheses.

Species	a_g	a_u	b_g	b_u
C_4H_6 (1,3-butadiene,**6**)	506 (0)	172 (0)	748.1 (0)	289 (2)
	898 (0)	524 (9)	898.1 (0)	989 (1)
	1219 (0)	896 (59)	970.7 (0)	1299 (3)
	1300 (0)	1027 (32)		1402 (3)
	1468 (0)			1638 (9)
	1701 (0)			3154 (18)
	3151 (0)			3168 (13)
	3164 (0)			3256 (27)
	3255 (0)			

Table A10. Harmonic vibrational frequencies (cm^{-1}) for isomers of C_4H_5, computed at the cc-pVDZ ROCCSD(T) level of theory. IR intensities (km mol^{-1}) are in parentheses.

Species	*a′*	*a″*
E-*n*-C_4H_5 (**7**)	199 (6)	171 (4)
	544 (4)	488 (0)
	849 (41)	507 (3)
	892 (1)	711 (33)
	1064 (1)	917 (19)
	1173 (1)	983 (1)
	1360 (1)	3192 (6)
	1489 (2)	
	1866 (3)	
	3109 (12)	
	3160 (7)	
	3172 (5)	
	3283 (7)	
Z-*n*-C_4H_5 (**8**)	287 (1)	155 (0)
	480 (2)	562 (0)
	871 (27)	695 (24)
	937 (7)	886 (27)
	1164 (0)	895 (26)
	1245 (1)	1000 (28)
	1301 (2)	
	1431 (1)	
	1597 (3)	
	1669 (4)	
	3141 (4)	
	3156 (8)	
	3177 (8)	
	3238 (1)	
	3258 (12)	
i-C_4H_5 (**9**)	292 (6)	165 (0)
	505 (3)	550 (40)
	817 (13)	713 (9)
	947 (2)	815 (0)
	1181 (3)	897 (30)
	1238 (1)	1002 (17)
	1300 (1)	
	1433 (1)	
	1602 (3)	
	1680 (3)	
	3074 (9)	
	3156 (7)	
	3184 (6)	
	3250 (1)	
	3258 (12)	

APPENDIX B

SUPPLEMENTARY MATERIAL FOR CHAPTER 4

Table B1. Incremental core-correlation focal point tables (kcal mol^{-1}) for the isomerization of propyne to allene.[a]

Basis Set	Δ_{fp}(core)[ZAPT2]	+δ[CCSD]	+δ[CCSD(T)]	Δ_{fp}(core)[CCSD(T)]
Propyne → Allene				
cc-pCVDZ	0.010	+0.006	–0.011	0.004
cc-pCVTZ	0.050	+0.014	–0.017	0.046
cc-pCVQZ	0.077	+0.021	–0.019	0.079
cc-pCV5Z	[0.086]	[+0.023]	[–0.019]	[0.090]
CBS limit	[0.096]	[+0.026]	[–0.020]	**[0.102]**
Fit	$a+bX^{-3}$	$a+bX^{-3}$	$a+bX^{-3}$	
Points (X=)	3,4	3,4	3,4	

[a] See footnote *a* of Table 4.4 for notation. This table pertains to the core correlation *correction* [Δ_{fp}(core)] to the reaction energy.

Table B2. Incremental core-correlation focal point tables (kcal mol^{-1}) for three isomerization reactions of propargyl radical.[a]

Basis Set	Δ_{fp}(core)[ZAPT2]	+δ[CCSD]	+δ[CCSD(T)]	Δ_{fp}(core)[CCSD(T)]
Propargyl → 1-propynyl (**2**)[b]				
cc-pCVDZ	–	0.132	–0.009	0.124
cc-pCVTZ	–	0.225	–0.018	0.207
cc-pCVQZ	–	0.258	–0.022	0.236
cc-pCV5Z	–	[0.270]	[–0.024]	[0.246]
CBS limit	–	[0.283]	[–0.025]	**[0.257]**
Propargyl → cycloprop-1-enyl (**3**)				
cc-pCVDZ	0.132	+0.013	–0.008	0.137
cc-pCVTZ	0.313	+0.012	–0.019	0.306
cc-pCVQZ	0.429	+0.021	–0.025	0.425
cc-pCV5Z	[0.470]	[+0.024]	[–0.027]	[0.467]
CBS limit	[0.513]	[+0.027]	[–0.029]	**[0.511]**
Propargyl → cycloprop-2-enyl (**4**)				
cc-pCVDZ	0.029	–0.002	+0.004	0.031
cc-pCVTZ	0.104	–0.004	+0.007	0.107
cc-pCVQZ	0.162	+0.002	+0.007	0.171
cc-pCV5Z	[0.182]	[+0.005]	[0.007]	[0.194]
CBS limit	[0.204]	[+0.007]	[0.007]	**[0.218]**
Fit	$a+bX^{-3}$	$a+bX^{-3}$	$a+bX^{-3}$	
Points (X=)	3,4	3,4	3,4	

[a] See footnote *a* of Table 4.4. This table pertains to the core correlation *correction* [Δ_{fp}(core)] to the reaction energy.

[b] For 1-propynyl radical (**2**), the necessity of restricting the molecular orbitals to posses C_{3v} symmetry to properly describe the ground state prohibits us from computing ZAPT2 energies, so they are excluded form the core-valence focal point table in this instance.

Table B3. Incremental core-correlation focal point tables (kcal mol^{-1}) for the formation of allene and propyne.[a]

Basis Set	Δ_{fp}(core)[MP2]	+δ[CCSD]	+δ[CCSD(T)]	Δ_{fp}(core)[CCSD(T)]
$H_2C{=}CH_2 + H_2C{=}CH_2 \rightarrow$ allene + CH_4				
cc-pCVDZ	–0.201	+0.009	+0.002	–0.190
cc-pCVTZ	–0.190	+0.018	+0.006	–0.166
cc-pCVQZ	–0.208	+0.018	+0.007	–0.183
cc-pCV5Z	[–0.214]	[+0.018]	[+0.008]	[–0.188]
CBS limit	[–0.221]	[+0.018]	[+0.008]	**[–0.195]**
$HC{\equiv}CH + H_3C{-}CH_3 \rightarrow$ propyne + CH_4				
cc-pCVDZ	–0.137	+0.001	+0.004	–0.133
cc-pCVTZ	–0.132	+0.004	+0.011	–0.116
cc-pCVQZ	–0.143	+0.005	+0.014	–0.124
cc-pCV5Z	[–0.148]	[+0.006]	[+0.015]	[–0.127]
CBS limit	[–0.152]	[+0.006]	[+0.017]	**[–0.129]**
Fit	$a + bX^{-3}$	$a + bX^{-3}$	$a + bX^{-3}$	
Points (X=)	3,4	3,4	3,4	

[a] See footnote *a* of Table IV. This table pertains to the core correlation *correction* [Δ_{fp}(core)] to the reaction energy.

Table B4. Incremental core-correlation focal point tables (kcal mol^{-1}) for the formation of propargyl radical.[a]

Basis Set	Δ_{fp}(core)[ZAPT2]	+δ[CCSD]	+δ[CCSD(T)]	Δ_{fp}(core)[CCSD(T)]
$H_2CCCH_2 + CH_3 \rightarrow HCCCH_2 + CH_4$				
cc-pCVDZ	–0.069	–0.003	+0.006	–0.066
cc-pCVTZ	–0.122	–0.002	+0.011	–0.114
cc-pCVQZ	–0.156	–0.005	+0.012	–0.149
cc-pCV5Z	[–0.167]	[–0.006]	[+0.012]	[–0.162]
CBS limit	[–0.180]	[–0.008]	[+0.012]	**[–0.175]**
$H_2CCCH_2 \rightarrow HCCCH_2 + H$				
cc-pCVDZ	0.116	+0.009	+0.013	0.138
cc-pCVTZ	0.020	+0.029	+0.023	0.072
cc-pCVQZ	–0.024	+0.037	+0.027	0.039
cc-pCV5Z	[–0.040]	[+0.039]	[+0.028]	[0.027]
CBS limit	[–0.057]	[+0.042]	[+0.029]	**[0.014]**
CH ($^2\Pi$) + HCCH $\rightarrow HCCCH_2$				
cc-pCVDZ	–0.482	–0.070	+0.009	–0.543
cc-pCVTZ	–0.731	–0.104	+0.022	–0.812
cc-pCVQZ	–0.837	–0.117	+0.025	–0.929
cc-pCV5Z	[–0.875]	[–0.122]	[+0.026]	[–0.970]
CBS limit	[–0.914]	[–0.127]	[+0.027]	**[–1.014]**
Fit	$a + bX^{-3}$	$a + bX^{-3}$	$a + bX^{-3}$	
Points (X=)	3,4	3,4	3,4	

[a] See footnote *a* of Table IV. This table pertains to the core correlation *correction* [Δ_{fp}(core)] to the reaction energy.

Table B5. Harmonic vibrational frequencies (cm^{-1}) for allene, computed at the TZ(2d1f,2p1d) ROCCSD(T) level of theory. IR intensities (km mol^{-1}) are in parentheses.

a_1	b_1	b_2	e
1082 (0)	869 (0)	1438 (2)	343 (6)
1487 (0)		2009 (44)	845 (51)
3151 (0)		3149 (2)	1015 (2)
			3232 (1)

Table B6. Harmonic vibrational frequencies (cm^{-1}) for propyne and 1-propynyl radical, computed at the TZ(2d1f,2p1d) ROCCSD(T) level of theory. IR intensities (km mol^{-1}) are in parentheses.

Species	a_1	e
propyne	933 (1)	317 (7)
	1424 (0)	634 (48)
	2176 (4)	1059 (0)
	3058 (15)	1493 (7)
	3467 (50)	3132 (7)
1-propynyl	933 (4)	110 (3)
	1420 (1)	1014 (21)
	2188 (11)	1488 (2)
	3061 (14)	3138 (4)

Table B7. Harmonic vibrational frequencies (cm^{-1}) for propargyl radical, computed at the TZ(2d1f,2p1d) ROCCSD(T) level of theory. IR intensities (km mol^{-1}) are in parentheses.

a_1	b_1	b_2
1057 (3)	322 (5)	376 (4)
1472 (0)	606 (48)	468 (57)
1979 (4)	1033 (2)	652 (41)
3171 (3)	3269 (0)	
3456 (50)		

Table B8. Harmonic vibrational frequencies (cm^{-1}) for cycloprop-1-enyl and cycloprop-2-enyl radicals, computed at the TZ(2d1f,2p1d) ROCCSD(T) level of theory. IR intensities (km mol^{-1}) are in parentheses.

Species	*a′*	*a″*
cycloprop-1-enyl	663 (1)	510 (0)
	882 (76)	644 (2)
	1010 (35)	804 (2)
	1036 (0)	3177 (2)
	1515 (1)	
	1711 (18)	
	3101 (33)	
	3342 (15)	
cycloprop-2-enyl	596 (67)	723 (33)
	922 (5)	852 (0)
	991 (16)	987 (4)
	1223 (6)	1040 (23)
	1625 (1)	3263 (2)
	3107 (43)	
	3306 (0)	